Filipe André Prata Ataíde

Mestrado integrado em Engenharia Química e Bioquímica

Oxygen transport enhancement by functionalized magnetic nanoparticles (FMP) in bioprocesses

Dissertação para obtenção do Grau de
Doutor em Engenharia Química e Bioquímica

Orientador: Rui Manuel Freitas Oliveira,
Prof. Associado com Agregação, Univ. Nova de Lisboa

Co-orientador: João Carlos dos Santos Silva e Pereira de Lima,
Prof. Associado, Univ. Nova de Lisboa

Júri:

Presidente:	Prof. Doutora Maria da Ascensão Carvalho Fernandes Miranda Reis
Arguentes:	Prof. Doutor José António Couto Teixeira
	Prof. Doutora Eulália Fernanda Alves de Carvalho Pereira
Vogais:	Prof. Doutor Rui Manuel Freitas Oliveira
	Prof. Doutor João Carlos dos Santos Silva e Pereira de Lima

FACULDADE DE CIÊNCIAS E TECNOLOGIA
UNIVERSIDADE NOVA DE LISBOA

Fevereiro, 2016

Oxygen transport enhancement by functionalized magnetic nanoparticles (FMP) in bioprocesses

Acknowledgements

O período de doutoramento é muitas vezes um percurso solitário e longo, que depende muito do trabalho e inspiração de quem o executa. No entanto, apesar de ser uma tarefa individual, é impossível chegar a bom porto sem a contribuição de um grupo de pessoas a vários níveis. Como tal gostaria de agradecer a todos os que me tenham ajudado a concluir este período de formação e que possam não estar mencionados nas próximas linhas.

Em primeiro lugar, gostaria de agradecer ao meu orientador, Prof. Rui Oliveira, por me ter dado a oportunidade de desenvolver o meu doutoramento no seu grupo de investigação. Foi certamente um grande desafio e penso que diferente dos outros trabalhos que costumam ser realizados neste grupo. O projecto das nanopartículas passou por alguns percalços iniciais, que à partida não estavam previstos, mas penso que conseguimos chegar a um bom resultado. Agradeço a disponibilidade que teve para me ouvir e discutir todas as questões que foram aparecendo ao longo do tempo e que com uma grande dose de inspiração e espírito de estratégia, me ajudou a combater alguma da minha "aversão" ao laboratório. Todo o conhecimento sobre transferência de massa e correlações que consegui absorver foram de extrema importância para a conclusão desta etapa. O seu espírito de liderança e batalhador são inspiradores, e não falo apenas relativamente à orientação no doutoramento mas também a várias outras experiências que temos passado durante os últimos anos. Um grande obrigado por tudo!

Em segundo lugar, ao meu co-orientador, Prof. João Carlos Lima, por ter abraçado

este projecto quando ele já ia a meio e por ter trazido a sua “nano-visão” para me ajudar no meu doutoramento. Todas as discussões que tivemos a três foram realmente muito produtivas e penso que o seu contributo foi determinante para o resultado final desta tese. Aumentou ainda mais o nível de espírito crítico sobre os mecanismos das nanopartículas e trouxe uma nova dinâmica ao trabalho experimental. Ver-nos aos três, num determinado período, diariamente pelo laboratório, de volta de todo o aparato experimental para sintetizar nanopartículas era algo que não me passava pela cabeça ver durante o doutoramento. Parecíamos uns miúdos de volta de um brinquedo novo!

Em terceiro lugar, Prof. Maria Ascensão Reis, que apesar de ter sido co-orientadora apenas durante um curto período do meu doutoramento, se mostrou sempre disponível para qualquer questão que eu pudesse ter, seja a nível de revisão de abstracts para conferências seja nível de planificação de trabalho no início do projecto. Gostaria também de lhe agradecer por me ter acolhido no grupo BIOENG, onde pude crescer a nível científico e conhecer um grupo de pessoas que, quando quer, consegue ser uma grande e agradável família.

Em seguida, gostaria de agradecer aos meus colegas do grupo Systems Biology and Engineering, que são realmente uns grandes companheiros de “guerra” e que conseguem trazer uns espírito leve, descontraído e de bom-humor ao dia-a-dia: Moritz von Stosch, Cristiana de Azevedo, Rodolfo Marques, Rui Portela, Mauro Luís, João Dias e Valter Frade. Gostava ainda de dar uma palavra de especial agradecimento à Cristiana de Azevedo, por ter contribuído na parte de desenvolvimento de correlações para a modelação matemática e ao Moritz von Stosch por ter sempre uma grande disponibilidade para discutir qualquer aspecto técnico sobre modelação e ter dado feedback sobre a tese em tempo record!! Um obrigado a todos.

Não poderia também de deixar de agradecer ao grupo BIOENG, já que foram a minha primeira “casa“ e onde pude desenvolver o meu trabalho laboratorial. Agradeço toda a ajuda que me deram tanto no laboratório como o convívio que pude ter com

alguns de vocês e com quem pude partilhar bons momentos dentro e fora da FCT: Mónica Carvalheira, Christophe Roca, Ricardo Marques, Luísa Neves, Carla Daniel, Henrique Marçal, Catarina Oliveira e Rita Ferreira. Gostaria de deixar uma palavra especial ao José Luís Santos com quem pude partilhar a secretária durante alguns anos e com quem pude aprender muito. O teu rigor científico e a inteligência com que abordas os problemas são inspiradores!

Gostaria ainda de agradecer ao Prof. José Carlos Lopes e ao Enis Leblebici, da FEUP, por terem colaborado neste projecto das nanopartículas e pelas várias discussões que tivemos tanto por Skype, como presencialmente. O vosso contributo para este projecto foi importante e penso que será ainda mais no futuro.

Gostaria também de agradecer à Prof. Cecília Roque e ao seu grupo (em particular à Íris Batalha) por me terem recebido no vosso laboratório e terem ensinado muito (quase tudo) do que sei hoje sobre síntese de nanopartículas magnéticas.

Ao Prof. António Lopes, do ITQB, gostaria de lhe agradecer toda a disponibilidade que mostrou sempre que precisei de fazer medições de DLS e potencial-ζ e me explicar os conceitos por trás destas técnicas de caracterização.

Para finalizar os agradecimentos "técnicos", gostaria de agradecer aos Prof. Vaclav Linek e Prof. Michal Kordac da Prague Institute of Chemical Technology, que são uma referência no campo da transferência de oxigénio e por me terem respondido aos emails sobre a técnica de oxidação do sulfito de sódio para medir a transferência de oxigénio. As vossas resposta exaustivas foram cruciais para dominar este sistema químico que tanto me deu cabo da cabeça. Gostaria também de agradecer o tempo que o Prof. Michal Kordac pode dispensar para se deslocar ao laboratório BIOENG e avaliar todo o método que construí e validar todo o trabalho experimental relativo à transferência de massa. Não menos importante, foi a disponibilidade do Doutor Bernat Olle do MIT, para me responder à várias questões sobre o seu trabalho e o qual serviu de base de comparação para o trabalho que desenvolvi. É agradável perceber que pessoas brilhantes podem ser

igualmente modestas em relação ao valor. Obrigado aos três, foram muito importantes no desenvolvimento desta tese.

Aos meus pais e irmãos, um obrigado por todo o apoio que sempre me deram. Obrigado!

À Cris, agradecer-te é pouco, por tudo o que fizeste durante este doutoramento: ouviste-me quando precisei, aconselhaste-me, ajudaste-me a organizar o trabalho; deste-me apoio, carinho, e tiveste paciência comigo, mesmo quando, dia-após-dia, precisei de trabalhar fora de horas, fins-de-semana, feriados ou mesmo nas férias. Obrigado por me teres dado tudo o que precisei neste período e me conseguires sempre por um sorriso com o teu humor, mesmo quando o cansaço já começa a vencer. OBRIGADO POR TUDO!

Por fim, agradeço à Fundação para a Ciência e Tecnologia o financiamento da minha bolsa de doutoramento.

Abstract

The enhancement of fluid properties, namely thermal conductivity and mass diffusivity for a wide range of applications, through the use of nanosized particles' suspensions has been gathering increasing interest in the scientific community. In previous studies, Olle et al. (2006) showed an enhancement in oxygen absorption to aqueous solutions of up to 6-fold through the use of functionalized nanosized magnetic particles with oleic acid coating. Krishnamurthy et al. (2006) showed a remarkable 26-fold enhancement in dye diffusion in water. These two publications are landmarks in mass transfer enhancement in chemical systems through the use of nanoparticles.

The central goal of this Ph.D. thesis was to develop functionalized magnetic nanoparticles to enhance oxygen transport in bioprocesses. The experimental protocol for magnetic nanoparticles synthesis and purification adopted in this thesis is a modification of that reported by Olle et al. (2006). This is facilitated by employing twice the quantity of ammonia, added at a slower rate, and by filtering the final nanoparticle solution in a cross-flow filtration modulus against 55 volumes of distilled water. This modification in the protocol resulted in improved magnetic nanoparticles with measurably higher mass transfer enhancement. Magnetic nanoparticles with oleic acid and Hitenol-BC coating were screened for oxygen transfer enhancement, since these particles are relatively inexpensive and easy to synthesize. A glass 0.5-liter reactor was custom manufactured

specifically for oxygen transport studies in magnetic nanoparticles suspensions. The reactor geometry, baffles and Rushton impeller are of standard dimensions. Mass transfer tests were conducted through the use of the sulphite oxidation method, applying iodometric back-titration. A 3-factor central composite circumscribed design (CCD) was adopted for design of experiments in order to generate sufficiently informative data to model the effect of magnetic nanoparticles on interfacial area and mass transfer coefficient. The parameters ranges used were: 250-750 rpm for stirring speed, 0-2 vvm for aeration and 0-0.00120 $\mathrm{g\,g^{-1}}$ magnetic nanoparticles mass fraction.

It was found that 36 nm-sized nanoparticles produced during the course of this dissertation enhanced the volumetric mass transfer coefficient up to 3.3-fold and the interfacial area up to 3.3-fold in relation to gas-liquid dispersions without nanoparticles. These results are concordant with previously published enhancement data ($k_{\mathrm{L}}a$ enhancement by 7.1-fold and a enhancement by 4.1-fold) (Olle et al. 2006). The magnetic nanoparticles synthesized in this thesis were stable (constant diameter) over a 1wide pH range (2-9). Statistical regression models showed that both $k_{\mathrm{L}}a$ and a have high sensitivity to the nanoparticles loading. Empirical correlation models were derived for $k_{\mathrm{L}}a$ and for interfacial area, a, as function of physical properties and nanoparticles loading. These correlations lay out a methodology that can help the scientific community to design and scale-up oxygen transfer systems that are based on nanoparticle suspensions.

Keywords: Oxygen mass transfer enhancement, magnetic nanoparticles, Fe_3O_4, oleate, Hitenol-BC, sulfite oxidation, statistical modeling, empirical modeling.

Resumo

A melhoria das propriedades de fluidos, nomeadamente condutividade térmica e difusão mássica para uma vasta gama de aplicações, através do uso de suspensões de partículas nanométricas, tem recebido cada vez maior interesse na comunidade científica. Em estudos anteriores, Olle et al. (2006) mostrou um aumento na absorção de oxigénio em soluções aquosas até 6 vezes, através do uso de nanopartículas magnéticas funcionalizadas com uma camada de ácido oleico. No estudo de Krishnamurthy et al. (2006) verificou-se um aumento de 26 vezes na difusão de um corante em água. Estas duas publicações são uma referência no aumento de transferência de massa em sistemas químicos através de nanopartículas.

O objectivo desta tese de doutoramento é desenvolver nanopartículas magnéticas funcionalizadas para aumentar o transporte de oxigénio em bioprocessos. Para tal, o protocolo experimental de síntese e purificação de nanopartículas magnéticas adoptado nesta tese é uma modificação ao apresentado por Olle et al. (2006), utilizando o dobro da amónia, adicionada através de um caudal mais baixo, e filtrando a solução final de nanopartículas num módulo de filtracção de fluxo-cruzado com 55 vezes o volume de água em relação ao volume de solução final. Esta modificação no protocolo resultou em nanopartículas magnéticas melhoradas, com um aumento de transferência ligeiramente superior. Foram testadas nanopartículas magnéticas com um revestimento de ácido oleico

e Hitenol-BC, já que a sua síntese tem um custo baixo e é um processo facil de realizar. Para os testes de transporte de oxigénio em suspensões de nanopartículas magnéticas foi desenhado um reactor de vidro à medida com as dimensões/rácios standard, assim como as chicanas e a turbina Rushton. Os testes de transferência de massa foram realizados através do método de oxidação do sulfito, utilizando titulação iodométrica. Para estimar o efeito das nanopartículas magnéticas na área interfacial e no coeficiente de transferência de massa adoptou-se um desenho central composto circunscripto (CCD) de três factores. As gamas para os parâmetros operatórios foram: 250-750 rpm para a velocidade de agitação, 0-2 vvm para o arejamento e 0-0.00120 $\mathrm{g\,g^{-1}}$ de fracção mássica de nanopartículas magnéticas.

As nanopartículas magnéticas produzidas neste doutoramento conseguem aumentar o coeficiente de transferência de massa volumétrica até 3.3 vezes e a área interfacial até 4.8 vezes, em relação a dispersões gás-liquido sem nanopartículas. Estes resultados confirmam os dados publicados anteriormente (aumento do $k_{\mathrm{L}}a$ de 7.1 vezes e aumento da área interfacial de 4.1 vezes) (Olle et al. 2006). As nanopartículas magnéticas sintetizadas nesta tese mostraram ser estáveis (diâmetro constante) para uma gama de pH entre 2 e 9. Através dos modelos estatísticos desenvolvidos, concluiu-se que tanto $k_{\mathrm{L}}a$ como a têm uma elevada sensibilidade à presença de nanopartículas. As correlações empíricas desenvolvidas para $k_{\mathrm{L}}a$ e a, são função de propriedades físicas e carga de nanopartículas. Estas correlações propõem uma metodologia que pode ajudar a comunidade científica a desenhar e aumentar a escala de sistemas de transferência de oxigénio que envolver suspensões de nanopartículas.

Palavras-chave: Aumento de transferência de massa de oxigénio, nanopartículas magnéticas, Fe_3O_4, ácido oleico, Hitenol-BC, oxidação de sulfito, modelação estatística, modelação empírica.

Contents

List of Figures

List of Tables

CHAPTER 1

Introduction

1.1 Background

In the last two decades, many studies investigated the role that fine particles ($< 1\,\text{mm}$) may play in chemical and biochemical (among other) engineering processes. The use of these particles showed to enhance mass transport in several binary systems (Dagaonkar et al. 2003; Demmink et al. 1998; Holstvoogd et al. 1988; Linek et al. 2008; Littlejohns and Daugulis 2007; Nagy 2003; Ruthiya et al. 2003b).

Holstvoogd et al. (1988) improved gas absorption by using a reactor with 1 % Pt on activated carbon particles ($d_p(50\,\%) < 10\mu\text{m}$), due to higher concentration of particles in the gas-liquid interface. Demmink et al. (1998) was a pioneer study in using fine (micron-sized) particles for mass transfer enhancement, using sulfur particles to enhance the absorption of acetylene into iron chelates solutions. They applied $2.4\,\mu\text{m}$ particles and achieved an enhancement factor of 4.65. In Dagaonkar et al. (2003), $3\,\mu$m-sized TiO_2 particles were used to improve CO_2 absorption into water, hexadecane and sun

flower oil solutions. Parameters (particle loading (0–15 $\mathrm{kg\,m^{-3}}$) and stirring speed (180–780 rpm)) were varied , reaching a maximum gas absorption enhancement of 2.0, 1.9 and 2.2 for water, hexadecane and sun flower oil, respectively, with low stirring speeds (198 rpm) and 1, 10 and 15 $\mathrm{kg\,m^{-3}}$ of particle loading, respectively. Ruthiya et al. (2003b) evaluated the most generally accepted mechanisms for the enhancement of gas-liquid mass transfer: boundary layer mixing, shuttling effect, coalescence inhibition and boundary layer reaction. The study used silica and carbon particles in different systems (AMS-H_2, glucose-O_2 and distilled water-electrolyte). The enhancements achieved are 1.4, 1.4 and 3.5, respectively for carbon particles while for silica the enhancements areup to 1.7, 1.1, 2.1, for each system respectively.

The enhancement of fluid properties, namely thermal conductivity and mass diffusivity, through the use of nanosized particles' suspensions have been gathering increasing interest in the scientific community. This trend is clearly shown by recording the evolution of the number of hits of the keyword 'nanoparticle enhancement' on *ISI Web of Knowledge* (Figure 1.1). In the investigation performed by Choi and Eastman (1995) the term *nanofluid* appeared for the first time, describing a new class of engineering heat transfer fluids, which contain about 10-nanometer-sized metallic particles.

In recent years, a very promising set of studies report the use of functionalized magnetic nanoparticles for oxygen transfer enhancement (Ditsch et al. 2005a,b, 2006; Kral 2005; Krishnamurthy et al. 2006; Olle 2006; Olle et al. 2006; Shen et al. 1999) in bioprocesses (Olle 2006; Olle et al. 2006). Functionalized magnetic nanoparticles are composed by a magnetic core and an organic coating, which form colloidal dispersions in water. The particles have usually a size of $\sim$10 nm in the single form but, if clustered, they can range up to several hundred nanometers.

Particles with size below 10 nm are to be avoided since magnetic forces cannot be used to direct particle behaviour; over 1 micrometer, particles tend to form aggregates thereby lowering the specific surface area. Also the coating can be used to prevent

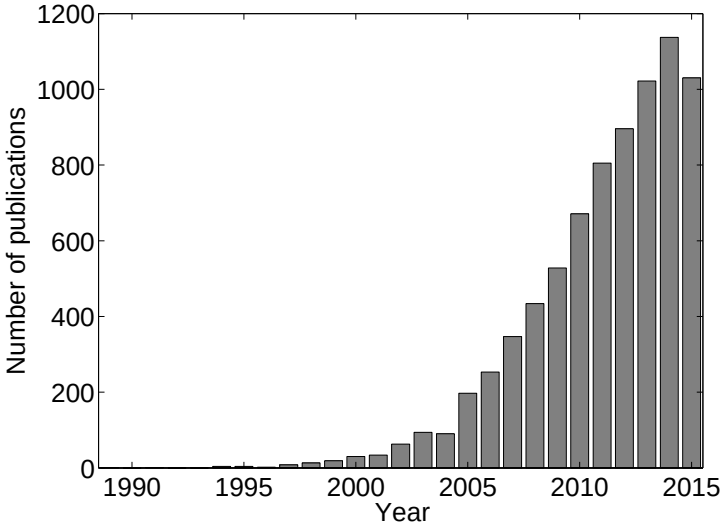

Figure 1.1: Number of hits evolution on *ISI Web of Knowledge* with the keyword 'nanoparticle enhancement' (accessed on December 2015)

the instability of unbound aggregates. These coatings are usually surfactants (Shen et al. 1999) or polymers (Ditsch et al. 2005a; Moeser et al. 2002) that provide colloidal stability to the particle and at the same time can be tailored for a specific application. The advantages of functionalized magnetic nanoparticles are manifold:

1. Ease of separation from the fermentation broth by magnetic filtration (Ditsch et al. 2005b);

2. Large interfacial area (mass transfer occurs in the time scale of micro to nanoseconds);

3. The particles are non-volatile, thus not lost in the reactor;

4. Better loading per fold enhancement of oxygen transfer ratio than pure hydrocarbons or perfluorocarbons;

5. Made from cheap raw materials and

6. Environmental friendly.

In 2006, the first study showing an enhancement in oxygen absorption to aqueous solutions of up to 6-fold was published by Olle et al. (2006). In the same year, the article by Krishnamurthy et al. (2006) showed a remarkable 26-fold enhancement in dye diffusion in water. These two publications boosted the study of mass transfer enhancement through nanoparticles use in order to fully understand this novel phenomenon (Fang et al. 2009; Kang et al. 2008; Kim et al. 2006, 2007; Komati and Suresh 2008, 2010; Lee et al. 2010; Ma et al. 2007, 2009; Zhu et al. 2008, 2009, 2010).

1.1.1 Effect of nanoparticles on transport mechanisms

In Krishnamurthy et al. (2006), the mean square displacement of the dye was measured and consequently, the dye mass diffusivity coefficient was determined by the mean displacement equation,

$$\left\langle (\Delta r)^2 \right\rangle = 2 D_{\mathrm{np}} t_{\mathrm{md}} \tag{1.1}$$

where D_{np} is the mass diffusivity inside nanoparticles and t_{md} is the time to travel the mean displacement. The mass transport rate showed an obvious relation with the nanofluid volume fraction. All experiments using nanoparticles enhanced mass transfer compared to pure water, with a peak at $\phi = 0.5\,\%\,(\mathrm{v/v})$. It was further demonstrated that Brownian motion exhibited by nanoparticles should not increase dye diffusion, since the travel time of a Brownian (nano)particle through its diameter, which is given by the Stokes-Einstein diffusivity equation in conjunction with Equation (1.1),

$$t_{\mathrm{B}} = \frac{3\pi\eta d^3}{2 k_{\mathrm{B}} T} \tag{1.2}$$

(ϕ is the nanoparticle volume fraction, t_{B} the time to travel a (Brownian) nanoparticle diameter, η the liquid viscosity, d the nanoparticle diameter, k_{B} the Boltzmann constant and T the temperature) is lower than the travel time of dye for the same distance,

$$t_{\mathrm{m}} = \frac{d^2}{2D} \tag{1.3}$$

where t_{m} is the time to diffuse dye through a nanoparticle diameter and D is the mass diffusivity of the solute in water, proving that nanoparticles are not physically pushing the dye. Rather, the effect of the induced motion in the fluid causes micro-convection currents, which travel faster than nanoparticles, might be the reason for the mass transport enhancement. Moreover, the peak at $\phi = 0.5\,\%\,(\mathrm{v/v})$ was explained as the more nanoparticles are present more convection currents are created but there is a time where the high amount of nanoparticles creates a smaller particle-to-particle distance, increasing the possibility of aggregation; this phenomenon will lead to bigger, heavier and more importantly, slower nanoparticles, lessening the previously presented Brownian motion, thus decreasing the mass transport.

Another investigation by Fang et al. (2009) came to confirm the previously discussed works, highlighting not only the mass transport enhancement by presence of nanoparticles but also showing a similar profile of mass transport enhancement against nanoparticle loading presented in Olle et al. (2006). Rhodamine B mass diffusion increased with higher volume fractions of nanofluid (enhancement of about 4 and 11 times for $\phi = 0.1$ and $0.5\,\%\,(\mathrm{v/v})$, respectively, compared to pure water, T=15 °C) vaguely indicating the presence of a plateau towards larger nanoparticle loadings. Higher temperatures lead to higher mass diffusion (diffusion coefficient increase of around 8- and 26-fold for $\phi = 0.1$ and $0.5\,\%\,(\mathrm{v/v})$, respectively, compared to pure water, T=25 °C), suggesting stronger

disturbances in the fluid created by Brownian motion thus increasing the Rhodamine B mass transfer.

1.1.2 The case of oxygen transport

Binary gas-liquid systems have always been given great emphasis in chemical and biochemical engineering, with gas absorption as one of the most important examples. Usually the major resistance is found in the liquid side due to solute diffusion and solubility issues. A typical problem is oxygen transport in fermentations since oxygen solubility in aqueous media is low ($\sim 8\,\mathrm{mg/L}$ at $20^{\mathrm{o}}\mathrm{C}$); with such low solubility, oxygen availability to cells may become compromised at certain periods. To answer this limitation, several strategies to improve the oxygen transfer rate (OTR) have been tried such as increased air pressure, pure oxygen supply, among others. One of the latest techniques being successfully used to enhance OTR is the addition of nanoparticles to the system. Recent studies have shown that different type of nanoparticles (alluminium- (Krishnamurthy et al. 2006), copper- (Fang et al. 2009) and functionalized iron-oxides (Olle et al. 2006), Cu-water-based (Li et al. 2006); silica (Turanov and Tolmachev 2009)) can effectively enhance mass transport; mass transport of different solutes was analyzed such as dye, Rhodamine B, and oxygen.

The investigation carried out in Olle et al. (2006) by physical and chemical methods, stated that the $k_{\mathrm{L}}a$ is enhanced up to 6-fold *via* convection in the fluid surrounding nanoparticles caused by random/Brownian motion.

The mass transfer coefficient showed a linear increase below a nanoparticle mass fraction of $\phi = 1\,\%$, converging to a plateau afterwards, presenting a similar behavior as the one in Krishnamurthy et al. (2006). As for the interfacial area contribution to mass transport enhancement, it was found that nanoparticles can increase interfacial area by two ways: by reducing the surface tension (above $\phi = 0.1\,\%\,(\mathrm{m/v})$ of nanoparticle

concentration the surface tension at the air-water interface was decreased from 72 mN/m to around 39 mN/m), which will enable an easier bubble break-up, and by preventing bubble coalescence (nanoparticles adsorb strongly at the gas-liquid interface) which accounts for an area enhancement of 50 %. It was also noted that the increase in interfacial area due to nanoparticles accounts for the largest fraction of the mass transfer enhancement.

The dispersion of nanoparticles ($\phi = 0.6$ % mass fraction) was afterwards applied to an *Escherichia coli* cultivation yielding an oxygen uptake rate enhancement of 40 %.

1.1.3 Mass transfer models

1.1.3.1 Aggregation models

Mass diffusion can be correlated with thermal conductivity. Prasher et al. (2006b) studied the effect of aggregation on thermal conductivity in nanofluid. As a major conclusion it was found that there is a nanoparticle size for which thermal conductivity can be enhanced the most. With increasingly smaller sized particles there is a higher probability of aggregation to occur, since, for a constant volume fraction, average interparticle distance is smaller. With the formation of aggregates, a larger mass of "new" particles is achieved, reducing Brownian motion, thus attenuating this contribution for thermal/mass conductivity/diffusion. Therefore there should exist an intermediate particle size large enough to prevent large aggregate formation but still small enough so that the aggregate mass does not become an issue.

Prasher et al. (2006b) compiled information on convective and conductive enhancement of thermal conductivity. The convective enhancement of thermal conductivity is given by,

$$\frac{k_{\mathrm{nf}}}{k_{\mathrm{f}}} = 1 + B \times \mathrm{Re}^{q}\mathrm{Pr}^{1/3}\phi \tag{1.4}$$

where k_{nf} is the nanofluid thermal conductivity, k_{f} the base liquid thermal conductivity, B and q are constants determined by experiments (Prasher et al. 2006a), Pr the Prandtl number ($\mathrm{Pr} = \frac{\nu}{\alpha} = \frac{c_{\mathrm{p}}\mu}{k}$ where ν the kinematic viscosity, c_{p} is the specific heat, μ the dynamic viscosity) and Re the Reynolds number ($\mathrm{Re} = \frac{\rho v d}{\mu}$ where ρ is the fluid density) which is calculated using the Brownian speed, v (for the case of an aggregate):

$$v = \sqrt{\frac{3k_{\mathrm{B}}T}{m}} \tag{1.5}$$

To account for the contribution of the conductive enhancement of k, Prasher et al. (2006b) used Bruggeman model, including the effect of percolation, since particles are in direct contact with each other,

$$\frac{k}{k_{\mathrm{f}}} = \frac{\left[k_{\mathrm{a}} + 2k_{\mathrm{f}}\right] + 2\phi_{\mathrm{a}}\left[k_{\mathrm{a}} - k_{\mathrm{f}}\right]}{\left[k_{\mathrm{a}} + 2k_{\mathrm{f}}\right] - \phi_{\mathrm{a}}\left[k_{\mathrm{a}} - k_{\mathrm{f}}\right]} \tag{1.6}$$

The equation to determine k_{a} is given by,

$$\left(1 - \phi_{\mathrm{int}}\right)\frac{k_{\mathrm{f}} - k_{\mathrm{a}}}{k_{\mathrm{f}} + 2k_{\mathrm{a}}} + \phi_{\mathrm{int}}\frac{k_{\mathrm{p}} - k_{\mathrm{a}}}{k_{\mathrm{f}} + 2k_{\mathrm{a}}} = 0 \tag{1.7}$$

where ϕ_{int} is the volume fraction of particles in the aggregate, which can be calculated by,

$$\phi_{\mathrm{int}} = \left(\frac{R_{\mathrm{a}}}{r_{\mathrm{p}}}\right)^{d_{\mathrm{f}}-3} = \left(1 + \frac{t}{t_{\mathrm{p}}}\right)^{\left(\frac{d_{\mathrm{f}}-3}{d_{\mathrm{f}}}\right)} \tag{1.8}$$

where R_{a} is the gyration radius of an aggregate, r_{p} the particle radius, d_{f} the fractal diameter of aggregates, t the time and t_{p} the aggregation time constant.

1.1.3.2 Pseudo-homogeneous and heterogeneous models

The approach used in Nagy (1995), Nagy and Moser (1995), and Nagy et al. (2007) was to develop models that can give some insight on how mass transfer can be enhanced through nanosized particles. Two models were constructed, a pseudo-homogeneous and a heterogeneous model. The first one should be used when the mass transport inside nanoparticles is considered instantaneous while the heterogeneous should be applied otherwise; the latter model should also be considered when the solubility of the component in the dispersed phase is much higher than in the liquid phase, which is the case when an organic phase is used to enhance oxygen mass transport.

The differential mass balance for the boundary layer at the gas-liquid interface (Nagy 1995) for the continuous (liquid) and dispersed phases is, respectively,

$$D\frac{\partial^2 C}{\partial x^2} - Q = \frac{\partial C}{\partial t} \tag{1.9a}$$

$$D_{\mathrm{d}}\frac{\partial^2 C_{\mathrm{d}}}{\partial x^2} - Q_{\mathrm{d}} = \frac{\partial C_{\mathrm{d}}}{\partial t} \tag{1.9b}$$

with the initial and boundary conditions:

$$\text{if } t = 0, x > 0 \text{ then } C = C_{\mathrm{d}} = 0, \tag{1.10a}$$

$$\text{if } t > 0, x = 0 \text{ then } C = C^*, \tag{1.10b}$$

$$\text{if } t > 0, x = \delta_1 \text{ and } x = \delta_2 \text{ then } C_{\mathrm{d}} = HC \text{ and } D\frac{\partial C}{\partial x} = D_{\mathrm{d}}\frac{\partial C_{\mathrm{d}}}{\partial x}, \tag{1.10c}$$

$$\text{if } t > 0, x = \delta \text{ (for } \delta_1 + d \leq \delta) \text{ then } C = C_{\mathrm{d}} = 0 \tag{1.10d}$$

or

$$\text{if } t > 0, x = \delta_1 + d \text{ then } C = C_{\mathrm{d}} = 0. \tag{1.10e}$$

where H is the partition coefficient of solute between dispersed and liquid phases, D and D_{d} are the solute mass diffusivities in liquid and dispersed phases, C, C_{d} and C^{*} are the solute concentrations in the liquid, dispersed phases and at gas-liquid interface, Q and Q_{d} are the reaction rates in the liquid and dispersed phases, $\delta_{1,2}$ are the distances between gas-liquid interface and each dispersed particle edge (one dimension), δ the gas-liquid boundary layer thickness.

The solute mass transfer rate (J) is derived by solving Equation (1.9) and applying the conditions in Equations (1.10a) to (1.10e),

$$J = \sqrt{D_{\mathrm{n}} s}\sqrt{1 + \frac{\phi H}{1-\phi}} \tag{1.11}$$

where D_{n} is the enhanced diffusion coefficient in the nanofluid, s the surface renewal frequency.

It is possible to calculate the enhanced diffusion coefficient by combining the Frössling equation,

$$\mathrm{Sh} = 2 + 0.6\mathrm{Re}^{0.5}\mathrm{Sc}^{0.3} \tag{1.12}$$

(Sh is the Sherwood number ($\mathrm{Sh} = \frac{k_{\mathrm{L}}L}{D}$), Sc the Schmidt number ($\mathrm{Sc} = \frac{\nu}{D} = \frac{\mu}{\rho D}$)) and the modified thermal conductivity equation – Equation (1.4) (Prasher et al. 2006a,b) – which results in,

$$D_{\mathrm{n}} = D\left(1 + B\mathrm{Re}^{q}\mathrm{Sc}^{1/3}\phi\right) \tag{1.13}$$

Thus, Equation (1.11) turns into,

$$J = \sqrt{D\left(1 + B\mathrm{Re}^{q}\mathrm{Sc}^{1/3}\phi\right)}\, s\sqrt{1 + \frac{\phi H}{1-\phi}} \tag{1.14}$$

1.1.4 Mass transfer parameters' determination in a gas-liquid system

A crucial review (Linek and Vacek 1981) in the field of gas-liquid mass transfer in which a comprehensive study was developed around the use of catalyzed sulfite oxidation kinetics for the determination of mass transfer characteristics in gas-liquid systems, providing both theoretical and practical knowledge around this redox reaction, which has been largely applied in the characterisation of mass transfer systems (Beenackers and Swaaij 1993; Cents 2003; Cooper et al. 1944; Fujasová et al. 2007; Kordač and Linek 2006; Kordač et al. 2011; Lewis and Roberts 2005; Linek et al. 2005a, 2006, 2008; Nagy and Hadik 2003; Nagy et al. 2007; Olle et al. 2006; Painmanakul et al. 2009; Sardeing et al. 2006; Suresh et al. 2009; Swiniarski 1992). The influence of several parameters such as pH, temperature, sulfite, oxygen and catalyst concentrations in homogeneous and heterogeneous conditions were evaluated and a methodology for application of the sulfite oxidation system to determine a and $k_{\mathrm{L}}a$ either individually or simultaneously (the latter will not be addressed due to the need of highly variable correction factors – $k_{\mathrm{L}}a$ corrections range from -4 – 90 % (Linek and Vacek 1981)) which is presented in the following subsections.

According to Danckwerts (1970), it is possible to determine the absorption of oxygen into a sulfite solution caused by a pseudo-n$^{\mathrm{th}}$-order reaction with the sulfite ions:

$$\mathrm{OUR} = a\left(C^{*}_{\mathrm{O}_2} - C_{\mathrm{O}_2,\mathrm{bulk}}\right)\sqrt{\frac{2}{n+1}k_n {C^{*}_{\mathrm{O}_2}}^{n-1} D_{\mathrm{O}_2,\mathrm{L}} + k_{\mathrm{L}}^2} \tag{1.15}$$

in which a is the specific area, n is the reaction order, k_n is the reaction rate constant, $D_{O_2,L}$ is the oxygen diffusion coefficient in the liquid phase, k_L is the mass transfer coefficient, $C^*_{O_2}$ and $C_{O_2,bulk}$ are the oxygen concentrations at saturation and in well-mixed bulk in equilibrium with oxygen partial pressures in gas ($p_{O_2,G}$) and liquid ($p_{O_2,L}$) phases, respectively:

$$C^*_{O_2} - C_{O_2,bulk} = H\left(p_{O_2,G} - p_{O_2,L}\right) \tag{1.16}$$

H is the Henry's law constant which enables one to calculate pure oxygen solubility in a sulfite solution (Linek and Vacek 1981):

$$H = 5.909 \times 10^{-6} \exp\left(\frac{1602.1}{T} - \frac{0.9407 C_{SO_3}}{1+0.1933 C_{SO_3}}\right) \tag{1.17}$$

in which H is the Henry's law constant and C_{SO_3} is the sulfite concentration inside the reactor.

1.1.4.1 Determination of volumetric mass transfer coefficient, $k_L a$

The rationale to determine the volumetric mass transfer coefficient is to, firstly, garantee 3 conditions:

$$C_{O_2,bulk} = 0 \tag{1.18a}$$

$$\mathrm{Ha} < 0.3 \tag{1.18b}$$

$$\mathrm{Ha} \ll \frac{C_{SO_3}}{z C^*_{O_2}} \tag{1.18c}$$

where z is the reaction stoichiometry coefficient (sulfite per oxygen moles reacted) and Ha is the Hatta number which is used to compare oxygen consumption and mass transfer rates

$$\mathrm{Ha} = \frac{\sqrt{\frac{2}{n+1} k_n {C^*_{\mathrm{O}_2}}^{n-1} D_{\mathrm{O}_2,\mathrm{L}}}}{k_\mathrm{L}} \tag{1.19}$$

To fulfill the 3 conditions stated in Equation (1.18a)–1.18c, the concentration of Co^{2+} (catalyst) should be under 1×10^{-5} M since below this concentration the reaction is not chemically enhanced (Olle et al. 2006). By accepting the previous constraints, it is possible to infer that the reaction rate is much slower than mass transfer rate but still fast enough to consume all the oxygen in the bulk solution. Thus, the Equation (1.15) can be rewritten as

$$\mathrm{OUR} = k_\mathrm{L}a \cdot C^*_{\mathrm{O}_2} = k_\mathrm{L}a \cdot H \cdot p_{\mathrm{O}_2,\mathrm{G}} \tag{1.20}$$

1.1.4.2 Determination of interfacial area, a

To determine the interfacial area it is needed to work the opposite way of the previous section, i.e.,

$$C_{\mathrm{O}_2,\mathrm{bulk}} = 0 \tag{1.21a}$$

$$\mathrm{Ha} \geq 3 \tag{1.21b}$$

$$k_\mathrm{L}a C^*_{\mathrm{O}_2} \ll k_n {C^*_{\mathrm{O}_2}}^n \tag{1.21c}$$

enhance the sulfite oxidation reaction by using a catalyst concentration above

1×10^{-5} M (Olle et al. 2006) reducing Equation (1.15) to

$$\mathrm{OUR} = aC^*_{\mathrm{O}_2}\sqrt{\frac{2}{n+1}k_n {C^*_{\mathrm{O}_2}}^{n-1} D_{\mathrm{O}_2,\mathrm{L}}} \tag{1.22}$$

Experiments to determine the gas-liquid interfacial area will be conducted with the experimental system as of the $k_\mathrm{L}a$ determination. The catalyst used will be Co_2^+ instead of Cu_2^+ because the former permits operation in a regime where absorption is kinetically enhanced.

1.2 Research Strategy

The principal objective of the study reported in this dissertation was to produce nanoparticles that enhance oxygen mass transfer in bioprocesses and to develop models to maximize oxygen transfer and to assist the scale up of such processes. To accomplish this goal, the thesis is divided in three main parts: synthesis of nanoparticles, mass transfer parameters' assessment in reactor experiments and modelling of mass transfer coefficients and interfacial area.

In the first part, the goal was to design/synthesize magnetic nanoparticles that behave at least as well as those found in the literature, in terms of mass transfer capabilities. Even though the general protocol to synthesize Hitenol-BC/oleic acid-coated iron oxide nanoparticles is well described in Olle et al. (2006), inconsistencies were detected when comparing to synthesis protocol of a bare iron oxide nanoparticle (Abareshi et al. 2010; Chen et al. 2012; Ingram et al. 2010; Khan 2008; Narita et al. 2009; Shen et al. 2009; Wang et al. 2012; Wang et al. 2011; Yang et al. 2010). After a deep analysis of the literature, it was possible to modify the protocol of Olle et al. (2006) in order to improve the production of these particles. Furthermore, a systematic approach to determine the reagents quantities was developed to serve as a model for

future works in the synthesis of iron oxide nanoparticles. Also, the final purification step was improved, which revealed to be more reproducible and less prone to error when compared to dialysis (Olle et al. 2006). This modification is crucial since the organic reagents are used in excess during the synthesis (and without the fine-tuned purification step) will contaminate the mass transfer tests, hindering the real impact of the nanoparticles in the mass transfer process.

In the second part, mass transfer tests were carried out in a custom design reactor in two ways: in absence of nanoparticles and in the presence of Hitenol-BC/oleic acid coated nanoparticles. The mass transfer tests were carried out in the specified conditions of Section 1.1.4. The first set of experiments was used to ensure the validity of the sulfite oxidation method. For the second set of experiments, statistical analysis was applied to a central composite design and an additional PLS analysis was also employed to assess the impact of each operational parameter on each mass transfer parameters.

Finally, empirical correlations models were developed based on the experimental designs used in order to provide knowledge to mass transfer mechanisms in the presence of nanoparticles. The $k_{\mathrm{L}}a$ correlations developed in this thesis were inspired in published empirical correlations of gas-liquid dispersion without magnetic nanoparticle, using the most common operational parameters as function of gassed power input (P_{G}), superficial gas velocity (V_{S}) and in our case also the nanoparticles. The interfacial area models were derived using correlations that are based on Weber (We) and the Eötvös number (Eo).

1.3 Thesis Outline

This Thesis is divided into six chapters, following the work performed during this PhD project, which resulted in 2 articles, presented in Chapters 2 to 5, respectively. Chapter 1 introduces this Thesis, by presenting the context and motivation for this PhD project,

and the research strategy followed. The article related to Chapter 2 was submitted for publication during the time of writing this Thesis, while the article that comprises Chapters 3 to 5 is in preparation for submission.

Chapter 2 presents both a new protocol for magnetic nanoparticles synthesis with Hitenol-BC and oleic acid coating and a new purification step. A model to determine the reagents quantities to use in the nanoparticle synthesis was developed. The results obtained through the new protocol and model showed that the synthesized magnetic nanoparticle increase the oxygen transport in an aerated and stirred tank and that similar mass transfer enhancements can be achieved with lower nanoparticles loadings.

In both Chapters 3 and 4, the magnetic nanoparticles synthesized in Chapter 2 were used in mass transfer tests to determine the volumetric mass transfer coefficient, $k_{\mathrm{L}}a$, interfacial area, a and the liquid side mass transfer coefficient, k_L. The experiments were carried out based on a central composite design which was analyzed using the statistical software MODDE. An additional sensitivity analysis was carried out to weight the impact of the operational variables (Q, ϕ and N) on the mass transfer parameters ($k_{\mathrm{L}}a$ and a).

In Chapter 5, correlations are proposed to predict the behaviour of $k_{\mathrm{L}}a$ and a (through Sauter mean diameter, d_{32}) in the presence of magnetic nanoparticles. For $k_{\mathrm{L}}a$, a similar correlation to the literature was found , while for d_{32}, two correlations are proposed since the ones in the literature either do not take into account the presence of nanoparticles or fall short in term of variables used. The results showed that the volumetric mass transfer can be generally well predicted while the Sauter mean diameter presents a rather low correlation with the nanoparticle loading.

Chapter 6 summarises the main results of this Ph.D. project and presents some possible challenges and suggestions for future research.

CHAPTER 2

Synthesis and characterization of functionalized magnetic nanoparticles

2.1 Introduction

Mass transfer resistances can often supersede kinetic resistances in multiphasic biological systems. A prominent example is the transport of oxygen from air bubbles into the cultivation medium. The major resistance in the O_2 transfer from air bubbles into the liquid is found in the liquid side boundary layer (Bailey and Ollis 1986). Classical strategies to improve the oxygen transfer rate (OTR) include the increase of air pressure or the use of pure oxygen (Charoenrat et al. 2006). However, in many high cell density cultivations these two strategies are not sufficient to avoid dissolved oxygen limitation (Ferreira et al. 2012).

Other nonconventional strategies exist to increase mass transfer in biological systems, including the use of organic phases and particle suspensions. Dispersion into an organic

phase in which oxygen has a higher solubility than in water is another approach to increase oxygen transfer (oil in water systems), since larger amounts of oxygen are removed from the aeration gas stream. There have been several reports on organic phases increasing mass transfer such as oleic acid (Linek and Benes 1976; Yoshida et al. 1970), toluene (Yoshida et al. 1970), n-hexadecane (Hassan and Robinson 1977; Ho et al. 1990; Ju and Ho 1989; Zhao et al. 1999), and perfluorochemicals (Lowe 2002; Mattiasson and Adlercreutz 1983, 1987; McMillan and Wang 1987, 1990). For the case of oleic acid, Yoshida et al. (1970) reported a $\sim 40\,\%$ $k_{\mathrm{L}}a$ enhancement while in Linek and Benes (1976) they reported that the addition of oleic acid resulted in an initial decrease in k_{L} but when the oleic acid fraction increased, so did the k_{L}.

In the last two decades, multiple studies investigated the role of fine particles ($< 1\,\mathrm{mm}$) in transport phenomena. The use of these particles has shown the ability to enhance mass transport in several binary systems (Dagaonkar et al. 2003; Demmink et al. 1998; Holstvoogd et al. 1988; Linek et al. 2008; Littlejohns and Daugulis 2007; Nagy 2003; Ruthiya et al. 2003b).

More recently the use of even smaller nanosized particles for enhancement of fluid properties, namely thermal conductivity and mass diffusivity, has been gathering greater interest in the scientific community. In the investigation performed by Choi and Eastman 1995 the term nanofluid appeared for the first time, describing a new class of engineering heat transfer fluids, which contain about 10-nanometer-sized metallic particles. In recent years, mass transfer in nanoparticle suspensions has been studied by several authors. A summary of results reported in different studies is presented in Table 2.1. The diffusivity of a solute in water suspensions has been studied by Krishnamurthy et al. 2006 who reported a 26-fold enhancement in fluorescein dye diffusivity in 20 nm sized Al_2O_3 nanoparticle/water suspensions. Fang et al. 2009 reported comparable results for Rhodamine B diffusivity in 25 nm Cu/water suspensions.

Olle et al. 2006 showed for the first time a mass transfer enhancement in stirred

Table 2.1: Sum-up of mass transfer systems using nanoparticles.

Nanoparticles	Coating	Size (nm)	Fraction (%)	Liquid phase	Solute	Enhancement	Parameter	System	Reference
Cu	—	25	0.1–0.5 (v)	H_2O	Rhodamine B	4–26	D	Quiescent liquid	Fang et al. 2009
Cu	—	50	0–0.1 (w)	H_2O	NH_3 vapor	2.3–3.2	m	Bubble absorber	Kim et al. 2006, Kim et al. 2007
CuO	—	47	0–0.1 (w)	H_2O	NH_3 vapor	2.1–3.0	m	Bubble absorber	Kim et al. 2006, Kim et al. 2007
Al_2O_3	—	33	0–0.1 (w)	H_2O	NH_3 vapor	2.1–3.0	m	Bubble absorber	Kim et al. 2006, Kim et al. 2007
Al_2O_3	—	35	0–0.06 (v)	H_2O	NH_3 vapor	1.10–1.18	m	Bubble absorber	Lee et al. 2010
Al_2O_3	—	20	0.1-1 (v)	H_2O	Dye	26	D	Quiescent liquid	Krishnamurthy et al. 2006
CNT	—	25	0.01 and 0.1 (w)	H_2O	NH_3 vapor	2.15–2.50	m	Refrigeration	Kang et al. 2008
CNT	—	25	0-0.08 (v)	H_2O	NH_3 vapor	1.10–1.18	m	Bubble absorber	Lee et al. 2010
CNT	—	20	0.05–0.5 (w)	H_2O	NH_3 vapor	1.0–1.2	m	Bubble absorber	Ma et al. 2009
MCM41	methyl groups	n.a.	0.6 (w)	H_2O	CO	1.38–2.01	H_2 yield	STR	Zhu et al. 2010
MCM41	methyl groups	250	0.4 (w)	H_2O	CO	1.05–1.94	k_La	STR	Zhu et al. 2008, Zhu et al. 2009
Fe_3O_4	Oleic acid	20	0.5–4 (v)	H_2O	O_2	3.0–6.0	k_La	STR	Olle et al. 2006
Fe_3O_4	PPO-PEO	80	0.5–4 (v)	H_2O	O_2	1.3–2.6	k_La	STR	Olle et al. 2006
Fe_3O_4	PEO	21.1	0.05-1.0 (v)	H_2O	O_2	1.55–2.70	$N.a$	WWC	Komati and Suresh 2010
Fe_3O_4	PEO	13.2	0.023–0.1 (v)	MDEA	CO_2	1.35-1.85	$N.a$	WWC	Komati and Suresh 2010
Fe_3O_4	Lauric acid	10.0	0.05–0.25 (v)	MDEA	CO_2	1.40-1.85	$N.a$	WWC	Komati and Suresh 2010
Fe_3O_4	TMAOH	21.1	0.023–0.4 (v)	MDEA	CO_2	1.20-1.85	$N.a$	WWC	Komati and Suresh 2010
Fe_3O_4	—	15	0–0.39 (v)	MDEA	CO_2	1.928	k_La	WWC	Komati and Suresh 2008
Fe	—	100	0.01 and 0.1 (w)	H_2O	LiBr	1.7–1.9	m	Refrigeration	Kang et al. 2008
Fe	—	100	0.01 and 0.1 (w)	H_2O	NH_3 vapor	1.7–1.9	m	Bubble absorber	Ma et al. 2007

gas-liquid systems. They reported an enhancement of oxygen absorption to aqueous solutions of up to 6-fold using 20 nm sized nanoparticles with oleic acid coating. Several other studies followed addressing different solvents (H_2O, LiBr ionic liquid, MDEA), solutes (O_2, NH_3 vapor, CO and CO_2) and nanoparticles (Cu, CuO, Al_2O_3, CNT, MCM41, Fe_3O_4 and Fe) with or without coating. The results by Kim et al. 2006, 2007 showed that different nanoparticles (Cu, CuO and Al_2O_3) in the range of 33-50 nm without any type of coating enabled up to 3.2 fold enhancement in the mass transfer rate of NH_3 into water. However, the oxygen transfer studies by Olle et al. 2006 showed that the functionalization with an organic coating was essential to increase substantially the mass transfer rate. The inclusion of an oleic acid coating resulted in a 6-fold increase of the oxygen transfer rate into water.

From the studies previously performed, it becomes apparent that the size of the nanoparticles, the material of the nanoparticles and the existence of the coating and its composition may have a large impact in the mass transfer enhancement. It is therefore essential to be able to synthesize high quality particles. In this chapter, we study how the synthesis protocol affects critical nanoparticle properties such as, size, particle composition and zeta potential, which are critical for the purpose of oxygen transfer enhancement. We show that the synthesis of high quality particles can enhance substantially the oxygen mass transfer air-water systems using Fe_3O_4 nanoparticles with oleic acid coating.

2.2 Materials and methods

2.2.1 Materials

The chemical compounds used in this study were the following: Na_2SO_3 – sodium sulfite anhydrous (Panreac, 98.0 %), $Na_2S_2O_3 \cdot 5\,H_2O$ – sodium thiosulfate 5-hydrate (Panreac,

99.5 %), KI – potassium iodide (Fischer Scientific), I_2 – iodine (Fischer Scientific), $FeCl_2 \cdot 4\,H_2O$ – iron (II) chloride tetrahydrate (Sigma-Aldrich, 99.0 %), $FeCl_3 \cdot 6\,H_2O$ – iron (III) chloride hexahydrate (Sigma-Aldrich, 97 %), NH_4OH – ammonia solution (Scharlau, 25 %), HCl – hydrochloric acid (Fischer Scientific, 37 %), KIO_3 – potassium iodate (BDH Chemicals Ltd., 99.9 %), $CoSO_4 \cdot 7\,H_2O$ – cobalt (II) sulfate heptahydrate (Merck, 99 %), Hitenol BC-10 (Daiichi Kogyo Seiyaku), Potassium oleate (Aldrich, 40 wt. % paste in H_2O), Oleic acid (Aldrich, 65.0-88.0 %).

2.2.2 Nanoparticle synthesis

94 g of $FeCl_3 \cdot 6\,H_2O$ were added to 100 g of water and stirred under nitrogen sparging for 20 min in a round-bottom flask; afterwards 34.4 g $FeCl_2 \cdot 4\,H_2O$ were added maintaining sparging and stirring for 5 min. At this stage, the temperature was raised to 80 °C and continued sparging for 50 min. Next, 100 g of potassium oleate was added, and the mixture was stirred for an additional 40 min. 200 mL of NH_4OH was added to the mixture, at a slow rate (7 mL min^{-1}), after which the solution immediately turned black because of the formation of magnetite. The reaction continued at 80 °C under stirring and nitrogen sparging for 20 min, after which it was assumed that oleic acid had completely coated the magnetite aggregates. 100 g of Hitenol BC were added at this point and 25 min later 5 g of ammonium persulfate were added to the reaction mixture. The reaction continued at 80 °C for 40 min, under nitrogen sparging and vigorous stirring. The solution was cooled to room temperature and was left in the oven at 80 °C overnight, after which most of the residual ammonium hydroxide evaporated, after which a gray foam was formed on top of the solution. The foam was removed and only the aqueous solution was used for the rest of the work.

2.2.3 Nanoparticle purification

100 mL of dispersion were diluted to 500 mL total volume. Then, the solution was filtered in a cross-flow filtration modulus (Carbosep, 56 cm long, 15 kDa pore-size) at a Δp=1.5 bar. The solution was filtered until the volume was down to 100 mL. At this point 400 mL of water were added to the solution. This procedure was repeated until about 5.5 L of permeate were obtained. At this point the retentate was considered to be free of most oleate and unreacted compounds from the synthesis. The solid contents were measured by keeping a 1.5 mL sample in the oven overnight at 80 °C, in triplicate. In the end of this step a suspension was obtained with solids' concentration in the range of 2.66-6.25 g L^{-1}.

2.2.4 Dynamic Light Scattering and ζ-potential

Dynamic light scattering measurements were performed in a Zetasizer Nano Series ZEN3600 (Malvern, UK) operating with a 633 nm laser. The detection uses a non-invasive back scattering technique (173°). Temperature in the cells was kept constant at $T = 298.2 \pm 0.1$ K and a minimum of two measurements were made. The reported values are the extrapolated values to zero concentration. For ζ-potential determination we used the Smoluchowski approximation of the Henry equation relating electrophoretic mobility, u, with ζ-potential, ζ,$u = \frac{\varepsilon\varepsilon_0\zeta}{\eta}$ where ε is the dielectric permittivity of the solution, ε_0 is the vacuum dielectric permittivity, and η is the solution viscosity. This apparatus avoids electro-osmosis through the application of a slow field reversal and a fast field reversal (phase analysis) hence making it possible to determine very low mobility of the scattering particles.

2.2.5 Transmission Electron Microscopy

TEM was utilized for the characterization of particle morphology and estimation of the size of the magnetic core. The dried nanoparticle samples were prepared by evaporating dilute suspensions on a carbon-coated film and TEM performed in an Analytical TEM Hitachi 8100 with Rontec standard EDS detector and digital image acquisition. The diameter of the nanoparticles was determined through the image analysis of a TEM scan using the line intersection method (10 lines used) through the MATLAB package Line Cut 2.0 (06/02/2012).

2.2.6 Inductively Coupled Plasma-Atomic Emission Spectrometer (ICP-AES)

The ICP-AES analysis was carried out in a Horiba Jobin-Yvon, Ultima equipment with a 40.68 MHz RF generator, 1 m sequential Czerny-Turner monocromator. Both iron and sulfur concentrations were determined with 1.5 mL sample of nanoparticles.

2.2.7 Elemental analysis

The elemental analysis to determine the carbon, nitrogen, hydrogen and sulfur content in nanoparticles used a 2-3 mg of homogeneous nanoparticles sample in an Elemental Analyzer Thermo Finnigan CE Instruments, model Flash EA1112 CHNS series.

2.2.8 Surface tension

The surface tension was determined in a KSV CAM 100 Optical Contact Angle and Pendant Drop Surface Tension Equipment using the software V4.00 W2XP. The CAM100 fits the Young-Laplace equation to the drop image for calculation of surface tensions. The measurements were carried out at room temperature in triplicate.

2.2.9 Mass transfer tests

The mass transfer tests used the sulfite oxidation method to determine oxygen transfer from gas to liquid phases. The method consists in bubbling air into a reactor filled with a 0.8 M sodium sulfite solution at 500 rpm stirring speed and 400 mL/min air sparging rate. The reactor and impeller dimensions follow the standard ratios of $D/T = 1/3, B/T = 1/10, l_B/D = 1/4, h_B/D = 1/5, C/D = 1$, with $T = 81$ mm.

The sulfite is monitored by iodometric back-titration (as used by Fujasová et al. 2007; Kies et al. 2004; Kordač et al. 2011; Lewis and Roberts 2005; Linek and Vacek 1981; Linek et al. 2005a, 2006, 2008; Nagy and Hadik 2003; Nagy et al. 2007; Olle 2006; Olle et al. 2006), from which is possible to derive the oxygen mass transfer rate by the slope of sulfite concentration profile:

$$OTR = -\frac{\Delta C_{SO_3}}{\Delta t}\frac{1}{z} \tag{2.1}$$

in which z is the sulfite-to-oxygen stoichiometry ratio in the sulfite oxidation reaction:

$$SO_3 + \tfrac{1}{2}\,O_2 \longrightarrow SO_4 \tag{2.2}$$

It is only possible to assume that all oxygen transferred to the liquid phase is consumed if the reaction is catalyzed. The catalyst used for this study is $CoSO_4 \cdot 7\,H_2O$ which is a well-known catalyst for the sulfite oxidation (Kordač et al. 2011; Lewis and Roberts 2005; Linek and Vacek 1981; Linek et al. 2006, 2008).

2.3 Results

2.3.1 Synthesis of functionalized magnetic nanoparticles

The synthesized magnetic nanoparticles are composed of 3 layers (Figures 2.1 and 2.2). The inner layer is the magnetite core composed of Fe_3O_4. The oleic acid molecules attach directly to the surface of the magnetic core by a covalent bond (Guardia et al. 2007), forming a second layer. Hitenol-BC molecules link covalently with the oleic acid forming the third (outer) layer. While the inner radius, R_1, can to some extent be controlled during synthesis, the thickness of the second and third layers are essentially set by the chemistry of the coating process. A theoretical model can be useful to design the synthesis of a given target amount of nanoparticle (M_1) with a given size, as shown below.

2.3.1.1 Fe^{3+}:Fe^{2+} ratio

The synthesis of the innermost magnetite core follows the following co-precipitation reaction with well-known stoichiometry:

$$Fe^{2+} + 2\,Fe^{3+} + 8\,OH^- \longrightarrow Fe_3O_4 + 4\,H_2O \tag{2.3}$$

The theoretical Fe^{3+}:Fe^{2+} ratio is thus 2:1. Indeed, the Fe^{3+}:Fe^{2+} molecular ratio is 2:1 for the majority of published studies (Abareshi et al. 2010; Chen et al. 2012; Ingram et al. 2010; Khan 2008; Narita et al. 2009; Olle et al. 2006; Shen et al. 2009; Wang et al. 2012; Wang et al. 2011; Yang et al. 2010) and also in the present study. From the studies presented in Table 2.2 there is only one study that uses a lower ratio, namely Wang et al. 2011 who used 1.50:1.

For a given target amount of nanoparticles (M_1 in grams), one can calculate the required amounts of $FeCl_2 \cdot 4\,H_2O$ and $FeCl_3 \cdot 6\,H_2O$ according to the following material

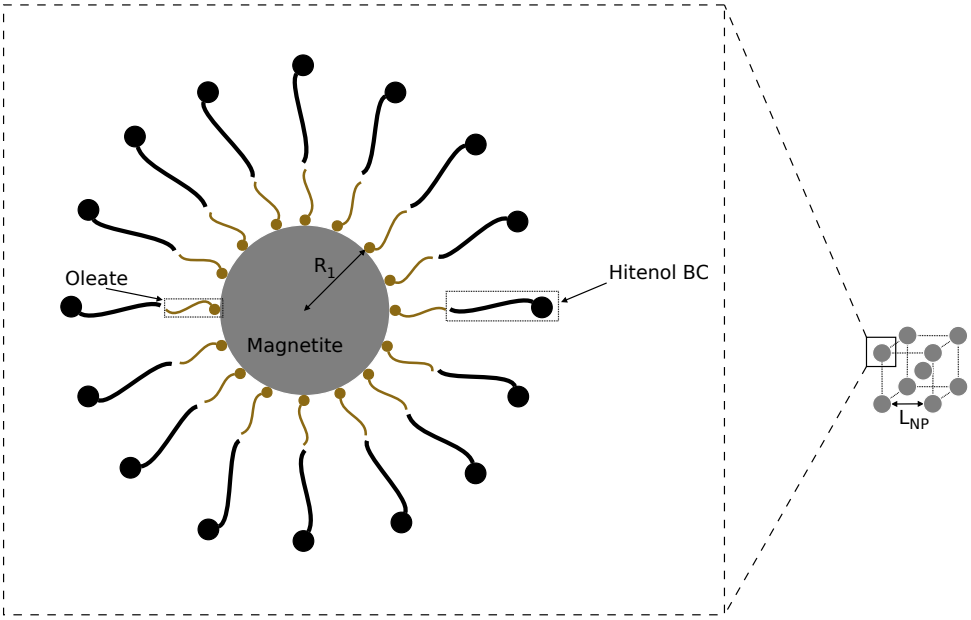

Figure 2.1: Schematics of magnetite nanoparticles coated with oleate and Hitenol BC. It is assumed a distance between nanoparticles of at least $L_{\mathrm{NP}} = 4d_{\mathrm{NP}}$, for an assumed distribution of particles in a cubic matrix (1 nanoparticle in each vertex and 1 nanoparticle at the center of the cube). The nanoparticle core radius is R_1.

balance equations:

$$m_{\mathrm{FeCl_2 \cdot 4\,H_2O}} = \frac{4\pi R_1^3}{3} \frac{N_{Fe}}{3A^3 N_A} \frac{MM_{\mathrm{FeCl_2 \cdot 4\,H_2O}}}{\mathrm{Purity}_{\mathrm{FeCl_2 \cdot 4\,H_2O}}} \frac{M_1}{m_{\mathrm{NP}}} \tag{2.4}$$

$$m_{\mathrm{FeCl_3 \cdot 6\,H_2O}} = \frac{4\pi R_1^3}{3} \frac{N_{Fe}}{3A^3 N_A} \frac{MM_{\mathrm{FeCl_3 \cdot 6\,H_2O}}}{\mathrm{Purity}_{\mathrm{FeCl_3 \cdot 6\,H_2O}}} \frac{M_1}{m_{\mathrm{NP}}} \tag{2.5}$$

with m_{NP} (g) the mass of a single nanoparticle (see Equation (2.10)), N_{Fe} the number of iron atoms in a unit cell of magnetite. The unit cell of magnetite is based on 32 $O^{2\breve{}}$ ions and has a face centered cubic symmetry with lattice constant $A = 8.3958$Å (Wechsler et al. 1984). Thus, it is possible to determine the total number of Fe ions in

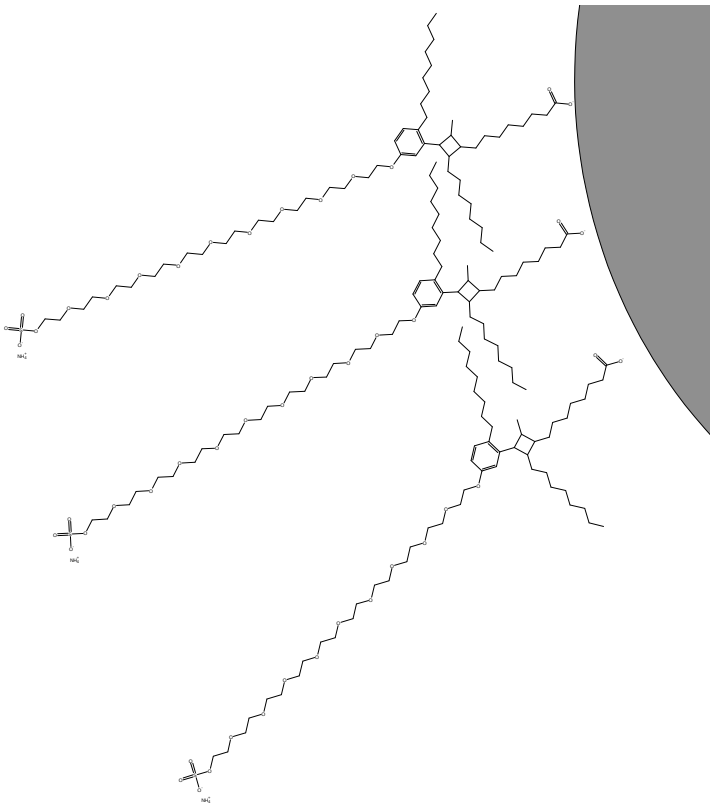

Figure 2.2: The schematics of the core and shell of magnetite nanoparticles with oleate+Hitenol BC coating.

the unit cell, which is $N_{Fe} = 24$.

2.3.1.2 OH^-:Fe^{2+} ratio

According to Equation (2.3) the theoretical OH^-:Fe^{2+} ratio is 8:1. There is however in the literature a wide range of OH^- concentrations used, leading to possible different nanoparticles morphologies. Nevertheless, the majority of the studies present either an excess in ammonia or a near 8:1 OH^-:Fe^{2+} ratio, in order to use all the iron present in the reaction. The total amount of NH_4OH (in mL) required to synthesize M_1 g of

Table 2.2: Fe^{3+}-, OH^-- and oleate-to-Fe^{2+} ratios in magnetite nanoparticles synthesis for recent studies

Fe^{3+}:Fe^{2+} ratio	OH^-:Fe^{2+} ratio	Oleate:Fe^{2+} ratio	Nanoparticles diameter (nm)	Reference
1.77:1	7.94:1	0.31:1	11.0	Wang et al. 2012
1.83:1	7.84:1	1.01:1	9.0	Chen et al. 2012
1.50:1	7.13:1	0.24:1	10.0	Wang et al. 2011
1.98:1	6.60:1	0.44:1	20.0	Yang et al. 2010
2.00:1	178.00:1	–	8.4	Abareshi et al. 2010
2.00:1	300.00:1	0.25:1	15.0	Ingram et al. 2010
2.00:1	3.00:1	–	12.0	Shen et al. 2009
2.02:1	63.83:1	1.57:1	7.8	Narita et al. 2009
2.01:1	4.92:1	1.17:1	10.0-15.0	Khan 2008
1.97:1	4.66:1	1.82:1	20.0	Olle et al. 2006

nanoparticles is given by the following:

$$V_{\mathrm{NH_4OH}} = \frac{4\pi R_1^3}{3}\frac{N_{Fe}}{3A^3N_A}\frac{8}{K_b}\left(\frac{4\pi R_1^3}{3}\frac{N_{Fe}}{3A^3N_A}+K_b\right)\frac{MM_{\mathrm{NH_4OH}}}{C_{\mathrm{NH_4OH}}}\frac{M_1}{m_{\mathrm{NP}}} \tag{2.6}$$

with K_b the base dissociation constant, $C_{\mathrm{NH_4OH}}$ the ammonium concentration (wt. %). In our work we used 200 mL of NH_4OH which can be converted to 1.28 mol of OH^- (by reacting with the iron mixture), which represents an OH^-:Fe^{2+} ratio of 8.25:1, slightly above the stoichiometric threshold, for the synthesis of nanoparticles.

2.3.1.3 Magnetite core coating

It is possible to calculate the theoretical amount of oleate required to cover the magnetic core surface at a given molecular density distribution. Assuming that an oleate molecule has a projection diameter of 1.38 nm (calculated from oleate projection using the software ChemBioDraw) and that the spacing between 2 adjacent molecules is Z, then

the theoretical oleate:Fe2+ ratio is given by:

$$\text{Oleate} : \text{Fe}^{2+} = \frac{R_1 N_{Fe} l^2}{9a^2} : 1 \tag{2.7}$$

The amounts of oleate and Hitenol-BC incorporated in the nanoparticles can be calculated by the following material balance equations:

$$m_{\text{Potassium oleate}} = \frac{4\pi R_1^2}{l^2 N_A} \frac{MM_{\text{Potassium Oleate}}}{\text{Purity}_{\text{Potassium Oleate}}} \frac{M_1}{m_{\text{NP}}} \tag{2.8}$$

$$m_{\text{Hitenol BC}} = \frac{4\pi R_1^2}{l^2 N_A} \frac{MM_{\text{Hitenol BC}}}{\text{Purity}_{\text{Hitenol BC}}} \frac{M_1}{m_{\text{NP}}} \tag{2.9}$$

with l (m) the length of each side of the unit cell drawn from the projection of oleate molecules on the surface of the nanoparticle as shown in Figure 2.3.

From the analysis of the nanoparticles sizes reported in the literature (Table 2.2), one can see that for R_1=3.85 nm and Z=0 (the smallest particles) the theoretical oleate:Fe^{2+} ratio is 0.058:1, while for R_1=10 nm (larger particles) the ratio decreases to 0.022:1. Literature values vary from 0.24:1 to 1.82:1 (Table 2.2) which reveals a large excess of oleate that could never be incorporated in the nanoparticles. Indeed, the presence of large excess of oleate prior to ammonia addition has two objectives: i) to coat the magnetic core immediately after formation thus avoiding a subsequent chemical synthesis step such as for instance the one suggested in (Ingram et al. 2010), and ii) to restrict the size of the magnetic core since the large oleate excess inhibits nuclei growth due to the premature formation of the coating.

In our work, we have R_1=4.4 nm sized nanoparticles (Figure 2.4b) thus the theoretical ratio is 0.050:1. We used 100 g of oleate which translates into 0.312 mol of oleate representing a 1.80:1 ratio value, well above the theoretical value.

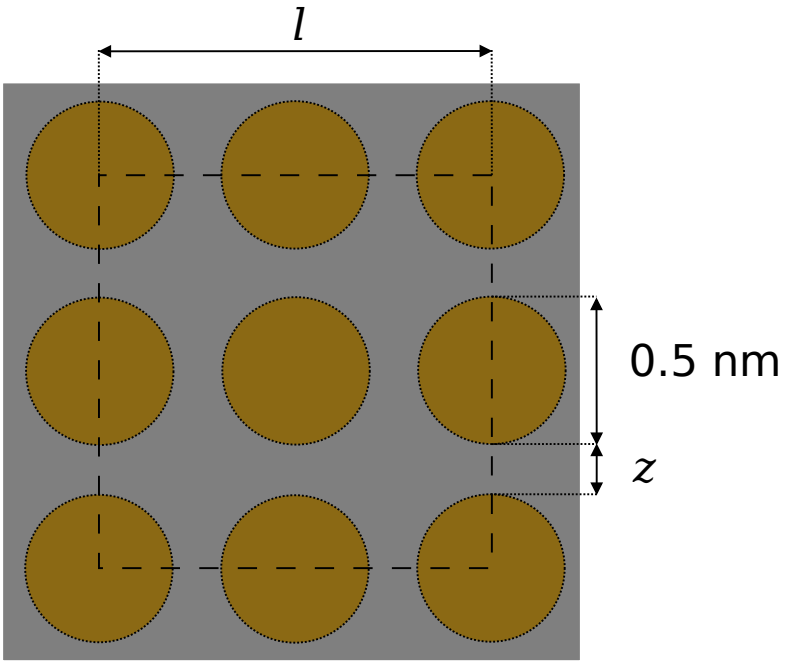

Figure 2.3: The projection of oleate chains (1.38 nm diameter) on the nanoparticle surface account for a total area of 4 oleate molecules for a square side of l, assuming the packing illustrated for the oleate molecules.

2.3.1.4 Total mass of nanoparticle

The total mass of the three layered nanoparticle can be calculated as the sum of the mass of the individual layers given by Equations (2.4), (2.5), (2.8) and (2.9) resulting in the following:

$$m_{\mathrm{NP}} = \frac{4\pi R_1^3}{3}\frac{N_{Fe}}{3A^3N_A}\left(\frac{MM_{\mathrm{FeCl_2\cdot 4\,H_2O}}}{\mathrm{Purity}_{\mathrm{FeCl_2\cdot 4\,H_2O}}} + 2\frac{MM_{\mathrm{FeCl_3\cdot 6\,H_2O}}}{\mathrm{Purity}_{\mathrm{FeCl_3\cdot 6\,H_2O}}} + \frac{8}{K_b}\left(\frac{4\pi R_1^3}{3}\frac{8N_{Fe}}{3A^3N_A} + K_b\right)\frac{MM_{\mathrm{NH_4OH}}}{C_{\mathrm{NH_4OH}}}\right) + \frac{4\pi R_1^2}{l^2N_A}\left(\frac{MM_{\mathrm{Potassium\ Oleate}}}{\mathrm{Purity}_{\mathrm{Potassium\ Oleate}}} + \frac{MM_{\mathrm{Hitenol\ BC}}}{\mathrm{Purity}_{\mathrm{Hitenol\ BC}}}\right) \quad (2.10)$$

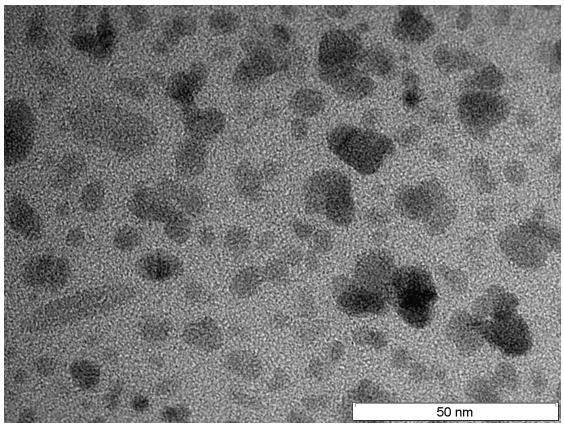

(a)

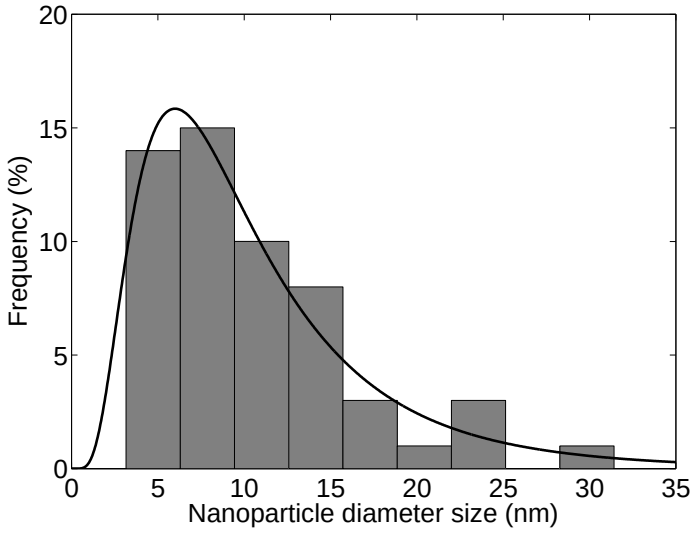

(b)

Figure 2.4: (a) TEM image of Fe_3O_4-oleate-Hitenol BC nanoparticles; (b) Nanoparticle core size distribution using the 10 line approach through Line Cut package for MATLAB - average size of 8.8 nm.

Table 2.3: Elemental composition of magnetic nanoparticles in N, C, H, S and Fe (wt. %)

Nitrogen	Carbon	Hydrogen	Sulfur	Iron
0.18	30.06	4.41	1.13	30.04

2.3.2 Magnetic nanoparticles characterization

2.3.2.1 Magnetic nanoparticles composition

For both the elemental and ICP-AES analysis a sample was used with solids' concentration of 3.76 $\mathrm{g\,L^{-1}}$. The Fe content in the nanoparticles was 391 $\mathrm{mg\,L^{-1}}$ as determined by ICP-AES. The Fe, N, C, H and S mass fractions (in weight %) are shown in Table 2.3. The iron mass fraction is calculated indirectly from the sulfur concentration measured by ICP-AES and the sulfur mass fraction measured by elemental analysis.

The mass fraction of each layer (iron core, oleate and Hitenol BC) was determined based on values of Table 2.3, which gives 47 % for the iron core, 21 % for the oleate layer and 32 % for the outer Hitenol BC layer (Table 2.4). Comparing these values with the ones by Olle 2006 one can see that the changes to the synthesis protocol introduced in this work resulted in a lower fraction of iron (58.3 %) concomitantly with higher fractions of oleate (18.74 %) and of Hitenol BC (22.92 %). The oleate:Fe^{2+} ratio can be verified by calculating the molar ratio of oleate to 1/3 of the total molar iron content. The calculated ratio is 0.361:1 for which we can assume that the nanoparticles are fully coated with a monolayer of oleate. It is also possible to calculate the amount of oleate per gram of nanoparticle which is 7.35×10^{-4} mol $\mathrm{g^{-1}}$ in the present work and 1.08×10^{-3} mol $\mathrm{g^{-1}}$ in the work by Olle 2006.

Table 2.4: Layer's composition of magnetic nanoparticles (wt. %)

Magnetite	Oleate	Hitenol BC
47.23	20.77	31.99

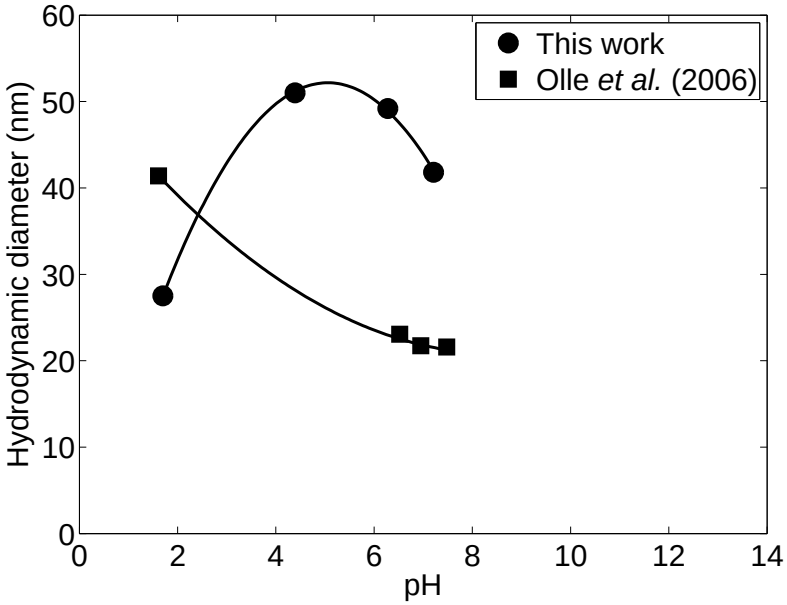

Figure 2.5: Nanoparticles' hydrodynamic diameter determined by dynamic light scattering across a wide range of pH.

2.3.2.2 Hydrodynamic diameter of the magnetic nanoparticles

The DLS analysis showed that the nanoparticle diameter does not change significantly (40-50 nm, Figure 2.5) for a wide range of pH values (4-8), decreasing to about half for a pH of 2. It is interesting to notice that the variation of the hydrodynamic diameter as function of pH present an opposite behavior when compared to Olle et al. 2006.

When moving from low to neutral pH, the hydrodynamic diameter in Olle et al. 2006 decreases, which was interpreted as the result a of less aggregation at higher pH. At very low pH, the sulfonate group in Hitenol BC becomes neutral and the oleate-Hitenol BC chains will shrink due to loss of repulsiveness and consequently reduce the hydrodynamic

diameter. From acid to slightly basic pH (4-8) the sulfonate group holds its negative charge which will strongly stabilize the oleate-Hitenol BC chains.

2.3.2.3 ζ-potential

The surface of the nanoparticles coating is negatively charged due to the sulfonate group in the end of the Hitenol BC chain, contributing to repulsion between nanoparticles and resulting in a colloidally stable solution. Moreover, the two long Hitenol BC side chains contribute to steric hindrance yielding an additional stabilizing factor.

As a result of these two contributions, nanoparticles remain stable over a wide range of pH (2-12), decreasing the ζ-potential value with pH increase (from -11 to -40 mV), as shown in Figure 2.6, while in Olle et al. 2006, the ζ-potential remains approximately unchanged for the whole pH range studied ($\sim$ 30 mV). Additionally, due to the sulfonate groups' ionization, when increasing the pH it is expected that the surface charge decreases, since the protons at the surface of the nanoparticle will travel to the bulk liquid, due to higher OH- concentration, which is clearly showed in Figure 2.6. At pH = 8.5, the zeta-potential of our synthesized nanoparticles and those from Olle et al. (2006)'s report is similar, and that is an appropriate pH for the sulphite oxidation method. Consequently, pH = 8.5 will be chosen for the mass transfer tests.

2.3.2.4 Diameter of magnetite core (TEM)

The diameter size of the magnetite core was determined by image analysis of TEM image (Figure 2.4a). The average value was 8.8 nm (Figure 2.4b) for a 10-line analysis which is close to the one reported by most authors (Abareshi et al. 2010; Khan 2008; Narita et al. 2009; Olle et al. 2006; Wang et al. 2011).

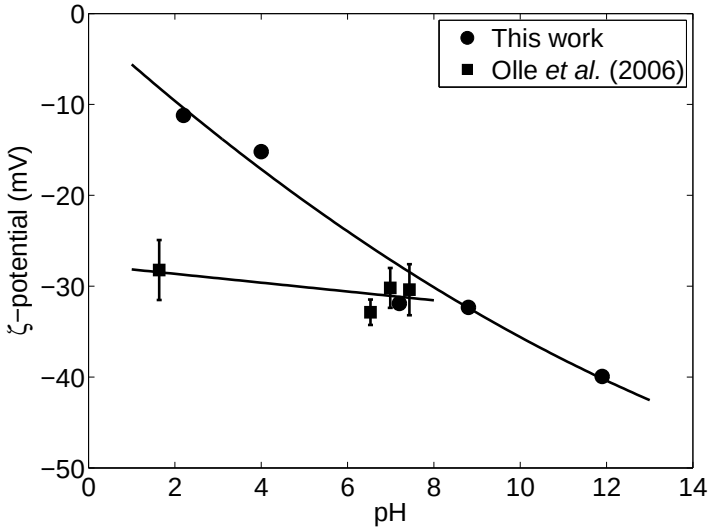

Figure 2.6: ζ-potential for nanoparticles across a wide range of pH.

2.3.3 Characterization of nanoparticles-water suspensions

2.3.3.1 Surface tension

If the surface tension of the oleate coated nanoparticles suspensions is compared with pure oleate in Figure 2.7a it can be seen that from $4 \times 10^{-5}\,\mathrm{g\,g^{-1}}$ onwards the surface tension of oleate solutions decreases in a steeper fashion than the nanoparticles suspensions, as expected. Comparing the surface tension of nanoparticle and oleate suspensions in terms of oleate concentration, for higher concentrations (above 4×10^{-4} M) oleate presents similar surface tension values (Figure 2.7b).

2.3.3.2 Oxygen mass transfer

For the whole range of nanoparticle loading there was an increase in the mass transfer rate of oxygen in relation to pure water-air dispersions as shown in Figure 2.8. The

(a)

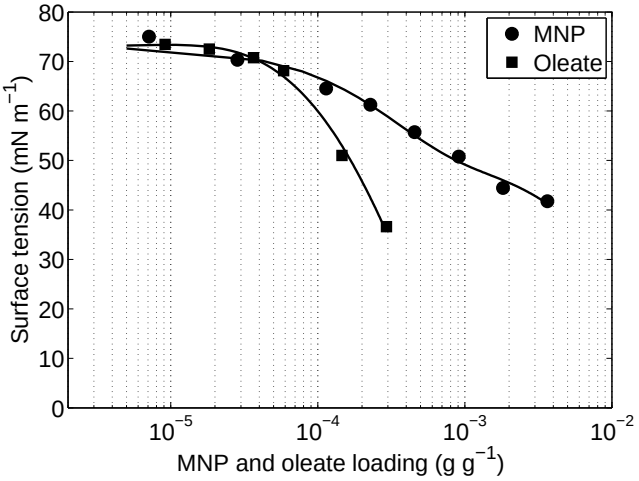

(b)

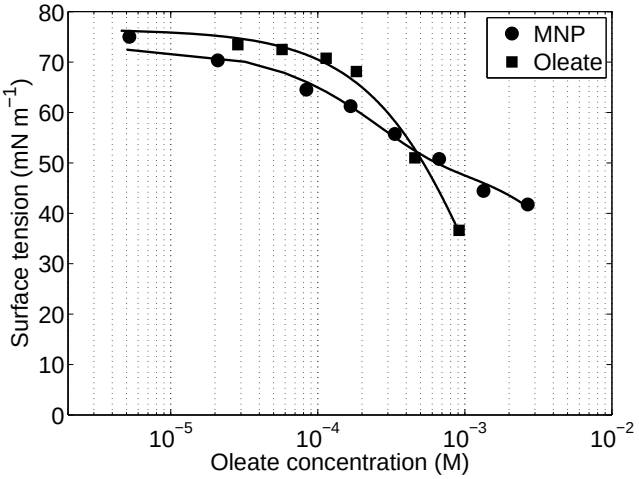

Figure 2.7: Surface tension of magnetic nanoparticles and oleate solutions for different (a) loadings and (b) oleate concentrations – for MNP solutions, it is presented the oleate concentration in its composition.

trend shown by the curve is that of an exponential convergence to a maximum mass transfer rate obtained at high nanoparticles loading. In the present study we reached a 4.3-fold mass transfer increase in relation to pure water for a nanoparticles loading of

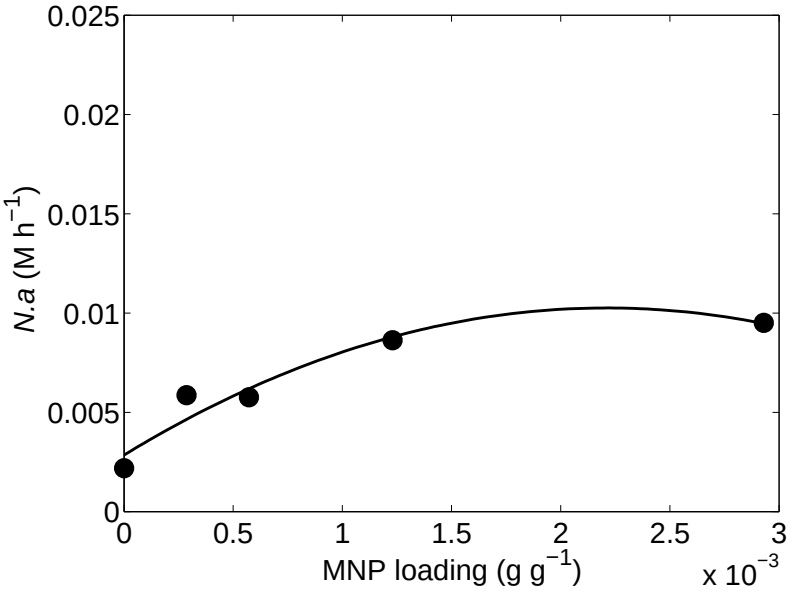

Figure 2.8: Mass transfer for different nanoparticle loadings.

$0.0029\,\mathrm{g\,g^{-1}}$.

When comparing with Olle et al. 2006 (maximum enhancement of 4.5-fold), our oxygen transfer enhancement is slightly lower (Figure 2.9a).It should be remarked that the reactor used in the present study is 10 times smaller than the one of Olle et al. 2006. The mass transfer coefficient is highly dependent of the reactor and impeller sizes, which precludes a direct comparison. In fact we used a much smaller power input (57 W $\mathrm{m^{-3}}$) than Olle et al. 2006 ($\sim$ 11 kW $\mathrm{m^{-3}}$), which however resulted in comparable oxygen transfer enhancement. When comparing the results in terms of oleate concentration in nanoparticles (Figure 2.9b), it is clear that for the same oleate concentration, the enhancement derived from our nanoparticles is similar to Olle et al. 2006.

Using surfactants as coating in nanoparticles in order to reduce surface tension and consequently to increase interfacial area seems to be a promising strategy for mass transfer enhancement. It should however be noted that the use of a pure surfactant or nanoparticles coated by the same surfactant might not produce equivalent results even

if the same amount of surfactant is introduced in the suspension. Figure 2.10 makes this comparison for the case of oleate, where it can be observed that there is a sharper increase in mass transfer rate and to higher values for pure oleate in relation to oleate coated nanoparticles. It becomes also evident that the surface tension mechanism is not sufficient to explain the differences observed as the surface tension values seems to be concordant for pure oleate and oleate coated nanoparticles (Figure 2.7b).

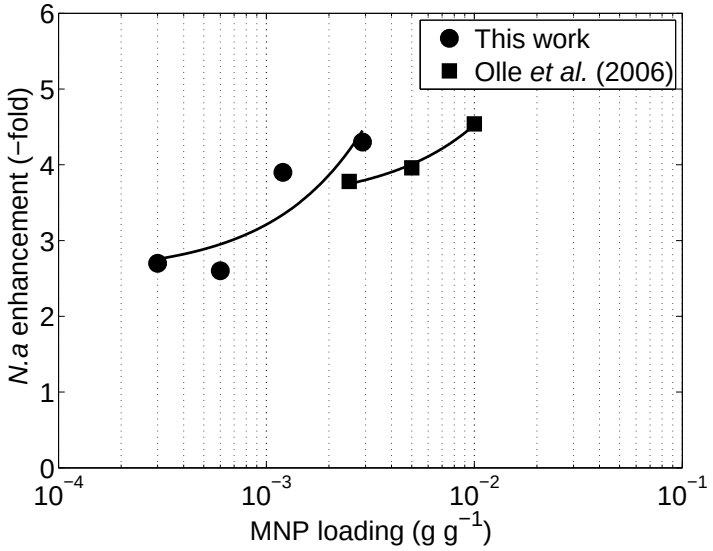

(a)

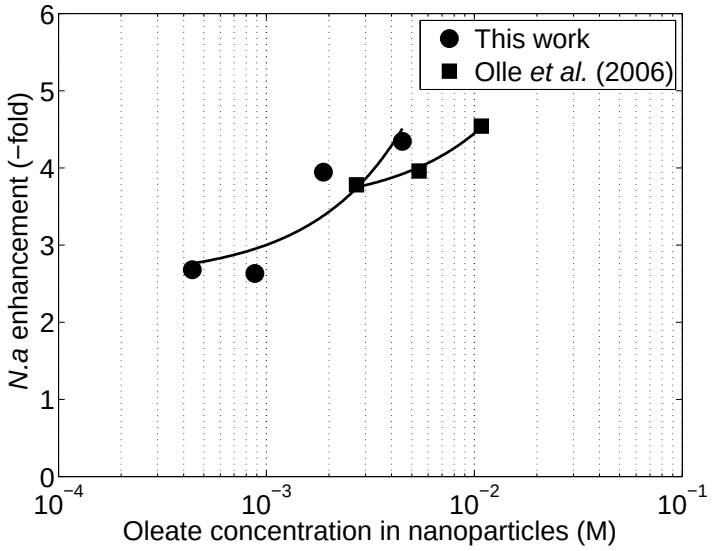

(b)

Figure 2.9: Comparison of mass transfer enhancement with Olle et al. 2006 for (a) different nanoparticle loadings and (b) different oleate concentration in nanoparticles.

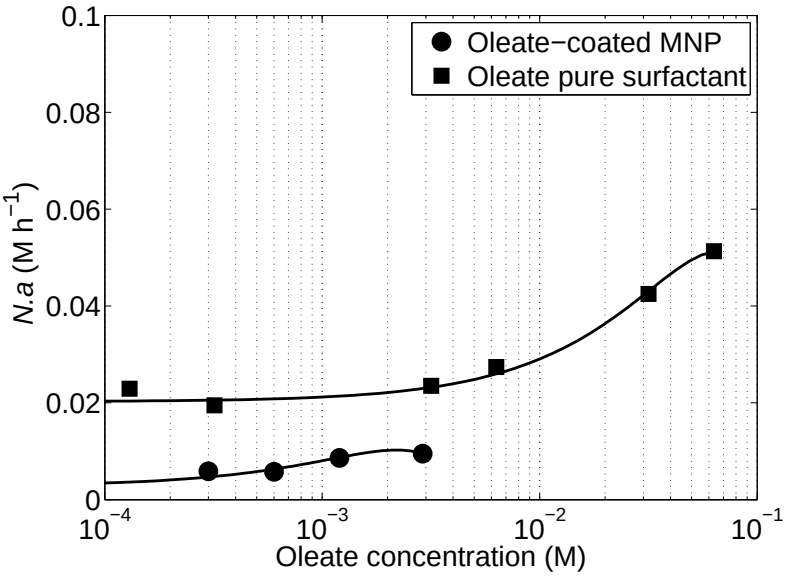

Figure 2.10: Mass transfer according to the different oleate concentrations with nanoparticles and pure surfactant.

2.4 Conclusions

Synthesis of nanoparticles using an improved protocol as outlined in the discussion above provided 8.8 nm core-sized particles stable for a wide range of pH (ζ-potential decreases from -10 to -40 mV with increasing pH) that enhance mass transfer up to 4.3-fold for a 0.29 % mass fraction. Comparing to Olle et al. 2006, our nanoparticles deliver higher enhancement for the same amount of oleate in nanoparticles with 3 orders of magnitude less power input per unit volume.

At pH = 8.5, the zeta-potential of our synthesized nanoparticles and those from Olle et al. (2006) report is similar, and that is an appropriate pH for the sulphite oxidation method. Consequently, pH = 8.5 will be chosen for the mass transfer tests.

The modification introduced in the protocols enhanced mass transfer up to 4.3-fold for a 0.29 % mass fraction. Compared to Olle et al. (2006), our nanoparticles deliver higher enhancement for the same amount of oleate with 3 orders of magnitude less power input per unit volume.

There is a correlation between the oxygen absorption rate and nanoparticle loading, with higher increases in oxygen absorption rates for low nanoparticle loading and smaller increases for high nanoparticle loading. The increase in oxygen absorption is also observed in mass transfer test using pure oleate surfactant. Therefore, the impact of the nanoparticles on oxygen absorption is presumably related to the presence of tensioactive agents on the composition of the nanoparticles. In the next chapter will be studied the impact of operational parameters (Q, ϕ and N) on the volumetric mass transfer coefficient, and the previous hypothesis will be validated as well as the reported mechanism of mass transfer.

CHAPTER 3

Effect of nanoparticles on the volumetric mass transfer coefficient ($k_{\mathrm{L}}a$)

3.1 Introduction

In the last few years, there has been an attempt to enhance mass transport and diffusion coefficients in gas-liquid systems through the use of nanoparticles, which has been a successful task by many authors (Amaris et al. 2014; Bahmanyar et al. 2011; Beiki et al. 2013a,b; Fang et al. 2009; Feng et al. 2005; Feng and Johnson 2012; Gerardi et al. 2009; Hwang et al. 2009; Jung et al. 2012; Kang et al. 2008; Keshishian et al. 2013; Kim et al. 2012; Kim et al. 2006, 2007; Kim et al. 2008; Komati and Suresh 2008, 2010; Krishnamurthy et al. 2006; Lee and Kang 2013; Lee et al. 2011; Lee et al. 2010; Lu et al. 2013; Ma et al. 2007, 2009; Manikandan et al. 2012; Moraveji et al. 2013; Nagy et al. 2007; Ozturk et al. 2010; Pang et al. 2012; Park et al. 2006a; Park et al. 2006b, 2007; Park et al. 2008; Saien and Bamdadi 2012; Sara et al. 2011; Subba-Rao et al.

2011; Turanov and Tolmachev 2009; Veilleux and Coulombe 2010; Wen et al. 2005; Wu et al. 2013; Yang et al. 2011; Zhu et al. 2008). Although a clear effect has been reported through the use of these nanoparticles, it is still not clear which mechanisms might be playing in the mass transport enhancement.

Most studies that try to explain the mass transport enhancement, postulate correlations that cannot predict the gas-liquid system behavior accurately in the presence of nanoparticles, but have been successfully applied in other systems (e.g., oil-in-water, small particles). Nevertheless, it seems that there is a general agreement that there are mechanisms affecting separately the specific interfacial area (a) and the mass transfer coefficient (k_{L}). The most noted mechanisms that have a high impact on mass transfer are the boundary layer mixing, shuttling effect, coalescence inhibition, grazing effect and Brownian motion of nanoparticles (Alper et al. 1980; Beenackers and Swaaij 1993; Dumont and Delmas 2003; Kars et al. 1979; Ruthiya et al. 2003a,b).

The boundary layer mixing is influenced by four major physical phenomena:

- Presence of small particles ($d_p < \delta_{\mathrm{L}}$) may decrease k_{L}, due to a decrease in the effective volume fraction of the liquid available for diffusion of gas at the interface.
- Presence of large particles ($d_p > \delta_{\mathrm{L}}$) can cause/induce local turbulence at the gas-liquid interface, increasing the renewal rate of the liquid in the gas-liquid boundary layer that flows from the bulk liquid (Godbole et al. 1990);
- Collisions of the particles with the boundary layer (Kluytmans et al. 2003; Zon et al. 1999) which increases the gas–liquid mass transfer coefficient ($k_{\mathrm{L}}a$), reducing the effective gas-liquid boundary layer thickness;
- Rate of coalescence of gas bubbles since: bubble coalescence may give rise to larger bubbles that have a more mobile interface (larger k_{L}) (Beenackers and Swaaij 1993; Kluytmans et al. 2003; Suresh et al. 1988), and can also cause re-dispersion of entrained gas, which means additional surface renewal (larger k_{L}).

The shuttling effect is defined by the adsorption of gas by particles (must have high specific surface area and porosity) that penetrate the liquid film close to the gas-liquid interface. Upon returning to the bulk liquid, the particles will desorb the solute gas, thus increase the transport of gas by the "shuttling" movement of the particles. In agitated slurry reactors, an increase of the volumetric mass transfer coefficient ($k_{\mathrm{L}}a$), is reported as being due to an increase in k_{L} of about 200–300 % due to this shuttle effect (Alper et al. 1980; Kars et al. 1979).

The grazing effect (or boundary layer reaction effect) is defined by the presence of small particles at the gas-liquid interface, catalyzing a chemical reaction and thus, increasing the consumption of gas in the diffusion layer around the bubbles. This increase in the solute consumption will therefore increase the rate of mass transfer. The mass transfer can be further enhanced as it is also subject of the lyophobicity and catalytic activity of the particles and the turbulence inside the reactor (Ruthiya et al. 2003a; Zon et al. 1999).

The Brownian motion is also considered as a mass transfer enhancement mechanism not for the Brownian motion of the particles itself, but the velocity disturbance field that is induced in the surroundings of the nanoparticles causing an enhanced mixing in the fluid (Komati and Suresh 2010; Krishnamurthy et al. 2006).

In this chapter, mass transfer tests are carried out following a central composite design varying three operational parameters: the stirrer speed, N (250-750 rpm), aeration rate, Q (0.00-2.00 vvm)m and nanoparticle loading, ϕ (0-1.20$\times10^{-3}$ g g^{-1}). To understand the impact of each operational parameter on mass transfer coefficients (volumetric and liquid-side), a statistical analysis was applied to the experimental data with the software MODDE and a PLS model was applied using the software MATLAB.

3.2 Materials and methods

3.2.1 Magnetic nanoparticles synthesis and characterization

Magnetic nanoparticles with an iron oxide core and two layers, oleic acid and Hitenol-BC, were synthesized as described in Olle et al. (2006) with the alterations proposed in Section 2.2.2.

3.2.2 Experimental Set up

The experiments were performed in a flat-bottomed cylindrical vessel equipped with a six flat vertical bladed Rushton impeller and an L-shaped tube sparger with 4 exit holes on the sides (Figure 3.1). The tank diameter (T) is 81 mm and the impeller diameter (D) is 27 mm. The reactor and impeller dimensions follow the standard ratios of turbine diameter, $D/T = 1/3$, baffle width, B/T=1/10, turbine blade length, l_B/D=1/4, turbine blade height, h_B/D=1/5 and off-bottom clearance, C/D=1 (Delafosse et al. 2009; Fujasová et al. 2007; Hashimoto et al. 2011; Linek et al. 1996; Nocentini et al. 1988; Olle et al. 2006; Zadghaffari et al. 2010). The liquid volume was 0.406 L, and liquid height (H) is approximately the same as the tank diameter and the horizontal part of the tube sparger is placed 10 mm below the turbine.

3.2.3 Mass transfer tests - Sulfite method

The mass transfer tests were carried out using the sulfite oxidation method to determine oxygen transfer from gas to liquid phases (Linek and Vacek 1981). The method consists in bubbling air into a reactor filled with a $C_{SO_3} = 0.8$ M solution in the presence of a catalyst ($CoSO_4 \cdot 7\,H_2O$ – 1×10^{-4} M); stirring speeds, air sparging rates and nanoparticle loadings were used within the ranges presented in Table 3.1. The sulfite

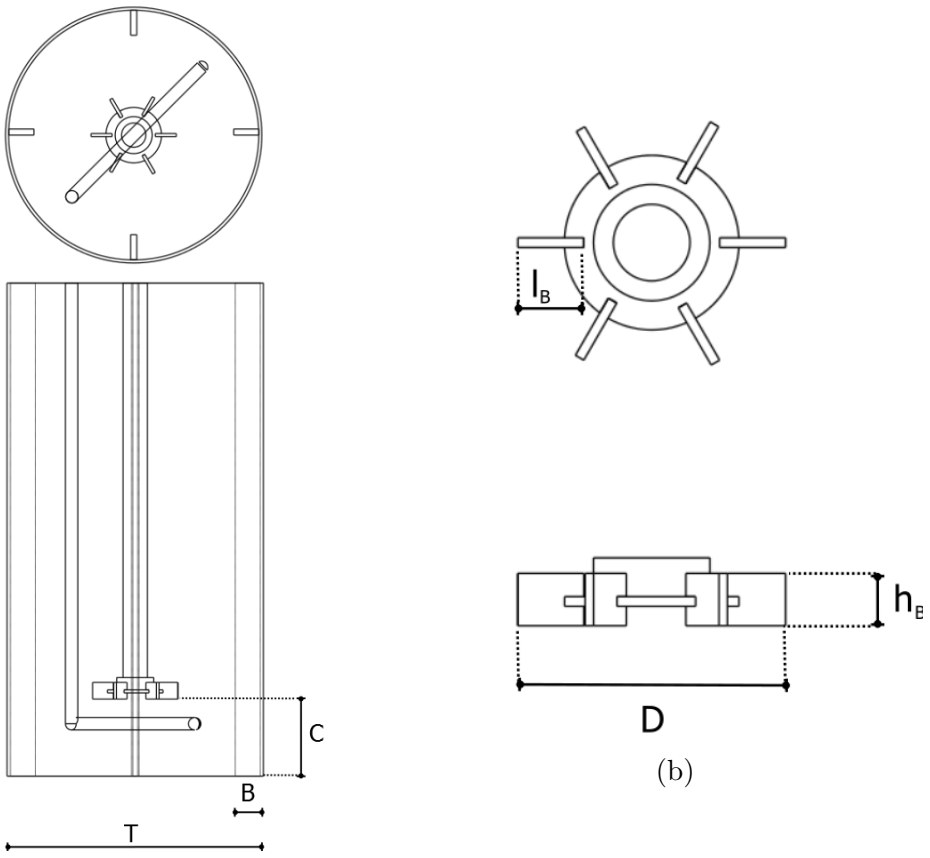

Figure 3.1: Sketch of the Rushton equipped reactor: (a) front and top views of reactor with Rushton turbine and L-shaped sparger and (b) front and top view of Rushton impeller.

concentration is monitored by iodometric back-titration (Fujasová et al. 2007; Kies et al. 2004; Kordač et al. 2011; Lewis and Roberts 2005; Linek and Vacek 1981; Linek et al. 2005b, 2006, 2008; Nagy and Hadik 2003; Nagy et al. 2007; Olle 2006; Olle et al. 2006), where a 1.5 mL reactor sample is mixed into a 50 mL of $C_{\mathrm{I}_2} = 0.026$ M; after quickly mixed, 10 mL of the resulting solution is titrated against $C_{\mathrm{S}_2\mathrm{O}_3} = 0.022$ M in triplicate. With this procedure it is possible to derive the oxygen mass transfer rate by the slope

of sulfite concentration profile

$$OTR = -\frac{\Delta C_{SO_3}}{\Delta t}\frac{1}{z} \tag{3.1}$$

in which z is the sulfite-to-oxygen stoichiometry ratio in the sulfite oxidation reaction:

$$SO_3 + \tfrac{1}{2}\,O_2 \longrightarrow SO_4 \tag{3.2}$$

It is only possible to assume that all oxygen transferred to the liquid phase is consumed if the reaction is catalyzed. The catalyst used for this study is $CoSO_4 \cdot 7\,H_2O$ which is a well-known catalyst for the sulfite oxidation (Kordač et al. 2011; Lewis and Roberts 2005; Linek and Vacek 1981; Linek et al. 2006, 2008).

3.2.4 Experimental mass transfer parameters' determination

3.2.4.1 Volumetric mass transfer coefficient (k_La)

The absorption of oxygen under a reaction with sulfite is widely used to measure the mass transfer coefficient in the interfacial area (Danckwerts 1970; Lewis and Roberts 2005; Linek and Vacek 1981; Nagy and Hadik 2003; Nagy et al. 2007; Olle et al. 2006) and is defined as follows:

$$N.a = a\left(C^*_{O_2} - C_{O_2,\text{bulk}}\right)\sqrt{\frac{2}{n+1}k_n {C^*_{O_2}}^{n-1} D_{O_2,L} + k_L^2} \tag{3.3}$$

where $N.a$ is the adsorption rate and n is the reaction order.

In order to determine the volumetric mass transfer coefficient, it is necessary to

fulfill the conditions presented in Equations (1.18a) to (1.18c). The condition in Equation (1.18a) is fulfilled by catalyzing the reaction, with a catalyst concentration of $C_{\mathrm{CoSO_4}} = 1 \times 10^{-4}$ M; Equation (1.18b) is related to the Hatta number which is calculated as

$$\mathrm{Ha} = \frac{\sqrt{\frac{2}{n+1} k_n C_{\mathrm{O_2}}^{*\ n-1} D_{\mathrm{O_2,L}}}}{k_{\mathrm{L}}} = \frac{\sqrt{\frac{2}{2+1} 12 \times 1.13 \times 10^{-4} \times 3.22 \times 10^{-9}}}{8.3 \times 10^{-4}} = 0.065 < 0.3 \tag{3.4}$$

where n is the order of (sulfite oxidation) reaction related to oxygen, which is 2; k_n is calculated from the literature (1300 $\mathrm{m^3\,mol^{-1}\,s^{-1}}$ at 20 °C and $C_{\mathrm{CoSO_4 \cdot 7\,H_2O}} = 3.56 \times 10^{-4}$ M – Laurent et al. (1974)) using an Arrhenius equation to the temperature of 37 °C and catalyst concentration, $C_{\mathrm{CoSO_4 \cdot 7\,H_2O}} = 1 \times 10^{-6}$ M; $C_{\mathrm{O_2}}^{*}$ is the oxygen concentration on the liquid and must be accounted for the reduced solubility of oxygen in a sulfite solution. Linek and Vacek (1981) proposed an equation to calculate the solubility of pure oxygen in a sulfite solution, H:

$$H = 5.909 \times 10^{-6} \exp\left(\frac{1602.1}{T} - \frac{0.9407 C_{\mathrm{SO_3}}}{1 + 0.1933 C_{\mathrm{SO_3}}}\right) = 5.32 \times 10^{-4} \mathrm{M\,atm^{-1}} \tag{3.5}$$

which allows to calculate the oxygen concentration in the liquid:

$$C_{\mathrm{O_2}}^{*} = H \times p_{\mathrm{O_2}} = 1.13 \times 10^{-4} \mathrm{M} \tag{3.6}$$

The diffusivity of oxygen in the liquid phase ($D_{\mathrm{O_2,L}}$) is 3.22 $\times 10^{-9}$ $\mathrm{m^2\,s^{-1}}$. To fulfill equation Equation (1.18c) ones must ensure that

$$\mathrm{Ha} \ll \frac{C_{\mathrm{SO_3}}}{z C_{\mathrm{O_2}}^{*}} \Longleftrightarrow 0.065 \ll 3532 \tag{3.7}$$

in order to turn mass transfer into the limiting step, allowing Equation (3.3) to be

reduced to

$$k_{\mathrm{L}}a = \frac{N.a}{C^{*}_{\mathrm{O}_2}} \tag{3.8}$$

3.2.5 Experimental design

A central composite design was applied to study variations in the three independent variables, volumetric flow rate (Q), nanoparticle loading (ϕ) and impeller rotation speed (N) whose -1 and +1 levels for each factor are: 0.41 and 1.59 vvm for Q, 2.40×10^{-4} and 9.60×10^{-4} g g^{-1} for ϕ and 351 and 649 rpm for N (Table 3.1). The 'ccdesign' function (MATLAB Statistics toolbox) generated 15 experiment designs, the respective factor variations for each of which are shown in Table 3.2. All the points were repeated for ϕ = 0 g g^{-1} in order to calculate $k_{\mathrm{L}}a$ enhancements.

MODDE 8.0 was used to analyze statistically the central composite design for the responses of $k_{\mathrm{L}}a$ and k_{L}. A second sensitivity analysis was performed by means of the npls function from the N-way Toolbox developed by Rasmus Bro & Claus A. Andersson (`http://www.models.life.ku.dk/nwaytoolbox/download`). This methodology had the purpose of weighting the impact of each of the operational parameters (Q, ϕ and N) on the outputs ($k_{\mathrm{L}}a$) (Bro 1996).

3.3 Results and discussion

3.3.1 Overall results - Mass transfer parameter ($k_{\mathrm{L}}a$) measurements (central composite design)

The proposed central composite design varied the aeration rate (Q), nanoparticle loading (ϕ) and stirring speed (N) from 0.00-2.00 vvm, 0-1.20×10^{-3} g g^{-1} and 250-750 rpm, respectively (Tables 3.1 and 3.2). The volumetric mass transfer coefficient ($k_{\mathrm{L}}a$) results

Table 3.1: Initial values and admissible range of independent variables.

α	-1.6818	-1	0	1	1.6818
Q (vvm)	0.00	0.41	1.00	1.59	2.00
ϕ ($g\,g^{-1}$)	0.00	2.40×10^{-4}	6.00×10^{-4}	9.60×10^{-4}	1.20×10^{-3}
N (rpm)	250	351	500	649	750

are shown in Table 3.2 and Figure 3.2. Additionally, a sensitivity analysis of the mass transfer parameters with respect to Q, ϕ and N was performed. A Partial Least Squared (PLS) model was developed and a number of two latent variables was scrutinized using cross-validation. Thereupon a PLS model with two latent variables was identified on the basis of all data and the regressions coefficients were computed. An additional set of runs were carried out for a control comparison in order to determine mass transfer enhancements, with the same conditions of the central composite design but without nanoparticles in the system (ϕ=0 $g\,g^{-1}$) (Table 3.2, runs A-H). The highest enhancement scores against the control batches were obtained in runs 12, with 3.30-fold enhancements for both $N.a$ and k_La.

Regarding the volumetric mass transfer coefficient, the results varied from 6.4-76.2 h^{-1}, achieving the highest values (>50 h^{-1}) for high nanoparticle loadings ($\geq$ 6.00×10^{-4} $g\,g^{-1}$), while no general correlation can be foreseen for the other two parameters, which comes in line with the regression coefficients derived from sensitivity analysis (linear regression coefficient (r.c.) of 0.72 for ϕ and under 0.26 for the other two variables, Figure 3.4). This phenomenon might be explained by collisions of the particles with the boundary layer (Kluytmans et al. 2003; Zon et al. 1999) which reduce the thickness of the gas-liquid boundary layer, thus enhancing the global mass transfer, i.e. the volumetric mass transfer coefficient; it can also be explained by the shuttling effect of the (nano)particles that decreases the travel time the oxygen takes in the diffusion layer around the bubbles (Alper et al. 1980; Kars et al. 1979); these mechanisms induced

Table 3.2: Oxygen absortion rate ($N.a$) and volumetric mass transfer coefficient ($k_{\mathrm{L}}a$) measurements for the first central composite design. Enhancement calculations are calculated as $E_{\mathrm{X}} = \frac{X_{Q_i,\phi_i,N_i}}{X_{Q_i,\phi_0,N_i}}$.

Run	Q (vvm)	ϕ ($\mathrm{g\,g^{-1}}$)	N (rpm)	$N.a$ ($\mathrm{M\,h^{-1}}$)	$E_{N.a}$	$k_{\mathrm{L}}a$ ($\mathrm{h^{-1}}$)	$E_{k_{\mathrm{L}}a}$
1	0.41	2.40×10^{-4}	351	0.00184	0.66	16.2	0.66
2	0.41	2.40×10^{-4}	649	0.00072	0.05	6.4	0.05
3	0.41	9.60×10^{-4}	351	0.00478	1.71	42.2	1.71
4	0.41	9.60×10^{-4}	649	0.00775	0.54	68.4	0.54
5	1.59	2.40×10^{-4}	351	0.00202	0.48	17.9	0.48
6	1.59	2.40×10^{-4}	649	0.00505	0.85	44.6	0.85
7	1.59	9.60×10^{-4}	351	0.00833	1.97	73.5	1.97
8	1.59	9.60×10^{-4}	649	0.00368	0.62	32.5	0.62
9	0.00	6.00×10^{-4}	500	0.00000	0.00	0.0	0.00
1	2.00	6.00×10^{-4}	500	0.00682	0.90	60.2	0.90
11	1.00	0.00	500	0.00262	1.00	23.1	1.00
12	1.00	1.20×10^{-3}	500	0.00863	3.30	76.2	3.30
13	1.00	6.00×10^{-4}	250	0.00103	0.26	9.1	0.26
14	1.00	6.00×10^{-4}	750	0.00389	0.75	34.4	0.75
15	1.00	6.00×10^{-4}	500	0.00576	2.20	50.8	2.20
A	0.41	0.00	351	0.00280		24.7	
B	0.41	0.00	649	0.01428		126.1	
C	1.59	0.00	351	0.00422		37.3	
D	1.59	0.00	649	0.00591		52.2	
E	2.00	0.00	500	0.00757		66.9	
F	1.00	0.00	500	0.00262		23.1	
G	1.00	0.00	250	0.00389		34.3	
H	1.00	0.00	750	0.00521		46.0	

by the presence of nanoparticles outweighs the impact of stirring and aeration.

Even though the study of these last two operational parameters is very well described in the literature, their results are analysed for the sake of completeness (Figure 3.3). In Figure 3.3a, it is possible to notice that there is a general increase trend in kLa with increasing aeration rate, which is expected since a higher air supply will translate into a higher oxygen transfer. On the other hand, in Figure 3.3b there are both ascending and descending profiles with the increasing of stirring speed, which means that there is no dominant behaviour concerning the agitation rate. A higher agitation rate should translate into smaller bubbles, and consequently smaller boundary layers, since the

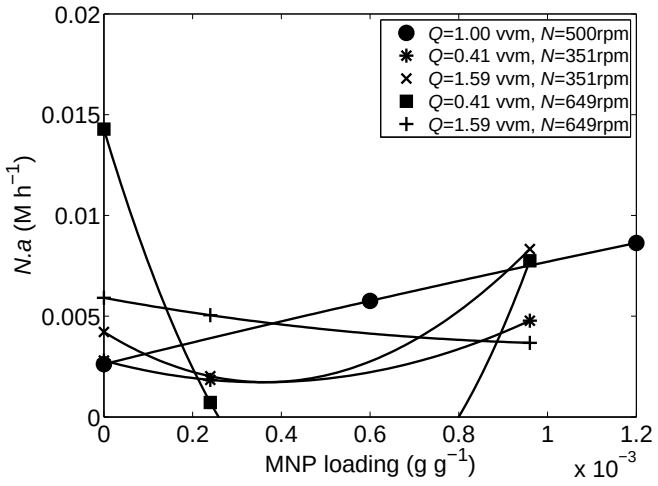

(a)

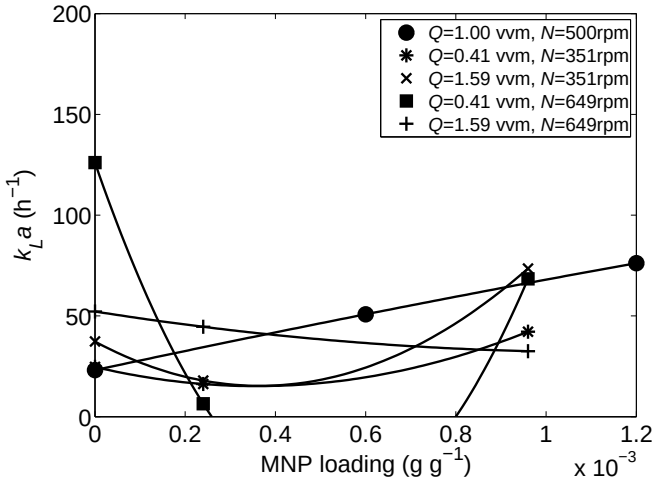

(b)

Figure 3.2: (a) Oxygen absorption rate and (b) volumetric mass transfer coefficient results for the central composite design.

stirrer blades would break the bubbles at a higher intensity. Since the nanoparticles already have an impact on the bubble and boundary layer sizes, the interaction of the nanoaparticle loading and the stirrer speed presents these unexpected results.

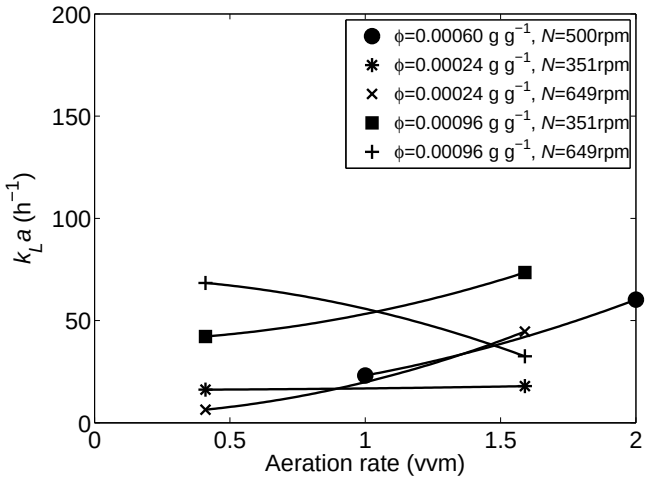

(a)

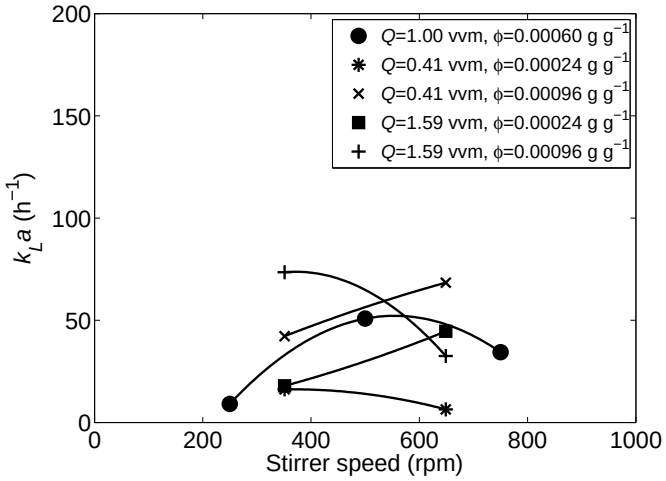

(b)

Figure 3.3: Volumetric mass transfer coefficient as a function of (a) aeration rate and (b) stirrer speed.

3.3.2 Sensitivity analysis of $k_{\mathrm{L}}a$ vs Q, ϕ and N

Beyond the sensitivity analysis of Q, ϕ and N on the volumetric mass transfer with main effects (Figure 3.4), a further analysis was carried out for interaction and quadratic effects for the same experimental design previously described using the statistical software

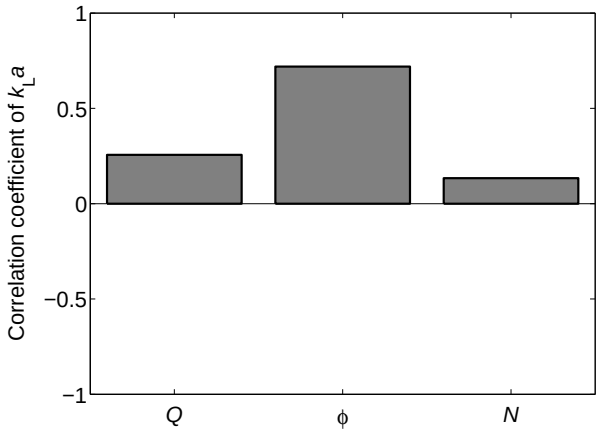

Figure 3.4: Regression coefficient values of Q, ϕ and N on the volumetric mass transfer coefficient k_La (r.c.=0.256, 0.719 and 0.133).

MODDE 8.0. Firstly, to analyze the correlation between experimental values and the statistical model proposed, it is necessary to derive the response equation for the model:

$$\begin{aligned} k_La =& 49.8 + 3.3N + 16.2\phi + 10.0Q - 9.0N^2 + 0.9\phi^2 - 6.0Q^2 - 4.0N \times \phi \\ & - 3.8N \times Q - 5.6\phi \times Q \end{aligned} \tag{3.9}$$

Comparing the experimental results against the application of Equation (3.9), it is possible to visualize that the statistical model adjusts well to the experimental results (Figure 3.5) and accounts for an R^2 of 0.795 for k_La for which the R^2 is at borderline of acceptable (R^2=0.80, according to Lundstedt et al. (1998)).

To fully understand the effect of the nanoparticle loading on mass transfer (aeration rate and stirring speed won't be studied since these are already vastly reported in the literature), a sensitivity analysis was carried out for the volumetric mass transfer coefficient as a function of ϕ (not showed). The nanoparticle loading contribution is remarkable for k_La, and shows a strong linear correlation with the nanoparticle loading

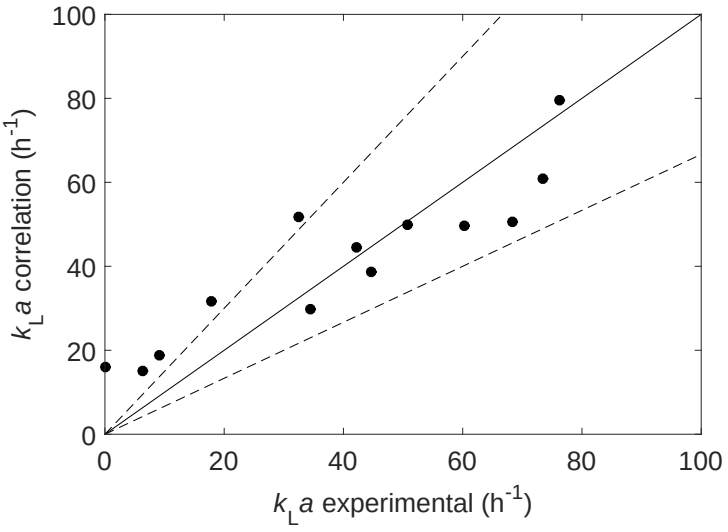

Figure 3.5: Observed results for $k_{\mathrm{L}}a$ for the central composite design against modelling estimations by MODDE 8.0. The dashed lines represent a 15 % deviation.

(Person correlation coefficient, r=0.999). These findings come in line with the reported results in Figure 3.4, which showed that the presence of nanoparticles severely affects the mass transfer behaviour of an air-water agitated reactor system.

One can also relate these results with the mechanisms reported in the literature, even though they have not been validated they have not been discarded, such as the increase of collision of particles in the boundary layer that increase the gas-liquid mass transfer coefficient by reducing the gas-liquid boundary layer thickness (Kluytmans et al. 2003; Zon et al. 1999); the increase of the rate of gas bubbles coalescence which ultimately lead to more mobile interface of the gas bubbles (Beenackers and Swaaij 1993; Kluytmans et al. 2003; Suresh et al. 1988); the increase in k_{L} due to the shuttling effect promoted by the (nano)particles (Alper et al. 1980; Kars et al. 1979); the mixing enhancement due to disturbance in the surroundings of the nanoparticles caused by their Brownian motion (Komati and Suresh 2010; Krishnamurthy et al. 2006).

3.4 Conclusions

Through the use of an experimental design, resorting to the sulfite oxidation method, it was possible to prove that nanoparticles can enhance both the oxygen absortion rate and the volumetric mass transfer coefficient in an air/water stirred tank reactor. A 230% enhancement was achieved for both values ($N.a$ and $k_{\mathrm{L}}a$) in the presence of nanoparticles. It was also concluded that, of the three operational parameters varied (Q, ϕ and N), nanoparticle loading (ϕ) has a higher impact on the $k_{\mathrm{L}}a$ (r.c. = 0.72) and strong linear correlation coefficient coefficient (r=0.999). The statistical model developed to describe the volumetric mass transfer coefficient behaviour accounted for an acceptable R^2 of 0.795.

Thus, it is possible to infer that the previous hypothesis from Chapter 2 that stated that the presence of tensioactive agents on the nanoparticles impacts positively on the mass transfer is not discarded. Nevertheless, to validate this hypothesis, one needs to determine if this effect has a higher impact on the interfacial area (a) or in the liquid side mass transfer coefficient (k_{L}), which will be studied in the following chapter.

As for the study of the impact of aeration rate and stirrer speed on the $k_{\mathrm{L}}a$, two conclusions can be withdrawn from our results: The aeration rate presents a positive (linear) impact on the volumetric mass transfer coefficient while the stirring speed does not present a clear trend regarding the $k_{\mathrm{L}}a$.

CHAPTER 4

Effect of nanoparticles on interfacial area and liquid-side mass transfer coefficient

4.1 Introduction

Even though the impact of nanoparticle loading on the volumetric mass transfer coefficient is receiving each year a higher attention by the scientific community, the splitting of the separate contributions same cannot be said for the impact caused by nanoparticles on of the interfacial area and mass transfer coefficient has not received much attention. Besides the grounding research by Olle et al. (2006) and Olle (2006), one of the few studies only one study that assesses the influence of nanoparticles on the interfacial area is Kim et al. (2014). However, prior to assessing the impact of the nanoparticles on the interfacial area, it is necessary to understand how gas-liquid interfacial area can be impacted by particles in general.

4.1.1 Mechanisms of interfacial area enhancement by particles

The adsorption of particles to the gas bubbles inhibits/reduces bubble coalescence and facilitates bubble breakup, thus increasing the specific interfacial area. The aforementioned adsorption is influenced by physical properties, such as surface tension of the liquid, viscosity and density of the liquid, ionic forces, lyophobicity/wettability of particles and the particle size:

- Bubble breaking effect mechanism: this mechanism is defined by the collision of particles with gas bubbles, during the gas absorption process, that leads to the particles colliding at the gas-liquid interface and consequently breaking the bubbles. With bubble breakage, the bubbles become smaller and the interfacial area becomes greater, yielding an increase in global mass transfer. However, as pointed out by Kim et al. (2014) bubbles in the presence of nanoparticles do not seem to break but rather to solely shrink.

- Bubble coalescence inhibition mechanism: it is known that the coalescence of two bubble takes place when the contact time of these two bubble exceeds the time that is necessary to drain the liquid film between them (Colella et al. 1999). In the presence of (nano)particles, these particles will inhibit the contact of the two bubbles by covering the bubble surface, thus preventing the bubble coalescing, and consequently keeping low-sized bubbles in the gas-liquid system.

In the study by Kim et al. (2014), the bubble shape and behaviour is studied on a CO2-methanol single bubble diffusion process, with and without nanoparticles in the liquid broth. It was hypothesized that bubble breakup is not a mechanism enhanced by the nanoparticle since to bubble breakup is observed throughout their experiments. The study by Olle (2006) proposed a correlation to measure the impact of nanoparticles

on the interfacial area but it does not use any nanoparticle loading related parameter (in fact, the correlation is solely a function of stirrer speed), and thus it is not possible to weigh the effect of these particles.

In the previous chapter, we used conditions for the mass transfer tests that favour the determination of the volumetric mass transfer coefficient $k_{\mathrm{L}}a$. In this chapter, the main objective is to decouple the effect of nanoparticles on the interfacial area (a) from the effect on the liquid side mass transfer coefficient (k_L). The mass transfer tests are carried out in the same fashion as in Chapter 3, subjecting the system to conditions that allow the calculation of the interfacial area.

The condition changed in this chapter when comparing with the previous chapter will be the increase of the catalyst concentration to 3×10^{-3} M, in which the mass transfer conditions are greatly enhanced and thus it is possible to calculate the interfacial area without interference of the diffusional effects.

To understand the impact of each operational parameter on interfacial area, a statistical analysis was applied to the experimental data and a PLS model.

4.2 Materials and methods

4.2.1 Magnetic nanoparticles synthesis and characterization

Magnetic nanoparticles with an iron oxide core and two layers, oleic acid and Hitenol-BC, were synthesized as described in Olle et al. (2006) with the alterations proposed in Section 2.2.2 on Page 21.

4.2.2 Experimental Set up

The experimental setup to run the experiments was the same as presented in Section 3.2.2 on Page 46.

4.2.3 Mass transfer tests - Sulfite method

The mass transfer tests were used as described in Section 3.2.3 on Page 46, with the only change being a higher $CoSo_4 \cdot 7\,H_2O$ catalyst concentration of 2×10^{-3} M used instead.

4.2.4 Experimental mass transfer parameters' determination

4.2.4.1 Specific (gas-liquid) interfacial area (a) determination

The specific (gas-liquid) interfacial area determination method used in this study follows the same methodology as described above. As duly noted by Olle et al. (2006), the sulfite oxidation method has the advantage that the gas-liquid interfacial area, a, can be separately determined by manipulating the concentration of catalyst. Thus, the reaction rate of the oxidation of sodium sulfite can be manipulated so that it becomes several times greater than the mass-transfer rate. A criterion of $Ha \geq 3$ is generally used. In order to achieve this condition we used a catalyst concentration of $C_{CoSO_4 \cdot 7\,H_2O} = 2 \times 10^{-3}$ M:

$$\mathrm{Ha} = \frac{\sqrt{\frac{2}{2+1} 24733 \times 1.13 \times 10^{-4} \times 3.22 \times 10^{-9}}}{8.3 \times 10^{-4}} = 3.0 \tag{4.1}$$

Under such conditions, the absorption rate ($N.a$) is greatly enhanced by the reaction and the effect of the hydrodynamic conditions can be ignored, i.e. the weight of the chemical reaction factor is such that k_L can be neglectable. Under these conditions, the

absorption rate depends only on the interfacial area and reaction kinetics,

$$N.a = aC^*_{O_2}\sqrt{\frac{2}{n+1}k_n {C^*_{O_2}}^{n-1} D_{O_2,L}} \tag{4.2}$$

4.2.4.2 Liquid-side mass transfer coefficient (k_L)

The volumetric mass transfer coefficient, k_La, is the product of the liquid-side mass transfer coefficient, k_L, and the interfacial area, a. Thus, the liquid-side mass transfer coefficient k_L is simply determined by:

$$k_L = \frac{k_La}{a} \tag{4.3}$$

4.3 Results and discussion

4.3.1 Overall results - mass transfer parameters (a and k_L) measurements (central composite design)

The central composite design referred to in Section 3.2.5 was also used for the assessment of interfacial area enhancement experiments (Table 4.1), with the same additional set of runs to determine mass transfer enhancements (ϕ=0 $g\,g^{-1}$) (Table 4.1). The interfacial area (a) and the liquid-side mass transfer coefficient (k_L) results are shown in Table 4.1 and Figure 4.1. Additionally, the sensitivity analysis was performed with the same methodology as in Section 3.2.5 with respect to Q, ϕ and N. The highest enhancement scores against the control batches were obtained in runs 6 and 3, with 4.8- and 1.44-fold enhancements for a and k_L, respectively.

Looking at the specific interfacial area results, the outcome ranged from 48.1-344.9 m^{-1}, having as major impact factors the stirring speed and the aeration rate – all values $> 200\,m^{-1}$ stem from $N \geq 649$ rpm (except for run 10). As for the aeration

Table 4.1: Interfacial area (a) and liquid-side mass transfer coefficient (k_{L}) measurements for the first central composite design. Enhancement calculations are calculated as $E_{\mathrm{X}} = \frac{X_{Q_i,\phi_i,N_i}}{X_{Q_i,\phi_0,N_i}}$.

Run	Q (vvm)	ϕ ($\mathrm{g\,g^{-1}}$)	N (rpm)	$N.a$ ($\mathrm{M\,h^{-1}}$)	$E_{N.a}$	a ($\mathrm{m^{-1}}$)	E_a	k_L ($\mathrm{m\,h^{-1}}$)	$E_{k_{\mathrm{L}}}$
1	0.41	0.00024	351	0.0152	0.57	48.1	0.58	0.337	1.14
2	0.41	0.00024	649	0.0766	3.31	242.3	3.32	0.026	0.02
3	0.41	0.00096	351	0.0313	1.17	99.2	1.19	0.425	1.44
4	0.41	0.00096	649	0.0692	2.99	219.4	3.00	0.312	0.18
5	1.59	0.00024	351	0.0539	2.71	168.7	2.70	0.106	0.18
6	1.59	0.00024	649	0.1090	2.94	344.9	2.96	0.129	0.29
7	1.59	0.00096	351	0.0348	1.75	110.4	1.76	0.666	1.12
8	1.59	0.00096	649	0.0963	2.59	305.5	2.62	0.106	0.24
9	0.00	0.00060	500	0.0000	0.00	0.0	0.00	0.000	0.00
10	2.00	0.00060	500	0.0677	1.65	214.8	1.67	0.280	0.54
11	1.00	0.00000	500	0.0222	1.00	71.8	1.00	0.322	1.00
12	1.00	0.00120	500	0.0534	2.40	171.1	2.38	0.445	1.38
13	1.00	0.00060	250	0.0273	0.95	86.4	0.96	0.105	0.28
14	1.00	0.00060	750	0.0933	2.41	295.6	2.44	0.116	0.31
15	1.00	0.00060	500	0.0554	2.49	177.6	2.47	0.286	0.89
A	0.41	0.00000	351	0.0000		83.6		0.296	
B	0.41	0.00000	649	0.0267		73.0		1.726	
C	1.59	0.00000	351	0.0231		62.6		0.596	
D	1.59	0.00000	649	0.0199		116.5		0.448	
E	2.00	0.00000	500	0.0371		128.8		0.519	
F	1.00	0.00000	500	0.0409		71.8		0.322	
G	1.00	0.00000	250	0.0222		90.5		0.379	
H	1.00	0.00000	750	0.0288		121.3		0.379	

rate, it is easy to spot a general ascending profile when plotting Q against a (plot not shown). These findings are in accordance with the sensitivity analysis (Figure 4.2a), which accounts for a linearity regression coefficient of r.c. = 0.966 for the aeration rate. This effect might be explained by the higher linear velocity of the air in the agitated reactor that results in a better distribution of the gas phase in the bulk liquid, i.e. smaller bubbles. The linear regression coefficient for N is around 0.83, accounts for a high impact on the interfacial area. This is due to the fact that the faster impeller blades movement will promote a higher bubble breakup, which leads to a higher specific interfacial area; The hypothesis proposed by Olle et al. (2006) that postulates that nanoparticles loading would prevent bubble coalescence (and produce a large interfacial

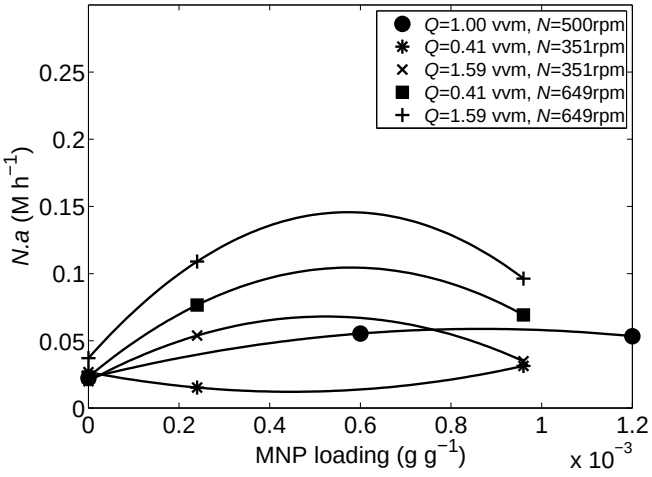

(a)

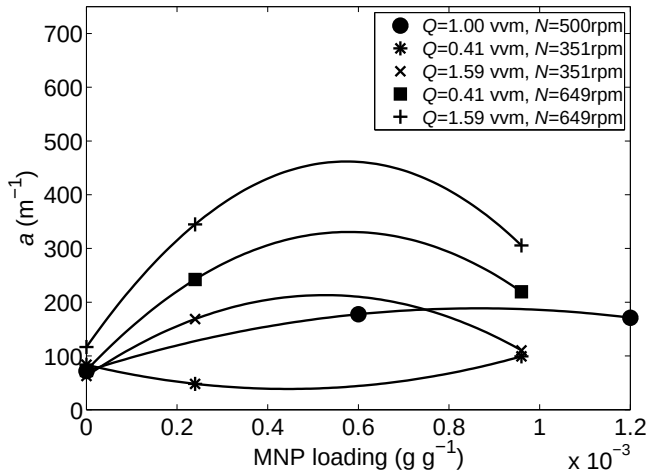

(b)

Figure 4.1: (a) Oxygen absorption rate and (b) interfacial area results for the central composite design, with two additional samples from Chapter 2 with $\phi = 3 \times 10^{-3}$ and 3×10^{-4} g g^{-1}, Q=1 vvm and N=500 rpm.

area enhancement) is rejected by our findings, since the linear regression coefficient between nanoparticle loading and interfacial area is around -0.103, which indicates that whichever physical impact the nanoparticles loading may have, is negligible.

The previous statement does not mean that the presence of nanoparticles is irrelevant, it means that the the enhancement of interfacial area is independent of the nanoparticle loading range studied ($0.00024 < \phi < 0.00120\ \mathrm{g\,g^{-1}}$). The nanoparticle' loading that serves as a threshold for the maximum enhancement of the interfacial area might be linked with the total surface area of the bubbles in the system. Whenever the loading is higher than the amount needed to cover the bubbles surface, the effect on the enhancement will not noticed.

Another possibility for the highest enhancement being for the interfacial area is that the nanoparticles are composed of an organic shell (oleic acid), which means they will tend to move away from the bulk liquid; with this dynamic they will firstly place themselves covering the bubbles' surface and only afterwards moving "freely" in the bulk liquid. This might promote a priority in the mechanisms at play in the presence of nanoparticles: the one with highest priority will be the bubble coalescence inhibition, while only afterwards the k_L affecting mechanisms will take place.

As for the liquid-side mass transfer coefficient, 0.026 and $0.666\,\mathrm{m\,h^{-1}}$ were the extreme values on the experimental design, achieving the highest outcomes ($> 0.400\,\mathrm{m\,h^{-1}}$) when the nanoparticle loading is at least $9.60\times10^{-4}\,\mathrm{g\,g^{-1}}$ agreeing with the reported results from the coefficient regression values that states that the only operational parameter with relevance for k_L is the nanoparticle loading 0.613 of linear regression coefficient for ϕ and less than 0.38 (in module) for Q and N, Figure 4.2b).

When comparing these results with the literature, one can see that the findings from Ruthiya et al. (2003a) that consider that the presence of small particles may decrease the k_L are denied, while the findings from Alper et al. (1980) and Kars et al. (1979) that state the k_L might be enhanced by the shuttling effect of small particles (nanoparticles) and a microconvection created in the surrounding fluid of the nanoparticles that disturbs the boundary layer, which increases greatly the mass transfer (Komati and Suresh 2010; Krishnamurthy et al. 2006) are supported.

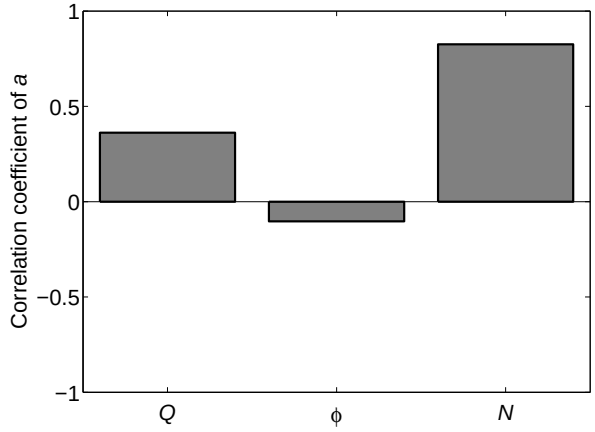

(a)

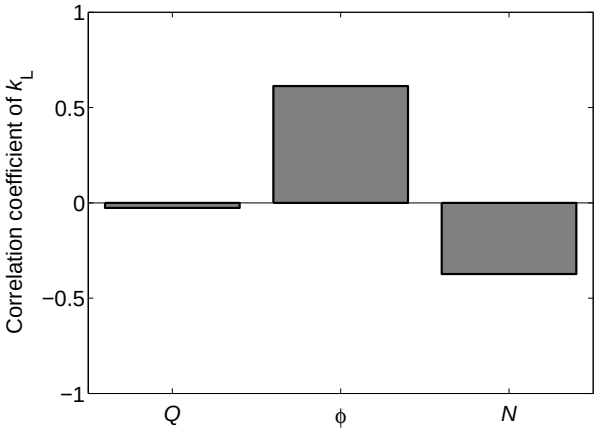

(b)

Figure 4.2: Coefficient values of Q, ϕ and N in the multilinear regression on (a) the interfacial area a (0.362, -0.103 and 0.826) and (b) liquid-side mass transfer coefficient k_{L} (-0.027, 0.613 and -0.374).

4.3.2 Sensitivity analysis of a and k_{L} vs Q, ϕ and N

Beyond the impact of the main effects of Q, ϕ and N on mass transfer parameters, a further analysis was carried out for interaction and quadratic effects for the same

experimental design previously described. The response equations for the model are:

$$\begin{aligned} a =& 167.2 + 76.0N + 7.1\phi + 50.0Q + 19.2N^2 - 5.4\phi^2 - 10.3Q^2 - 6.9N \times \phi \\ &+ 7.1N \times Q - 15.7\phi \times Q \end{aligned} \tag{4.4a}$$

$$\begin{aligned} k_{\mathrm{L}} =& 0.275 - 0.069N + 0.081\phi + 0.027Q - 0.047N^2 + 0.049\phi^2 - 0.037Q^2 \\ &- 0.048N \times \phi - 0.014N \times Q + 0.020\phi \times Q \end{aligned} \tag{4.4b}$$

The application of Equations (4.4a) and (4.4b) to the experimental results is shown in Figures 4.3a and 4.3b. The interfacial area model accounts for an acceptable R^2 of 0.880 (according to (Lundstedt et al. 1998)) and 0.651 for k_{L}, which is rather low and might be due to k_{L} being derived from the ratio of $\frac{k_{\mathrm{L}}a}{a}$ and not directly measured.

Since it was shown before that the nanoparticle's loading linear correlation with the interfacial area is rather small, the sensitivity analysis (using the software MODDE) was carried out for all three operational parameters and not only for ϕ as in the $k_{\mathrm{L}}a$ case. Firstly, as for the aeration rate, the sensitivity analysis seems to illustrate a much higher linear correlation with the interfacial area (Pearson coefficient, r=0.983), with an increasing behaviour throughout the scope of aeration rate used (not showed). Regarding the nanoparticle loading, there seems to be a smaller linear dependence to the interfacial area (r=0.827), remaining mainly constant throughout the nanoparticles' loading range, which comes in line with the previous results from the PLS model. Finally, the agitation rate shows a very high linear correlation (r=0.975), with a monotonical ascending behaviour (not showed).

Regarding the sensitivity analysis of the k_{L}, only the nanoparticle loading will be studied since it was the only parameter that showed a very higher linear correlation in the PLS model. The sensitivity analysis showed that the linear relation between the

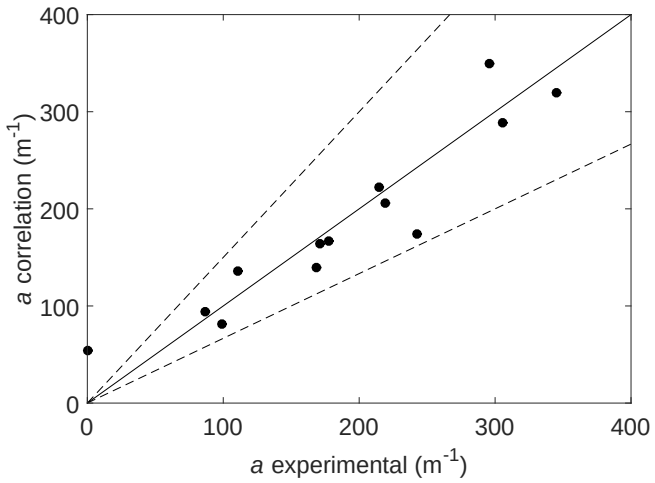

(a)

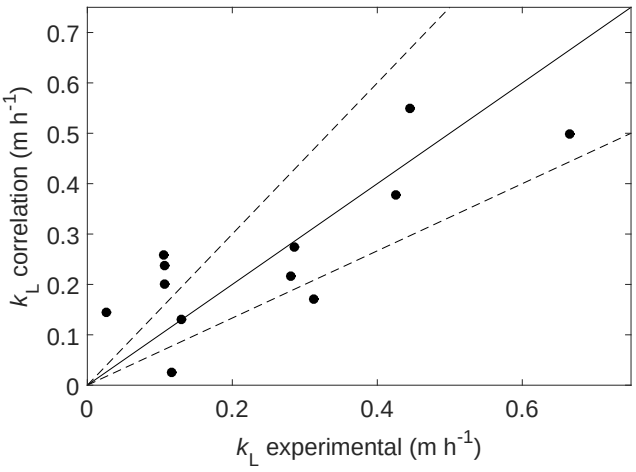

(b)

Figure 4.3: Estimated over experimental (a) a and (b) k_{L} values, for the central composite design against modeling estimations by MODDE 8.0. The dashed lines represent a 15 % deviation.

k_{L} and the nanoparticle is high, as in the PLS model, with an r=0.877, although it maintains constant in the first part of the range studied an increasing in the second (not shown).

As a general result of the sensitivity analysis through the use of MODDE, mostly confirmed the results from the PLS model, regarding the influence of nanoparticles on a and k_{L}. There seems to be a no great impact on the interfacial area, as opposed to an increasing linear profile by the liquid side mass transfer coefficient in the presence of the nanoparticles.

4.3.3 Liquid-side mass transfer coefficient, k_{L}

Regarding the liquid-side mass transfer coefficient k_{L}, the experimental k_{L} values range between 0.026 and 0.666 $\mathrm{m\,h^{-1}}$ for bubble sizes varying between 0.3 and 4 mm as it is shown in Figure 4.4. The bubbles' diameters are calculated from the study of Calderbank (1958):

$$d_{\mathrm{B}} = 2.25 \left(\frac{P_{\mathrm{G}}}{V}\right)^{-0.4} \sigma^{0.6} \rho^{-0.2} \varepsilon^{0.4} \left(\frac{\mu_{\mathrm{G}}}{\mu_{\mathrm{L}}}\right)^{0.25} \tag{4.5}$$

where the gassed power (P_{G})

$$P_{\mathrm{G}} = \left(\frac{P_{\mathrm{U}}^2 N D^3}{Q_{\mathrm{G}}^{0.56}}\right)^{0.45} \tag{4.6}$$

is derived from Michel and Miller (1962), with $P_{\mathrm{U}} = N_{\mathrm{imp}} N_{\mathrm{P}} N^3 D^5$, while the gas holdup ($\varepsilon$)

$$\frac{\varepsilon}{1-\varepsilon} = 0.819 \times \frac{V_{\mathrm{S}}^{2/3} N^{2/5} T^{4/15}}{g^{1/3}} \times \left(\frac{\rho_L}{\sigma}\right)^{1/5} \times \left(\frac{\rho_L}{\rho_L - \rho_G}\right) \times \left(\frac{\rho_L}{\rho_G}\right)^{-1/15} \tag{4.7}$$

is derived from Garcia-Ochoa and Gomez (2004).

These k_{L} experimental values are compared to the theoretical k_{L} values from two correlations: i) Frössling (Frössling 1938) valid for "smaller" spherical bubbles having rigid interface ($0.1\,\mathrm{mm} < d_{\mathrm{B}} < 2\,\mathrm{mm}$)

$$\frac{k_L d_{\mathrm{B}}}{D} = 2 + 0.6 \left(\frac{\rho u d_{\mathrm{B}}}{\mu}\right)^{0.5} \left(\frac{\mu}{\rho D}\right)^{0.33} \tag{4.8}$$

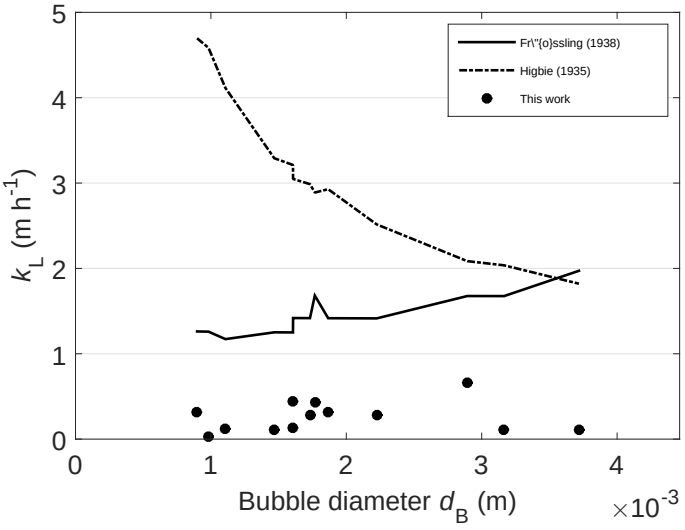

Figure 4.4: Comparison of experimental and predicted liquid-side mass transfer coefficient for different bubble diameters.

and ii) Higbie (Higbie 1935) valid for "big" mobile spherical bubbles ($d_B > 2.5\,mm$)

$$k_L = \left(\frac{4Du}{\pi d_B}\right)^{0.5} \tag{4.9}$$

having short contact times with the liquid . Through an analysis of Figure 4.4 it can be stated that the k_L values experimentally obtained are closer to those deduced from Equation (4.8) which is what would be expected since this equation is valid for "small" bubbles ($d_B < 2.5\,mm$). The inability of fitting accurately k_L values may be due to i) the bubble array is within the transition phase of rigid spherical bubbles to mobile ellipsoidal bubbles and ii) the nanoparticles adsorbed at the bubble surface, lowering the surface tension of the membrane, decreasing the resistance to the oxygen diffusion, therefore increasing the liquid-side mass transfer coefficient k_L.

4.4 Conclusions

After conducting this study, it was possible to conclude that the interfacial area is enhanced up to 332 % while the liquid side mass transfer coefficient is enhanced by 44 %, in the presence of nanoparticles. Thus, it is fair to conclude that the largest contributor for the overall mass transfer enhancement is the interfacial area, through bubble coalescence inhibition (bubble breakage mechanism by nanoparticles is discarded as pointed out by Kim et al. (2014)).

It was possible to describe fairly well the interfacial area using a statistical model (R^2 of 0.880) while the liquid side mass transfer coefficient presented a low score for the statitical estimation due to its indirect determination.

It was concluded that the parameter that impacts most on k_{L} is the nanoparticle loading, showing a 0.706 linear regression coefficient. For all the conditions tested, there seems to be a comparable profile, with a decrease in kL for mid-range nanoparticle loading.

As for the interfacial area, the behaviour was the opposite, having as most impactful both aeration rate with a 0.966 linear regression coefficient. Nevertheless, there seems to exist an agreement between interfacial area enhancement and nanoparticle loading, for most tested conditions; there is a rapid increase in interfacial area and afterwards it is maintained. This effect might be caused by the presence of surfactants on the nanoparticles. It was proved in Chapter 2 that for the same surfactant concentration, nanoparticles can yield up to 50 % of oxygen absorption of the pure surfactant. Thus, in the following chapter, in order to attempt to elucidate on possible mechanisms of oxygen transfer enhancement using nanoparticles, correlations will be developed that take into account the surfactant effect.

CHAPTER 5

Model based analysis of interfacial area and volumetric mass transfer coefficient

5.1 Introduction

5.1.1 Volumetric mass transfer coefficient

Unlike heat transfer, mass transfer enhancement by means of nanoparticles has not been extensively studied (Komati and Suresh 2010), though it has been hypothesized that mainly two possible mechanisms are responsible for the mass transfer enhancement – an increase in the gas-liquid interfacial area a, or by an increase of the mass transfer coefficient $k_{\mathrm{L}}a$ (Kim et al. 2006, 2007; Komati and Suresh 2010; Krishnamurthy et al. 2006; Nagy et al. 2007; Olle et al. 2006; Yu and Tan 2012).

Olle et al. (2006) reported that the enhancement in interfacial area was responsible for the largest part of the enhancement in total mass transfer and this conclusion is in agreement with our our observations so far (interfacial area enhancement is always

greater than k_L enhancement). The mechanism acts likely through the nanoparticle accumulation at the gas-liquid interface that stabilize gas bubbles against coalescence, and therefore maintains smaller bubble sizes and greater interfacial areas. The threshold for the enhancement is obtained at very small nanoparticle loading, and after that a plateau is reached and increase of NP loading no longer impacts the interfacial area.

Therefore, the goal of this work is to develop a new mass transfer correlation. Various correlations have been suggested for the overall k_La, in particular for stirred tank reactors and Newtonian liquids (Albal et al. 1983; Bartholomew 1960; Calderbank and Moo-Young 1961; Cichy and Russell 1969; Cooper et al. 1944; Kawase and Moo-Young 1991; Montes et al. 1999; Moo-Young and Blanch 1981; Nielsen et al. 1994; Perez and Sandall 1974; Richards 1961; Smith et al. 1977; Van't Riet 1979; Yagi and Yoshida 1975) (Table 5.2). Most of these correlations were derived from individual correlations for either k_L or a, which were determined by Calderbank and Moo-Young (1961) and taken in consideration the geometrical agitator-tank configurations, and take the form of

$$k_La = \alpha \left(\frac{P_G}{V}\right)^{\beta} V_S^{\gamma} \tag{5.1}$$

Correlations have been proposed based on the aforementioned mechanisms for general mass transfer systems. Only Olle et al. (2006) has proposed correlations that uses a parameter that reflects the nanoparticle loading:

$$k_La = 12.9 \left(\frac{P_G}{V}\right)^{0.63} V_S^{0.57} \left(1 + 4\phi^{0.34}\right) \tag{5.2}$$

and

$$d_B = e^{14.16} N^{-1.39} \tag{5.3}$$

These correlations take into account operation parameters and while the $k_{\mathrm{L}}a$ correlations seems to be consider the most important parameters, the bubble diameter correlation seems somewhat incomplete, since it employs only the stirring speed as a estimation parameter.

5.1.2 Interfacial area

Correlations to predict interfacial area in stirred tanks have also received considerable attention. The first cornerstone has been set by Calderbank (1958) study:

$$\frac{d_{32}}{D} = \alpha \left(1 + b\phi^{\beta}\right) \mathrm{We}^{\gamma} \tag{5.4}$$

determining the interfacial area by

$$a = \frac{6\varepsilon}{d_{32}} \tag{5.5}$$

The aforementioned correlation predicts the (Sauter) diameter, d_{32}, based on the volume fraction of a dispersed phase and the Weber number,

$$\mathrm{We} = \frac{\rho N^2 l^3}{\sigma} \tag{5.6}$$

a very useful dimensionless number in fluid mechanics, which takes into account the main fluid properties, i.e. density, agitation speed, droplet diameter and surface tension. This study initiated a high number of studies with correlations with the similar format (Brown and Pitt 1970; Chatzi et al. 1989; Chen and Middleman 1967; Coulaloglou and Tavlarides 1976; Godfrey and Grilc 1977; Heuven and Beek 1971; Mlynek and Resnick 1972; Sprow 1967) (Table 5.3) or slight variations either using the Weber number,

$$\mathrm{We} = \frac{\rho N^2 L}{\sigma} \tag{5.7}$$

or a “viscosity group” number,

$$Vi = \frac{\mu_d}{\sqrt{\rho_d \sigma_d}} \tag{5.8}$$

instead of the dispersed fraction, ϕ (Arai et al. 1977; Calabrese et al. 1986; Lagisetty et al. 1986; Nishikawa et al. 1987a,b; Wang and Calabrese 1986).

In this chapter, the correlations will be developed based on the experimental design from Chapters 3 and 4. Since one of the physical parameters that might affect the interfacial area is the surface tension, we will present the calculated values for the central composite design based on the profile presented in Figure 2.7a.

5.2 Materials and methods

For the identification of the models' parameters, a gradient based optimization algorithm was applied, namely the “lsqnonlin” MATLAB routine. Analytically derived derivatives were provided, by means of the Jacobian solution:

$$J_{kj}(x) = \frac{\partial F_k(x)}{\partial x_j} \tag{5.9}$$

for each correlation, where $F_k(x)$ are the correlations for $k_{\mathrm{L}}a$ and a, while the x_j will be the coefficients of the correlations, i.e. α, b, β, γ and δ. As additional details on the computational effort of the optimization code, the 'lsqnonlin' options used were a maximum of 1000 iterations aswell as a maximum of 1000 function evaluations, the lower bound on the size of a step is 10^{-10}, while the lower bound on the function change per iteration is 10^{-12}.

In all correlations, the identification was restarted 1000 times from random initial values, using a wide range for each parameter, to ensure global optimality of the optimal parameter values, which were selected to be those that provided the smallest estimation

error. The optimal parameters were derived from the median of the end results of each calculation.

5.3 Results and discussion

5.3.1 Mechanisms affecting the liquid side mass transfer coefficient, k_{L}

In the previous chapters, the mechanisms that were hypothesized as affecting the mass transfer coefficient were several, namely, boundary layer mixing, shuttling effect, coalescence inhibition, grazing effect and Brownian motion of nanoparticles. To elucidate which might actually be at play in the present work, it is needed to validate or exclude each one in light of our results. All the calculations of the following subsections are showed in Table 5.1.

Table 5.1: Sum-up of calculations of variables of mechanisms at play in the presence of nanoparticles. The enhancements are calculated as $E_{\mathrm{X}} = \frac{X_{Q_i,\phi_i,N_i}}{X_{Q_i,\phi_0,N_i}}$

Run	D_n (m^2/s)	$E(=\frac{D_n}{D})$	δ_L, Equation (5.14) (m)	$\frac{\delta_L}{\delta_{L_0}}$	δ_L Equation (4.8) (m)	$\frac{\delta_L}{\delta_{L_0}}$
1	3.25×10^{-9}	1.008	3.47×10^{-5}	0.87	3.80×10^{-6}	1.80
2	3.25×10^{-9}	1.008	4.43×10^{-4}	65.39	7.10×10^{-7}	0.31
3	3.26×10^{-9}	1.014	2.76×10^{-5}	0.69	1.92×10^{-6}	0.91
4	3.26×10^{-9}	1.014	3.77×10^{-5}	5.56	8.15×10^{-7}	0.36
5	3.25×10^{-9}	1.008	1.10×10^{-4}	5.62	2.67×10^{-6}	0.38
6	3.25×10^{-9}	1.008	9.05×10^{-5}	3.46	1.22×10^{-6}	0.35
7	3.26×10^{-9}	1.014	1.76×10^{-5}	0.90	4.24×10^{-6}	0.61
8	3.26×10^{-9}	1.014	1.11×10^{-4}	4.23	1.43×10^{-6}	0.41
9	3.26×10^{-9}	0.000	–	0.00	–	0.00
10	3.26×10^{-9}	1.011	4.18×10^{-5}	1.86	2.39×10^{-6}	0.63
11	3.22×10^{-9}	1.000	3.60×10^{-5}	1.00	4.37×10^{-6}	1.00
12	3.27×10^{-9}	1.015	2.64×10^{-5}	0.73	1.97×10^{-6}	0.45
13	3.26×10^{-9}	1.011	1.12×10^{-4}	3.62	4.05×10^{-6}	1.10
14	3.26×10^{-9}	1.011	1.01×10^{-4}	3.26	1.06×10^{-6}	0.43
15	3.26×10^{-9}	1.011	4.10×10^{-5}	1.14	1.84×10^{-6}	0.42

5.3.1.1 Brownian motion

As detailed in Chapter 1, Brownian motion is one of the most cited mechanisms that might be enhancing mass transfer in the presence of nanoparticles. To prove if this mechanism is in fact affecting the process, it is necessary to compare the time the solute takes to travel a given distance against the time that a nanoparticle takes to travel the same given distance subjected to its Brownian motion. The distance used to compare both times will be a nanoparticle diameter, and according to Equation (1.2) the time to travel 36 nm with brownian motion is,

$$t_{\mathrm{B}} = \frac{3\pi\eta d^3}{2k_{\mathrm{B}}T} = 3.55 \times 10^{-5}\mathrm{s}$$

while the time that oxygen takes to travel the same distance is Equation (1.3),

$$t_{\mathrm{m}} = \frac{d^2}{2D} = 2.01 \times 10^{-7}\mathrm{s}$$

It is then clear that the diffusion rate of oxygen is 2 orders of magnitude faster than the travel rate of Brownian motioned particles, thus it is seems safe to state the these particles are not physically pushing the solute molecules increasing their speed. It is then concluded that the Brownian motion as a mechanism per se is not responsible by the mass transfer enhancement observed in the previous chapters.

5.3.1.2 Microconvection in the nanoparticle' surrounding fluid

Nanoparticles in a bulk liquid are constantly colliding against the fluid's molecules which might increase the travel speed of the surrounding molecules. The velocity is simply calculated as,

$$v_{\mathrm{thermal}} = \frac{d}{t_c} \tag{5.10}$$

To keep the same approach as the previous section, it will be necessary to compare

the time a nanoparticle (and the surrounding fluid) to travel across a nanoparticle diameter (t_c) against the time that oxygen takes to diffuse through the same distance. By applying the kinetic theory to liquids and from the average molecular kinetic energy from the Boltzmann distribution, it is possible to derive:

$$\frac{1}{2}Mv_{\text{thermal}}^2 = \frac{3}{2}k_BT \tag{5.11}$$

Which in fact can be simplified to

$$v_{\text{thermal}} = \sqrt{\frac{3k_BT}{M}} \tag{5.12}$$

Where M is the mass of the nanoparticle. Therefore, a 36nm nanoparticle (and its surrounding fluid) which weighs around 5.98×10^{-18} g can travel as fast as 1.44 m/s, having has travel time through its diameter $t_c = 2.5 \times 10^{-8}$ s. Since this time is in the same order of magnitude (it is even smaller than t_m) of the oxygen diffusion rate in water, it means that the mechanism of microconvection promoted by the nanoparticles has an impact on the oxygen mass transfer.

5.3.1.3 Shuttling effect

As for the shuttling effect, the impact of this mechanism on the mass transfer would be an enhancement of the effective diffusion of oxygen across the boundary layer. Nagy et al. (2007) derived a pseudo-homogeneous model that estimates the diffusion coefficient of oxygen in a nanofluid,

$$D_n = D\left(1 + BRe_{np}^m Sc^{1/3}\phi\right) \tag{5.13}$$

Where B and m are experimentally determined parameters, for which this work was not intended for, thus it will not be possible to determine the impact of the

shuttling effect on the diffusion of the oxygen across the boundary layer. In the case of being possible to assume B and m parameters determined in Nagy et al. (2007) to be the same for this work, an increase in the diffusion rate of oxygen of up to 1.5 % ($Re_{\mathrm{np}} = 3.86 \times 10^{-3}$, ϕ=0.00120 g g^{-1}) could be observed.

5.3.1.4 Boundary layer mixing

From the previously describe physical phenomena that may impact on the boundary layer mixing, only the first one (reduction of stagnant film around a bubble) can be quantified. To determine the effect of nanoparticles on the boundary layer thickness, it is needed to calculate δ_L, using Lewis and Whitman's film theory (Lewis and Whitman 1924):

$$\delta_L = \frac{D_{\ n}}{k_{\mathrm{L}}}, \tag{5.14}$$

where D is derived from Equation (5.13). δ_L in the presence of nanoparticles ranges from 17.6 to 443 μm while the δ_L in the absence of nanoparticles ranges from 6.8 to 39.8 μm. It is possible to estimate the boundary layer change which can increase up to 65 times or decrease down to 69 %. It should be noted that the δ_L is calculated from the k_L which is determined indirectly ($= \frac{k_L a}{a}$). Taking this fact into account, there might be errors associated to the boundary layer length, which lower the confidence on these values. On the other hand, if one uses the Frossling equation (Equation (4.8)) to determine k_L (the experimental bubble range is valid for this equation), there will be an average reduction of the boundary layer thickness to 61 % of the original size with only two runs showing a thickness increase. These results mean that the boundary layer mixing mechanism can be responsible for an increase of almost 2 times in the presence of nanoparticles.

5.3.1.5 Grazing effect

As stated before, the grazing effect is defined by the presence of small particles at the gas-liquid interface that catalyze a chemical reaction, which ultimately increases the consumption of gas in the diffusion layer around the bubbles. However in our work, the synthesized nanoparticles are inert in what concerns the mass transfer tests. Therefore, the grazing effect will not impact as a mass transfer enhancement mechanism, in the presence of nanoparticles.

5.3.2 Mechanisms affecting the interfacial area, a

5.3.2.1 Coalescence inhibition (hydrodynamics effect)

The coalescence inhibition is greatly influenced by the time it takes to complete the film drainage between the bubbles. If this time is lower than the contact time between bubbles then the coalescence process takes place. There are several equations to calculate the film drainage time and the bubble contact time in the literature, but it would be necessary to determine several bubble properties experimentally thus it will not be possible to assess the impact of nanoparticles on the coalescence inhibition mechanism. However, it might be possible to hypothesize that since the turbulence in the surrounding fluid of nanoparticles is increased, it will possibly lead to a decrease in the bubble contact time, thus reducing the probability of bubble coalescence to occur. Again, since no experimental work was planned to quantify this effect, it will not be possible to weigh the impact of the nanoaprticles on this mechanism.

Table 5.2: Fit of experimental results to various $k_{\mathrm{L}}a$ correlations from literature for stirred tanks in the form of $k_{\mathrm{L}}a = \alpha \left(\frac{P_{\mathrm{G}}}{V}\right)^{\beta} V_{\mathrm{S}}^{\gamma} \left(1 + b\phi^{\delta}\right)$.

Reference	Systems	α (s^{-1})	β	γ	b	δ
Calderbank (1959); Cichy and Russell (1969)	coalescing	2.4×10^{-2}	0.400	0.500		
Van't Riet (1979)	coalescing	2.6×10^{-2}	0.400	0.500		
Fujasová et al. (2007)	coalescing	6.1×10^{-3}	0.687	0.530		
Karimi et al. (2011)	coalescing	2.3×10^{-1}	0.660	0.580		
Van't Riet (1979)	non-coalescing	2.0×10^{-3}	0.700	0.200		
Linek et al. (1987)	non-coalescing	1.4×10^{-3}	0.946	0.400		
Fujasová et al. (2007)	non-coalescing	7.8×10^{-4}	1.254	0.572		
Linek et al. (1987)	viscuous	1.1×10^{-3}	0.944	0.400		
Karimi et al. (2011)	viscuous	1.2	0.340	0.420		
Olle et al. (2006)	non-coalescing + + nanoparticles	6.1×10^{-3}	0.630	0.570	4	0.34
This work, Equation (5.15)	non-coalescing + + nanoparticles	1.40×10^{-2}	0.0578	0.166	2.36×10^{5}	1.71

5.3.3 Correlation for volumetric mass transfer coefficient, $k_{\mathrm{L}}a$

In the present work, the correlation to be used for the volumetric mass transfer coefficient will incorporate factors b and δ to account for the nanoparticles loading:

$$k_{\mathrm{L}}a = \alpha \left(\frac{P_{\mathrm{G}}}{V}\right)^{\beta} V_{\mathrm{S}}^{\gamma} \left(1 + b\phi^{\delta}\right) \tag{5.15}$$

The same strategy was adopted by Olle et al. (2006). Similar approaches were conducted to account for the impact of: i) an immiscible, organic liquid phase (Hassan et al. 1995; Nielsen et al. 2003); ii) the presence of microbial cells (Amaral et al. 2008; Cascaval et al. 2006; Galaction et al. 2004, 2005).

The results for the $k_{\mathrm{L}}a$ correlation are plotted against the experimental values in Figure 5.1. It can be seen that for lower $k_{\mathrm{L}}a$ values (under $10\,\mathrm{h}^{-1}$) are scattered, which may indicate still a difficulty in modeling the effect of the nanoparticles on the mass transfer mechanisms for low mass transfer conditions; for $k_{\mathrm{L}}a$ values above $10\,\mathrm{h}^{-1}$ there

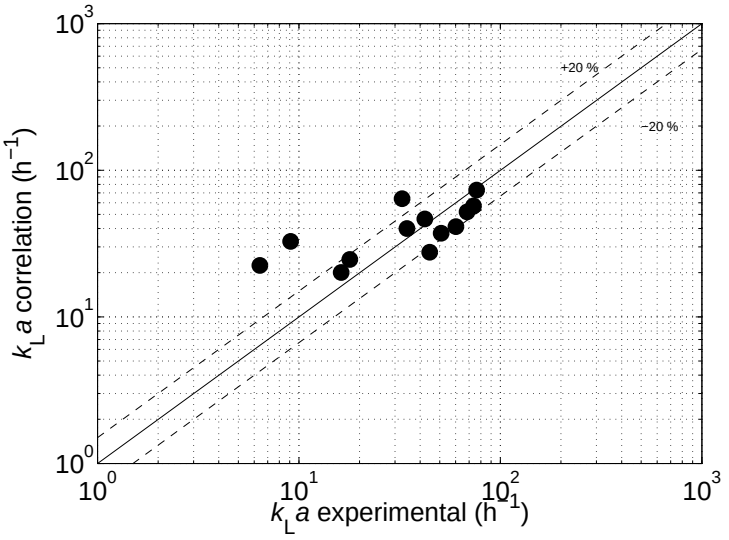

Figure 5.1: $k_{\mathrm{L}}a$ correlation from model vs observed $k_{\mathrm{L}}a$ results. The dashed lines represent a 20 % deviation.

seems to be a better agreement between observed and modelled results. The plot shows an R^2 of 53.2 % which is higher than most correlations described in the literature, including Olle et al. (2006), which is the most comparable study to ours. As a side note, Olle et al. (2006) presents an R^2 of 97 % (graphically), while we obtained a value -17.1 % after replicating their data and applying the suggested correlation parameters.

While there is no general agreement in the literature about α values, typically β exponents assume values of 0.4 and 0.7 for water-coalescing and –non-coalescing systems. On the other hand,γ exponent is placed at 0.5 and 0.2, for the aforementioned systems, respectively (Van't Riet 1979). Karimi et al. (2011) developed a mass transfer correlation for silicon oil (0-20 %), using simply the first three parameters (α, β and γ). It seems that the only noticeable trend is that β values decrease with the increase of fraction of the organic phase. β decreases from 0.66 to 0.30 from a fraction of 0 % to 20 %. Fujasová et al. (2007) studied the mass transfer in a coalescing system of water/air with

multiple impellers and achieved β and γ values of 0.687 and 0.530, respectively, which is not in line with the literature for coalescing systems for β (Van't Riet 1979). The same study was also performed for a Na_2SO_4 non-coalescing system with 1.254 and 0.572 for β and γ, respectively, which are clearly above. When comparing the physical properties with our obtained results, it is not possible to conclude wether our system is a non-coalescing system (β=0.0578 and γ=0.166). Even though γ values are closer to non-coalescing system, there is a small gap that might be due to the experiment values falling outside of the validity range for which Van't Riet (1979) tested his hypothesis ($500 < \frac{P_G}{V} < 10000\,\mathrm{W\,m^{-3}}$, $2 < V < 4000\,\mathrm{L}$).

When comparing with the results from Olle et al. (2006), one can see that our results seem to be somewhat consistent with the literature only for the γ exponent (γ=0.166, non-coalescing) while Olle et al. (2006)'s exponents reveal an antagonic behaviour, i.e. β=0.630 (non-coalescing) while γ=0.570 (coalescing).

On another note, when looking at b and δ coefficients (2.36×10^5 and 1.71, respectively), it is easy to quantify the theoretical enhancement with the lowest nanoparticle mass fraction used is: $1 + 2.36 \times 10^5 \times 0.00024^{1.71} = 1.098$, which translates into a 15.2 % mass transfer enhancement. On the other hand, for the highest nanoparticle mass fraction used the enhancement is 239.0 %.

As for Olle et al. (2006), this theoretical enhancement is: $1 + 4 \times 0.0025^{0.34} = 1.522$, resulting in a 52.2 % enhancement for the lowest nanoparticle mass fraction and 83.6 % for the highest mass fraction. Thus, our correlation seems to estimate fairly well the enhancement range by only means of nanoparticle loading (the maximum reported k_La enhancement in Chapter 3 is 230 %), whereas Olle et al. (2006)' correlation does not predict the mass transfer enhancement very accurately, since their k_La enhancements are up to 710 %.

5.3.4 Correlation for the interfacial area, a

The interfacial area was calculated for our results using Equation (5.4). In addition, a new correlation was also used with the inclusion of the Eötvos number

$$\mathrm{Eo} = \frac{(\rho - \rho_{\mathrm{G}})\, g L^2}{\sigma} \tag{5.16}$$

and a new exponent coefficient (δ),

$$\frac{d_{32}}{D} = \alpha \left(1 + b\phi^{\beta}\right) \mathrm{We}^{\gamma} \mathrm{Eo}^{\delta} \tag{5.17}$$

The Eötvos number is used to have an additional parameter that takes into account surface tension forces in the system, but detached from the impeller speed, which is included in the Weber number. The results showed for the first correlation an R^2 of 79.9 % (Figure 5.2a), which means the correlation that is used in gas-liquid systems holds somewhat applicable in the presence of nanoparticles. When considering the Eötvös number in the correlation, a higher 93.3 % R^2 (Figure 5.2b) is achieved. Thus, since the agreement between the experimental values and the estimation it might indicate than this nondimensional number is physically relevant and its use can improve the accuracy of the bubbles' diameter.

In terms of coefficients, it can be seen that both α coefficients are placed in the same order of magnitude (10^{-4}) for the correlationss. α values are two orders of magnitude lower than in the literature, although usually α values might not translate into any physical meaning. b seems to be 1-2 order of magnitude higher. It should be noted that our b values might be much higher than the literature (Brown and Pitt 1970; Calderbank 1958; Chatzi et al. 1989; Coulaloglou and Tavlarides 1976; Godfrey and Grilc 1977; Heuven and Beek 1971; Mlynek and Resnick 1972), since this is a new type of system tested for interfacial area enhancement, i.e. nanofluids, as opposed to classic organic

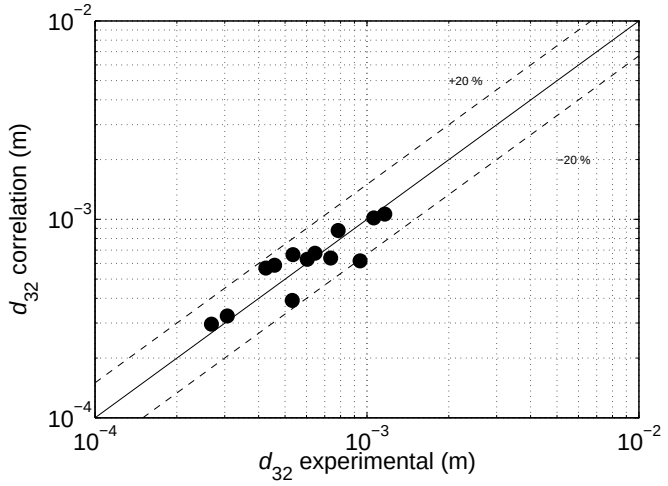

(a)

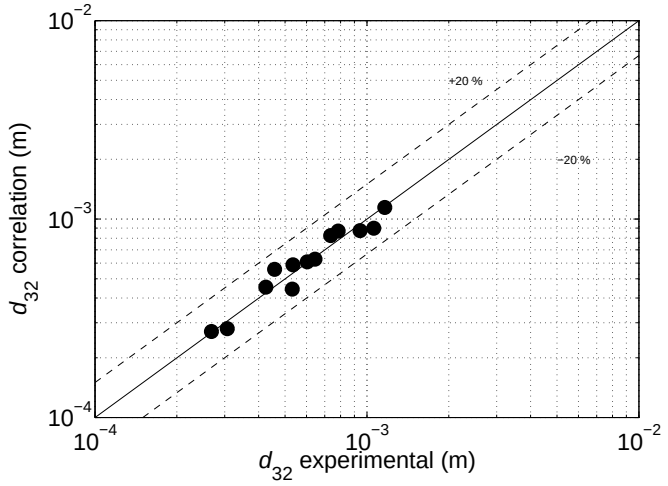

(b)

Figure 5.2: d_{32} correlation from model vs observed results for (a) Equation (5.4) and (b) Equation (5.17). The dashed lines represent a 20 % deviation.

phases. As for the β, both correlations present low values ($\sim 10^{-2}$). when compared with previous studies; again, in the past, only a linear relation was tested for the impact of an organic phase while for the nanoparticle loading, the impact might not be linear at all, as one can see from the results. As for the γ, Equation (5.4) yielded a positive

Table 5.3: Parameter values to various d_{32} correlations from literature for stirred tanks in the form of $\frac{d_{32}}{D} = \alpha\left(1 + b\phi^{\beta}\right)\mathrm{We}^{\gamma}\mathrm{Eo}^{\delta}$.

Reference	α	b	β	γ	δ
Calderbank (1958)	6.00×10^{-2}	9.00	1.00	−0.6000	
Chen and Middleman (1967)	5.30×10^{-2}	0		−0.6000	
Sprow (1967)	5.24×10^{-2}	0		−0.6000	
Brown and Pitt (1970)	5.10×10^{-2}	3.14	1.00	−0.6000	
Heuven and Beek (1971)	4.70×10^{-2}	2.50	1.00	−0.6000	
Mlynek and Resnick (1972)	5.80×10^{-2}	5.40	1.00	−0.6000	
Coulaloglou and Tavlarides (1976)	8.10×10^{-2}	4.47	1.00	−0.6000	
Godfrey and Grilc (1977)	5.80×10^{-2}	3.60	1.00	−0.6000	
Chatzi et al. (1989)	5.60×10^{-2}	11.0	1.00	−0.6000	
This work, Equation (5.4)	7.41×10^{-4}	503	0.0886	0.367	
This work, Equation (5.17)	3.07×10^{-5}	512	-0.098	−0.0886	0.441
This work, Equation (5.19)	1.75×10^{-2}			−0.115	0.457

coefficient which does not come in line with the usual effect of the Weber number on interfacial area. This result seems odd since the Weber number is impacted by the bubble diameter to the power of 3, thus the coefficient obtained should be negative since the interfacial area has a inversely proportinal relation to the bubble diameter. Moreover, Equation (5.17) yielded an expected negative γ of -0.0886, which, even though is not on the same level of previous studies, has a much more explainable behaviour than the previous γ. This might be due to the inclusion of the additional Eötvos number term, that may have affected the outcome of the γ coefficient. The new exponent δ deals with similar variables (ρ, d_B, σ) when comparing with γ and yielded a value of 0.441.

Regarding the theoretical interfacial area enhancement, it can be quantified as follows:

$$E_a = \frac{a_{\phi\neq 0}}{a_{\phi=0}} = \frac{\varepsilon_{\phi\neq 0}}{\varepsilon_{\phi=0}} \left(\frac{\mathrm{We}_{\phi=0}}{\mathrm{We}_{\phi\neq 0}}\right)^{\gamma} \left(\frac{\mathrm{Eo}_{\phi=0}}{\mathrm{Eo}_{\phi\neq 0}}\right)^{\delta} \frac{1}{(1 + b\phi^{\beta})} \tag{5.18}$$

which means that the enhancement can be quantified by the nanoparticle fraction.

Table 5.4: Gas holdup, Weber and Eötvös numbers sum-up for both experimental designs

Run	Gas holdup, ε	$\frac{\varepsilon_{\phi\neq0}}{\varepsilon_{\phi=0}}$	We	$\frac{\mathrm{We}_{\phi=0}}{\mathrm{We}_{\phi\neq0}}$	Eo	$\frac{Eo_{\phi=0}}{\mathrm{Eo}_{\phi\neq0}}$	σ (N m^{-1})
1	0.008	1.0	1.69×10^{-6}	0.2	0.161	0.3	0.0670
2	0.011	1.0	5.06×10^{-8}	33.3	0.010	10.1	0.0670
3	0.009	1.0	2.53×10^{-7}	1.2	0.048	1.0	0.0565
4	0.011	1.0	8.95×10^{-8}	18.8	0.016	6.6	0.0565
5	0.021	1.0	5.83×10^{-7}	17.9	0.079	6.7	0.0670
6	0.026	1.0	2.59×10^{-7}	23.6	0.031	8.1	0.0670
7	0.021	1.0	2.73×10^{-6}	3.8	0.236	2.3	0.0565
8	0.027	1.0	4.88×10^{-7}	12.5	0.050	5.0	0.0565
9	0.000	0.0					0.0615
10	0.028	1.0	1.08×10^{-6}	3.7	0.098	2.3	0.0615
11	0.017	1.0	5.96×10^{-6}	1.0	0.290	1.0	0.0710
12	0.018	1.1	6.95×10^{-7}	8.6	0.076	3.8	0.0533
13	0.014	1.0	9.46×10^{-7}	0.7	0.142	0.7	0.0615
14	0.021	1.0	2.59×10^{-7}	11.5	0.029	4.9	0.0615
15	0.018	1.0	4.95×10^{-7}	12.0	0.058	5.0	0.0615
A	0.008		2.93×10^{-7}		0.049		0.0710
B	0.011		1.68×10^{-6}		0.105		0.0710
C	0.020		1.04×10^{-5}		0.533		0.0710
D	0.026		6.12×10^{-6}		0.248		0.0710
E	0.027		4.00×10^{-6}		0.222		0.0710
F	0.017		5.96×10^{-6}		0.290		0.0710
G	0.013		6.55×10^{-7}		0.106		0.0710
H	0.020		2.99×10^{-6}		0.140		0.0710

While the variation between the maximum and minimum ratios for gas holdup (under 10 % change) are rather small, the change in the Weber number and the Eötvös number (from 20 to 3330 % and from 30 to 8830 %, respectively, Table 5.4) are much more pronounced. Thus, it is evident that even though the gas holdup has physical relevance, only the Weber and the Eötvös numbers seem to introduce the enhancement effect produced by the presence of nanoparticles (besides the nanoparticle loading). The theoretical enhancement for the highest nanoparticle loading is $1.1 \times 8.6^{-0.0886} \times 3.8^{0.441} \times \frac{1}{1+498\times0.00120^{0.0255}} = 0.0039$, which is in fact an interfacial area reduction of 99.61 %.

One puzzling fact from the results is that even though the bubble diameter estimation is of moderate accuracy (R^2 of 48.2 and 64.9 %), there seems to be a good agreement between the predicted and experimental values of interfacial area (R^2 of 70.9 and 85.8 %,

Figures 5.3a and 5.3b). This might be one additional confirmation that the loading of nanoparticles is not an important parameter for the estimation of bubble diameters, but probably the gas holdup plays an important role to predict the interfacial area, since it is the only one not being taken into consideration in the correlations with a weighting parameter.

Following this consideration an additional correlation was investigated. This time, Equation (5.17) was adjusted to the previous findings, and the nanoparticle loading was discarded. After applying the same methodology as before for the optimization of the parameters, the resulting equation is

$$\frac{d_{32}}{D} = 0.0175 \times \mathrm{We}^{-0.115}\mathrm{Eo}^{0.457} \tag{5.19}$$

The R^2 for this correlation was 84.2 % for the interfacial area and 64.8 % for the Sauter mean diameter (Figures 5.4a and 5.4b), which is similar to the accuracy achieved by Equation (5.17), but without the impact of the nanoparticle loading (since it has a nearly null impact). As for the theoretical interfacial area enhancement, it will be is calculated as $1.1 \times 8.6^{-0.115} \times 3.8^{0.457} = 1.5802$, which translate into an increase of around 58 %, as opposed to the 138 % improvement reported in Chapter 4. Even though it is much lower than the expected result, this shows that Equation (5.19) is much more suited to predict the interfacial area enhancement by simply resorting to operational and physical parameters.

Even though there is only one work (Olle et al. 2006) that provides a correlation for bubble diameter and consequently for interfacial area, in the presence of nanoparticles, it falls short for a complete comparison, since the only variable that is taken into account is the stirrer speed (Equation (5.3)). This might not be enough to predict bubbles behaviour in the presence of nanoparticles, since many (complex) forces are at play and there is still very few information on the mechanisms that are crucial for interfacial area

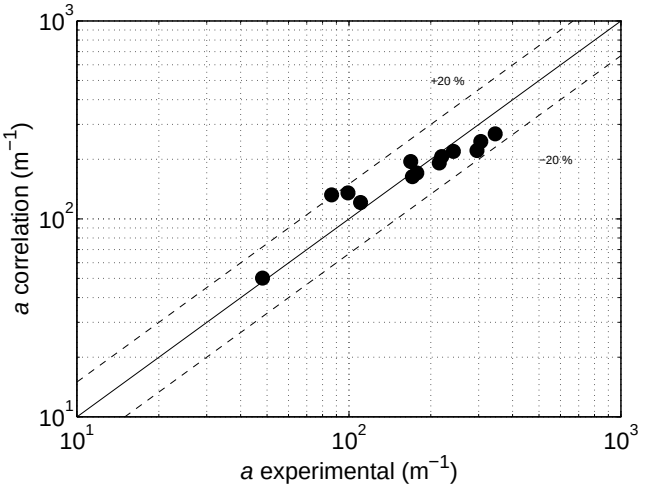

(a)

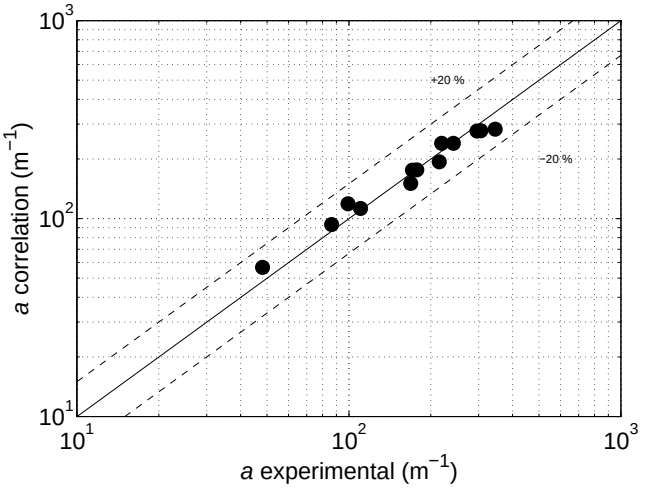

(b)

Figure 5.3: Interfacial area correlation from model vs observed results for (a) Equation (5.4) and (b) Equation (5.17). The dashed lines represent a 20 % deviation.

enhancement. In our work, we propose the first correlation for interfacial area (through Sauter mean diameter) with an above 80 % R^2 agreement with the experimental results.

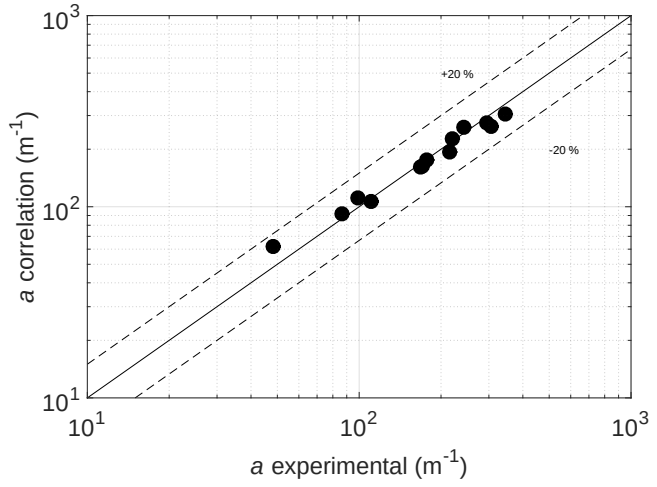

(a)

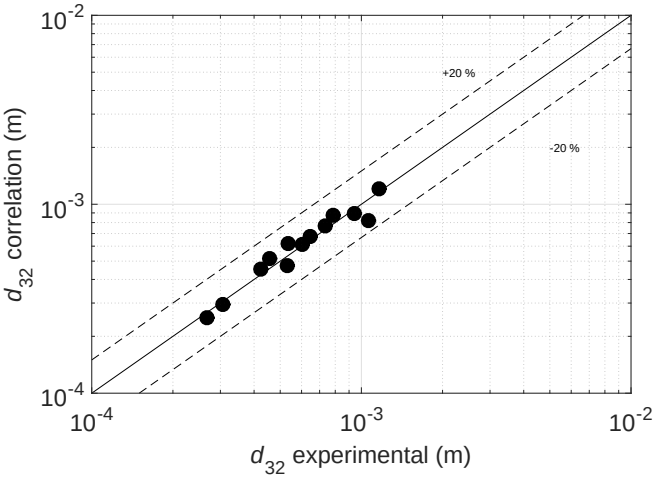

(b)

Figure 5.4: (a) Interfacial area and (b) d_{32} correlations from model vs observed results for Equation (5.19). The dashed lines represent a 20 % deviation.

5.4 Conclusions

In this chapter, it was possible to confirm the impact of some of the mechanisms that are referenced in the literature.

Firstly, it was possible to conclude that the Brownian motion is not responsible for the mass transfer enhancement since it takes a Brownian motioned particle ∼100 times longer to travel the same distance as the oxygen molecules take to diffuse. Still on the subject of particles motion, it was concluded that the microconvection in the nanoparticle' surrounding fluid impacts on the mass transfer since it takes the same time magnitude for a surrounding fluid particle to travel the previously mentioned distance as the oxygen diffusion.

Additionally, it was proved that the diffusion rate of oxygen (and consequently, the k_L) can be increased up to 8 % by the shuttling effect mechanism, but only if two experimental parameters taken from the literature can be assumed constant for our work. Through our results it was also possible to conclude that the boundary layer mixing mechanism might account for increase in the kL nearly up to 2-fold, since it reduces the boundary layer thickness down to 65 % (in average). Regarding the coalescence inhibition, there was no possible conclusion drawn from our results since there was no experimental apparatus set to determine drainage and bubble contact times, leaving the effect of this mechanism on mass transfer in the presence of nanoparticles as unknown.

Based on the central composite design it was possible to derive the correlation for $k_{\mathrm{L}}a$: $k_{\mathrm{L}}a = 1.40 \times 10^{-2} \left(\frac{P_{\mathrm{G}}}{V}\right)^{0.0578} V_{\mathrm{S}}^{0.166} \left(1 + 2.36 \times 10^{5} \phi^{1.71}\right)$. Solely resorting to the nanoparticle loading factor, it is possible to reasonably estimate the mass transfer enhancement. Therefore, (at least) some of the hypothesized mechanisms that impact on the liquid-side mass transfer coefficient (boundary layer mixing, shuttling effect and Brownian motion), indicated in the previous chapters, seem to be at play in the presence of our nanoparticles. Although it is not possible to validate the mechanisms at play through the proposed correlation, it is possible to hint that indeed the nanoparticle loading plays a very important role in the $k_L a$ enhancement.

As for the interfacial area, the correlation proposed is based on the Sauter mean diameter: $\frac{d_{32}}{D} = 0.0175 \times \mathrm{We}^{-0.115}\mathrm{Eo}^{0.457}$, $a = \frac{6\varepsilon}{d_{32}}$. The agreement of the results with

the correlation values is high, with an R^2 of 0.842, for the interfacial area. One of the conclusions that might be retained from the correlation developed for the interfacial area is that using dimensionless numbers that include the surface tension are of good use for the interfacial area estimation, which might validate the hypothesis of previous chapters. Thus, it can be concluded that, in fact, nanoparticles that include surfactants in its composition might assume a similar role as of a surfactant in the presence of a gas-liquid system.

The correlation proposed for the interfacial area estimation, in the presence of nanoparticle, uses the most complete set of physical parameters (ρ, ρ_G, σ, L, N) with highest impact on the interfacial area up to now.

CHAPTER 6

Conclusions and future work

6.1 Experimental Section

The oxygen mass transfer was assess in the presence of magnetic nanoparticles coated with an organic phase (oleic acid + Hitenol BC). The synthesized nanoparticles are composed of a 8.8 nm core, stable for a wide range of pH. The presence of the nanoparticles showed to be able to enhance the oxygen transfer up to 430 % for a 0.29 % mass fraction of nanoparticles. These nanoparticles showed also to achieve the comparable enhancements in oxygen mass transfer with 1000 times less power-input per unit volume. This might be a critical aspect when considering the scale up of any gas-liquid process in the chemical and biochemical industries, since the power input is usually one of the parameters mostly impacted by the up scaling.

With the application of an experimental design it was possible to derive the impact of the nanoparticles on mass transfer parameters: $k_{\mathrm{L}}a$, a and k_{L}. The $k_{\mathrm{L}}a$ achieved a maximum enhancement of 230 %, and the decoupled effect of the nanoparticles on each

a and k_{L} are 230 % and a 44 % enhancement, respectively.

It is possible to conclude that the mechanisms triggered by the nanoparticles are the ones that affect the interfacial area, which is most probably by the adsorption of the nanoparticle to the bubbles surface, inhibiting the coalescence of bubbles.

Another concluding remark from this study is that the enhancement of the interfacial area is physically constrained by the bubbles' total surface. The liquid side mass transfer coeffficient can be enhanced indefinitely, as long as the nanoparticles' loading does not cause the nanoparticles to collide with each other instead of travelling freely in their "shuttling" path.

6.2 Modeling section

Statistical models can describe fairly well the behaviour of the mass transfer parameters studied, in the presence of nanoparticles, with both $k_{\mathrm{L}}a$ and a presenting an R^2 around 0.80, while for k_{L} is around 0.65 (which might be explained by the indirect determination of this parameter).

As for mechanistic modeling, two models were proposed:

$$k_{\mathrm{L}}a = 1.40 \times 10^{-2} \left(\frac{P_{\mathrm{G}}}{V}\right)^{0.0578} V_{\mathrm{S}}^{0.166} \left(1 + 2.36 \times 10^{5} \phi^{1.71}\right)$$

and

$$\frac{d_{32}}{D} = 0.0175 \times \mathrm{We}^{-0.115}\mathrm{Eo}^{0.457}, a = \frac{6\varepsilon}{d_{32}}$$

The first correlation shows a rather low R^2 of 0.532, while for the interfacial area correlation the coefficient of determination is 0.842. This latter correlation is of particular importance since it uses the most complete set of physical parameters with highest impact on the interfacial area up to now.

6.3 Recommendations for future work

In terms of the synthesis of nanoparticles, it would be interesting to test different coatings that might have an even higher impact on both k_{L} and a such as other type of (stronger) surfactants. Stronger surfactants might lead to strong adsorption of the nanoparticles to the gas-liquid interface of the bubbles.

Another aspect that should be tested is the impact of the nanoparticle diameter on the k_{L} since higher/lower diameters would impact on the diffusion and Brownian motion of the particles and consequently the mass transfer rate.

A third aspect that would shed some light on the interfacial area enhancement by nanoparticles would be to use a smaller nanoparticle loading of the same synthesized nanoparticles. With this study it would be possible to conclude if there is a range where the interfacial area in directly proportional to to nanoparticle loading.

As a final recommendation, one of the downside of the current study is the determination of k_L indirectly. It would add value to this study to have a direct determination of k_{L}, such as by measuring the bubble diameters, using high speed cameras and further elaborate on the mechanism of bubble coalescence.

Nomenclature

$\left\langle (\Delta r)^2 \right\rangle$ Mean square displacement, m^2

A Lattice constant of unit cell of magnetite, Å

a Specific area, m^{-1}

B Baffle length, mm

B Constant determined by experiments in Equation (1.4), dimensionless

C Off-bottom clearance of impeller, mm

C Solute concentration in the liquid phase, $\mathrm{mol\,m}^{-3}$

C^* Solute concentration at gas-liquid interface, $\mathrm{mol\,m}^{-3}$

$C^*_{\mathrm{O}_2}$ Oxygen concentration at saturation, $\mathrm{mol\,m}^{-3}$

C_i Concentration of component i, M

$C_{\mathrm{NH_4OH}}$ Ammonium concentration, wt. %

$C_{\mathrm{O}_2,\mathrm{bulk}}$ Oxygen concentration in well-mixed bulk, $\mathrm{mol\,m}^{-3}$

C_{SO_3} Sulfite concentration, $\mathrm{mol\,L}^{-1}$

C_{d} Solute concentration in the dispersed phase, $\mathrm{mol\,m}^{-3}$

c_{p} Specific heat, $\mathrm{J\,kg}^{-1}\,\mathrm{K}^{-1}$

D Impeller diameter, mm

D Mass diffusivity of solute in water, $\mathrm{m^2\,s^{-1}}$

d Nanoparticle diameter, m

d_{NP} Diameter of nanoparticle, m

$D_{\mathrm{O_2,L}}$ Oxygen diffusion coefficient in the liquid phase, $\mathrm{m^2\,s^{-1}}$

D_{d} Mass diffusivity of solute in the dispersed phase, $\mathrm{m^2\,s^{-1}}$

d_{f} Fractal diameter of aggregates, m

D_{np} Mass diffusivity inside nanoparticles, $\mathrm{m^2\,s^{-1}}$

D_{n} Enhanced diffusion coefficient in the nanofluid, $\mathrm{m^2\,s^{-1}}$

H Henry's law constant, $\mathrm{mol\,L^{-1}\,atm^{-1}}$

H Partition coefficient of solute between dispersed and liquid phases, dimensionless

h_{B} Impeller blade height, mm

J Solute mass transfer rate, $\mathrm{m\,s^{-1}}$

k Thermal conductivity, $\mathrm{W\,m^{-1}\,K^{-1}}$

k_{L} Liquid side mass transfer coefficient, $\mathrm{m\,s^{-1}}$

K_b Base dissociation constant, M

k_n Reaction rate constant, $\mathrm{L^3\,mol^{-1}\,s^{-1}}$

k_{B} Boltzmann constant, $\mathrm{J\,K^{-1}}$

$k_{\mathrm{L}}a$ Volumetric mass transfer coefficient, $\mathrm{s^{-1}}$

l Length of each side of the unit cell in Figure 2.3, m

L_{NP} Distance between nanoparticles in a given cubic matrix, m

l_{B} Impeller blade length, mm

m Mass, kg

M_1 Mass of synthesized nanoparticles, g

m_i Mass of component i, g

m_{NP} Mass of a single nanoparticle, g

MM_i Molar mass of component i, $\mathrm{g\,mol^{-1}}$

n Reaction order, dimensionless

N_A Avogadro number, $\mathrm{mol^{-1}}$

N_{Fe} Number of iron atoms in a unit cell of magnetite, dimensionless

$p_{\mathrm{O_2,G}}$ Oxygen partial pressure in the gas phase, atm

$p_{\mathrm{O_2,L}}$ Oxygen partial pressure in the liquid phase, atm

$Purity_i$ Purity of component i, wt. %

Q Reaction rate in the liquid phase, $\mathrm{mol\,m^{-3}\,s^{-1}}$

q Constant determined by experiments in Equation (1.4), %

Q_{d} Reaction rate in the dispersed phase, $\mathrm{mol\,m^{-3}\,s^{-1}}$

R_1 Radius of nanoparticle core, m

R_{a} Gyration radius of an aggregate, m

r_p Particle radius, m

s Surface renewal frequency, s^{-1}

T Tank diameter, mm

T Temperature, K

t Time, s

t_B Time to travel a (Brownian) nanoparticle diameter, s

t_{md} Time to travel the mean displacement, s

t_m Time to diffuse dye through a nanoparticle diameter, s

t_p Aggregation time constant, s

V_{NH_4OH} Volume of ammonium, mL

x Distance in perpendicular direction to gas-liquid interface, m

Z Spacing between 2 adjacent molecules of oleate at nanoparticle surface, m

z Sulfite oxidation stoichiometry coefficient, dimensionless

Abbreviations

z Sulfite-to-oxygen stoichiometry ratio, dimensionless

OUR Oxygen uptake rate, $\mathrm{mol\,m^{-3}\,s^{-1}}$

Ha Hatta number, dimensionless

Pr Prandtl number, dimensionless

Re Reynolds number, dimensionless

Sc Schmidt number, dimensionless

Sh Sherwood number, dimensionless

Greek letters

α Thermal diffusivity, $\mathrm{m^2\,s^{-1}}$

δ Gas-liquid boundary layer thickness, m

$\delta_{1,2}$ Distance between gas-liquid interface and dispersed particles in the boundary layer, m

η Water viscosity, $\mathrm{N\,s\,m^{-2}}$

μ Dynamic viscosity, $\mathrm{kg\,m^{-1}\,s^{-1}}$

ν Kinematic viscosity, $\mathrm{m^2\,s^{-1}}$

ϕ Nanoparticle volume fraction, % (v/v)

ρ Fluid density, $\mathrm{kg\,m^{-3}}$

a Aggregate

f Fluid

int Primary particles in an aggregate

nf Nanofluid

p Primary particles

Bibliography

Abareshi, M., E. K. Goharshadi, S. M. Zebarjad, H. K. Fadafan, and A. Youseffi (2010). "Fabrication, characterization and measurement of thermal conductivity of Fe3O4 nanofluids". In: *Journal of Magnetism and Magnetic Materials* 322, pp. 3895–3901.

Albal, R. S., Y. T. Shah, A. L. Shumpe, and N. Carr (1983). "Mass transfer in multiphase agitated contactors." In: *Chemical Engineering Journal* 27, pp. 61–80.

Alper, E., B. Wichtendahl, and W.-D. Deckwer (Jan. 1980). "Gas absorption mechanism in catalytic slurry reactors". In: *Chemical Engineering Science* 35.1-2, pp. 217–222.

Amaral, P. F. F., M. G. Freire, M. H. M. Rocha-Leão, I. M. Marrucho, J. a. A. P. Coutinho, and M. A. Z. Coelho (2008). "Optimization of Oxygen Mass Transfer in a Multiphase Bioreactor With Perfluorodecalin as a Second Liquid Phase". In: *Biotechnology and Bioengineering* 99.3, pp. 588–598.

Amaris, C., M. Bourouis, and M. Vallès (Apr. 2014). "Passive intensification of the ammonia absorption process with NH3/LiNO3 using carbon nanotubes and advanced surfaces in a tubular bubble absorber". In: *Energy* 68, pp. 519–528.

Arai, K., M. Konno, Y. Matunaga, and S. Saito (1977). “Effect of dispersed-phase viscosity on the maximum stable drop size for breakup in turbulent flow”. In: *Journal of Chemical Engineering of Japan* 10.4, pp. 325–330.

Bahmanyar, A., N. Khoobi, M. R. Mozdianfard, and H. Bahmanyar (Aug. 2011). “The influence of nanoparticles on hydrodynamic characteristics and mass transfer performance in a pulsed liquid–liquid extraction column”. In: *Chemical Engineering and Processing: Process Intensification* 50.11-12, pp. 1198–1206.

Bailey, J. E. and D. F. Ollis (1986). *Biochemical Engineering Fundamentals*. 2nd editio. New York, United States of America: McGraw-Hill, Inc.

Bartholomew, W. H. (1960). “Scale-up of submerged fermentation”. In: *Advances in Applied Microbiology* 2, pp. 289–300.

Beenackers, A. A. C. M. and W. P. M. van Swaaij (1993). “Mass transfer in gas–liquid slurry reactors”. In: *Chemical Engineering Science* 48.18, pp. 3109–3139.

Beiki, H., M. N. Esfahany, and N. Etesami (Feb. 2013a). “Laminar forced convective mass transfer of γ-Al2O3/electrolyte nanofluid in a circular tube”. In: *International Journal of Thermal Sciences* 64, pp. 251–256.

— (Mar. 2013b). “Turbulent mass transfer of Al2O3 and TiO2 electrolyte nanofluids in circular tube”. In: *Microfluidics and Nanofluidics* 15.4, pp. 501–508.

Bro, R. (1996). “Multiway calibration. Multilinear PLS”. In: *Journal of Chemometrics* 10.1, pp. 47–61.

Brown, D. E. and K. Pitt (1970). “Drop break-up in a stirred liquid-liquid contactor”. In: *Proceedings Chemeca* 70, pp. 83–97.

Calabrese, R. V., C. Y. Wang, and N. P. Bryner (1986). "Drop breakup in turbulent stirred-tank contactors. Part III: correlations for mean size and drop size distribution". In: *AIChE Journal* 32.4, pp. 677–681.

Calderbank, P. H. (1958). "The interfacial area in gas-liquid contacting with mechanical agitation". In: *Transactions of the Institution of Chemical Engineers* 36, pp. 443–463.

— (1959). "Physical Rate Processes in Industrial Fermentation: Part II-The Interfacial Area in Gas-Liquid Contacting with and without Mechanical Agitation". In: *Transactions of the Institution of Chemical Engineers* 37, pp. 173–185.

Calderbank, P. H. and M. B. Moo-Young (Dec. 1961). "The continuous phase heat and mass transfer properties of dispersions." In: *Chemical Engineering Science* 16.1–2, pp. 39–54.

Cascaval, D., A.-I. Galaction, E. Folescu, and M. Turnea (Aug. 2006). "Comparative study on the effects of n-dodecane addition on oxygen transfer in stirred bioreactors for simulated, bacterial and yeasts broths". In: *Biochemical Engineering Journal* 31.1, pp. 56–66.

Cents, A. H. G. (2003). "Mass transfer and hydrodynamics in stirred gas-liquid-liquid contactors". PhD thesis. University of Twente.

Charoenrat, T., M. Ketudat-Cairns, M. Jahic, A. Veide, and S.-O. Enfors (2006). "Increased total air pressure versus oxygen limitation for enhanced oxygen transfer and product formation in a Pichia pastoris recombinant protein process". In: *Biochemical Engineering Journal* 30.2, pp. 205–211.

Chatzi, E. G., Asterios D. Gavrielides, and C. Kiparissides (1989). "Generalized Model for Prediction of the Steady-State Drop Size Distributions in Batch

Stirred Vessels". In: *Industrial & Engineering Chemistry Research* 28, pp. 1704–1711.

Chen, G., Y. Ma, P. Su, and B. Fang (Aug. 2012). "Direct binding glucoamylase onto carboxyl-functioned magnetic nanoparticles". In: *Biochemical Engineering Journal* 67, pp. 120–125.

Chen, H. T. and S. Middleman (1967). "Drop size distribution in agitated liquid-liquid systems". In: *AIChE Journal* 13.5, pp. 989–995.

Choi, S. U. S. and J. A. Eastman (1995). *Enhancing thermal conductivity of fluids with nanoparticles*. Ed. by D. A. Siginer and H. P. Wang. New York.

Cichy, P. T. and T. W. F. Russell (1969). "Reactor model parameters". In: *Industrial and Engineering Chemistry* 61.8, pp. 15–26.

Colella, D., D. Vinci, R. Bagatin, M. Masi, and E. ABu Bakr (1999). *A study on coalescence and breakage mechanisms in three different bubble columns*.

Cooper, C. M., G. A. Fernstrom, and S. A. Miller (1944). "Performance of agitated gas-liquid contactors". In: *Industrial and Engineering Chemistry* 36.6, pp. 504–509.

Coulaloglou, C. A. and L. L. Tavlarides (1976). "Drop size distribution and coalescence frequencies of liquid—liquid dispersions in flow vessels". In: *AIChE Journal* 22.2, pp. 289–297.

Dagaonkar, M. V., H. J. Heeres, A. A. C. M. Beenackers, and V. G. Pangarkar (Apr. 2003). "The application of fine TiO2 particles for enhanced gas absorption". In: *Chemical Engineering Journal* 92.1-3, pp. 151–159.

Danckwerts, P. V. (1970). *Gas-Liquid Reactions*. McGraw-Hill, Inc.

Delafosse, A., J. Morchain, P. Guiraud, and A. Liné (Apr. 2009). "Trailing vortices generated by a Rushton turbine: Assessment of URANS and large Eddy

simulations". In: *Chemical Engineering Research and Design* 87.4, pp. 401–411.

Demmink, J. F., A. Mehra, and A. A. C. M. Beenackers (1998). "Gas absorption in the presence of particles showing interfacial affinity: case of fine sulfur precipitates". In: *Chemical Engineering Science* 53.16, pp. 2885–2902.

Ditsch, A., P. E. Laibinis, D. I. C. Wang, and T. A. Hatton (June 2005a). "Controlled clustering and enhanced stability of polymer-coated magnetic nanoparticles." In: *Langmuir* 21.13, pp. 6006–18.

Ditsch, A., S. Lindenmann, P. E. Laibinis, D. I. C. Wang, and T. A. Hatton (Aug. 2005b). "High-Gradient Magnetic Separation of Magnetic Nanoclusters". In: *Industrial & Engineering Chemistry Research* 44.17, pp. 6824–6836.

Ditsch, A., J. Yin, P. E. Laibinis, D. I. C. Wang, and T. A. Hatton (2006). "Ion-exchange purification of proteins using magnetic nanoclusters". In: *Biotechnology Progress* 22.4, pp. 1153–1162.

Dumont, E and H Delmas (June 2003). "Mass transfer enhancement of gas absorption in oil-in-water systems: a review". In: *Chemical Engineering and Processing* 42.6, pp. 419–438.

Fang, X., Y. Xuan, and Q. Li (2009). "Experimental investigation on enhanced mass transfer in nanofluids". In: *Applied Physics Letters* 95.20, p. 203108.

Feng, W., J. Wen, J. Fan, Q. Yuan, X. Jia, and Y. Sun (Dec. 2005). "Local hydrodynamics of gas–liquid-nanoparticles three-phase fluidization". In: *Chemical Engineering Science* 60.24, pp. 6887–6898.

Feng, X. and D. W. Johnson (June 2012). "Mass transfer in SiO2 nanofluids: A case against purported nanoparticle convection effects". In: *International Journal of Heat and Mass Transfer* 55.13-14, pp. 3447–3453.

Ferreira, A. R., F. Ataíde, M. von Stosch, J. M. L. Dias, J. J. Clemente, A. E. Cunha, and R. Oliveira (Nov. 2012). "Application of adaptive DO-stat feeding control to Pichia pastoris X33 cultures expressing a single chain antibody fragment (scFv)". In: *Bioprocess and Biosystems Engineering* 35.9, pp. 1603–1614.

Frössling, N. (1938). "Über die Verdünstung fallenden Tropfen". In: *Gerlands Beitage Geophys.* 52, pp. 170–216.

Fujasová, M., V. Linek, and T. Moucha (2007). "Mass transfer correlations for multiple-impeller gas–liquid contactors. Analysis of the effect of axial dispersion in gas and liquid phases on "local" kLa values measured by the dynamic pressure method in individual stages of the vessel". In: *Chemical Engineering Science* 62, pp. 1650–1669.

Galaction, A.-I., D. Cascaval, C. Oniscu, and M. Turnea (Aug. 2004). "Prediction of oxygen mass transfer coefficients in stirred bioreactors for bacteria, yeasts and fungus broths". In: *Biochemical Engineering Journal* 20.1, pp. 85–94.

Galaction, A.-I., D. Cascaval, M. Turnea, and E. Folescu (2005). "Enhancement of oxygen mass transfer in stirred bioreactors using oxygen-vectors 2. Propionibacterium shermanii broths". In: *Bioprocess and Biosystems Engineering* 27.4, pp. 263–271.

Garcia-Ochoa, F. and E. Gomez (June 2004). "Theoretical prediction of gas–liquid mass transfer coefficient, specific area and hold-up in sparged stirred tanks". In: *Chemical Engineering Science* 59.12, pp. 2489–2501.

Gerardi, C., D. Cory, J. Buongiorno, L.-W. Hu, and T. McKrell (2009). "Nuclear magnetic resonance-based study of ordered layering on the surface of alumina nanoparticles in water". In: *Applied Physics Letters* 95.25, p. 253104.

Godbole, S. P., A. Schumpe, and Y. T. Shah (1990). “The effect of solid wettability on gas–liquid mass transfer in a slurry bubble column”. In: *Chemical Engineering Science* 45, pp. 3593–3595.

Godfrey, J. C. and V. Grilc (1977). “Drop size and drop size distribution for liquid–liquid dispersions in agitated tanks of square cross section”. In: *Proceedings of the 2nd European Conference on Mixing*, C1: 1–20.

Guardia, P., B. Batlle-Brugal, A. G. Roca, O. Iglesias, M. P. Morales, C. J. Serna, A. Labarta, and X. Batlle (2007). “Surfactant effects in monodisperse magnetite nanoparticles of controlled size”. In: *Journal of Magnetism and Magnetic Materials* 316.2, e756–e759.

Hashimoto, S., K. Natami, and Y. Inoue (2011). “Mechanism of mixing enhancement with baffles in impeller-agitated vessel, part I: A case study based on cross-sections of streak sheet”. In: *Chemical Engineering Science* 66, pp. 4690–4701.

Hassan, I. T. M. and C. W. Robinson (1977). “Oxygen transfer in mechanically agitated systems containing dispersed hydrocarbon”. In: *Biotechnology and Bioengineering* 19, pp. 661–682.

Hassan, M. A., N. D. N. Sin, B. A. Ghani, and M. I. A. Karim (1995). “Correlation between volumetric oxygen transfer coefficient and power requirement in citric acid fermentation by Aspergillus niger”. In: *Pertanika Journal Tropical Agric Science Agric Science* 18.3, pp. 183–186.

Heuven, J. W. van and W. J. Beek (1971). “Power input, drop size and minimum stirrer speed for liquid-liquid dispersions in stirred vessels”. In: *Proceedings of the International Solvent Extraction Conference*. Vol. 70.

Higbie, R. (1935). “The rate of absorption of a pure gas into still liquid during short periods of exposure”. In: *Transactions of the American Institution Chemical Engineers* 35, pp. 36–60.

Ho, C. S., L. K. Ju, and R. F. Baddour (1990). “Enhancing penicillin fermentations by increased oxygen solubility through the addition of n-hexadecane”. In: *Biotechnology and Bioengineering* 36, pp. 1110–1118.

Holstvoogd, R., W. P. M. van Swaaij, and L. van Dierendonck (1988). “The absorption of gases in aqueous activated carbon slurries enhanced by adsorbing or catalytic particles”. In: *Chemical Engineering Science* 43.8, pp. 2181–2187.

Hwang, B.-J., S.-W. Park, D.-W. Park, K.-J. Oh, and S.-S. Kim (May 2009). “Absorption of carbon dioxide into aqueous colloidal silica solution with different sizes of silica particles containing monoethanolamine”. In: *Korean Journal of Chemical Engineering* 26.3, pp. 775–782.

Ingram, D. R., C. Kotsmar, K. Y. Yoon, S. Shao, C. Huh, S. L. Bryant, T. E. Milner, and K. P. Johnston (Nov. 2010). “Superparamagnetic nanoclusters coated with oleic acid bilayers for stabilization of emulsions of water and oil at low concentration.” In: *Journal of Colloid and Interface Science* 351.1, pp. 225–32.

Ju, L. K. and C. S. Ho (1989). “Oxygen diffusion coefficient and solubility an n-hexadecane”. In: *Biotechnology and Bioengineering* 34, pp. 1221–1224.

Jung, J.-Y., J. W. Lee, and Y. T. Kang (Aug. 2012). “CO2 absorption characteristics of nanoparticle suspensions in methanol”. In: *Journal of Mechanical Science and Technology* 26.8, pp. 2285–2290.

Kang, Y. T., H. J. Kim, and K. I. Lee (Aug. 2008). "Heat and mass transfer enhancement of binary nanofluids for H2O/LiBr falling film absorption process". In: *International Journal of Refrigeration* 31.5, pp. 850–856.

Karimi, A., F. Golbabaei, M. Neghab, M. R. Mehrnia, K. Mohammad, M. R. Pourmand, and A. Nikpey (2011). "Investigation of oxygen transfer in a Two-phase partition stirred tank bioreactor in the presence of silicone oil". In: *Chemical and Biochemical Engineering Quarterly* 25.2, pp. 209–219.

Kars, R., R. Best, and A. Drinkenburg (June 1979). "The sorption of propane in slurries of active carbon in water". In: *The Chemical Engineering Journal* 17.3, pp. 201–210.

Kawase, Y. and M. Moo-Young (1991). "Oxygen transfer in slurry bioreactors." In: *Biotechnology and Bioengineering* 37.10, pp. 960–966.

Keshishian, N., M. N. Esfahany, and N. Etesami (Aug. 2013). "Experimental investigation of mass transfer of active ions in silica nanofluids". In: *International Communications in Heat and Mass Transfer* 46, pp. 148–153.

Khan, A. (Mar. 2008). "Preparation and characterization of magnetic nanoparticles embedded in microgels". In: *Materials Letters* 62.6-7, pp. 898–902.

Kies, F. K., B. Benadda, and M. Otterbein (Nov. 2004). "Experimental study on mass transfer of a co-current gas–liquid contactor performing under high gas velocities". In: *Chemical Engineering and Processing* 43.11, pp. 1389–1395.

Kim, H., J. Jeong, and Y. T. Kang (May 2012). "Heat and mass transfer enhancement for falling film absorption process by SiO2 binary nanofluids". In: *International Journal of Refrigeration* 35.3, pp. 645–651.

Kim, J. H., C. W. Jung, and Y. T. Kang (2014). “Mass transfer enhancement during CO2 absorption process in methanol/Al2O3 nanofluids”. In: *International Journal of Heat and Mass Transfer* 76, pp. 484–491.

Kim, J.-K., J. Y. Jung, and Y. T. Kang (Jan. 2006). “The effect of nano-particles on the bubble absorption performance in a binary nanofluid”. In: *International Journal of Refrigeration* 29.1, pp. 22–29.

— (Jan. 2007). “Absorption performance enhancement by nano-particles and chemical surfactants in binary nanofluids”. In: *International Journal of Refrigeration* 30.1, pp. 50–57.

Kim, W.-g., H. U. Kang, K.-m. Jung, and S. H. Kim (Aug. 2008). “Synthesis of Silica Nanofluid and Application to CO2 Absorption”. In: *Separation Science and Technology* 43.11, pp. 3036–3055.

Kluytmans, J. H. J., B. G. M. van Wachem, B. F. M. Kuster, and J. C. Schouten (Oct. 2003). “Mass transfer in sparged and stirred reactors: influence of carbon particles and electrolyte”. In: *Chemical Engineering Science* 58.20, pp. 4719–4728.

Komati, S. and A. K. Suresh (2008). “CO2 absorption into amine solutions: a novel strategy for intensification based on the addition of ferrofluids”. In: *Journal of Chemical Technology and Biotechnology* 83, pp. 1094–1100.

— (Jan. 2010). “Anomalous Enhancement of Interphase Transport Rates by Nanoparticles: Effect of Magnetic Iron Oxide on Gas-Liquid Mass Transfer”. In: *Industrial & Engineering Chemistry Research* 49.1, pp. 390–405.

Kordač, M. and V. Linek (2006). “Mechanism of enhanced gas absorption in presence of fine solid particles. Effect of molecular diffusivity on mass transfer coefficient in stirred cell”. In: *Chemical Engineering Science* 61, pp. 7125–7132.

Kordač, M., M. Opletal, and V. Linek (Jan. 2011). "Measurement of mass transfer characteristics of gas/liquid reactors by sulphite system using on-line monitoring UV absorption". In: *Chemical Engineering Journal*.

Kral, K. M. (2005). "Compatibility and toxicity of polymer-coated magnetic nanoparticles on mammalian cell systems". M.Sc. Massachusetts Institute of Technology.

Krishnamurthy, S, P. Bhattacharya, P. E. Phelan, and R. S. Prasher (Mar. 2006). "Enhanced mass transport in nanofluids." In: *Nano Letters* 6.3, pp. 419–23.

Lagisetty, J., P. Das, R. Kumar, and K. Gandhi (1986). "Breakage of viscous and non-Newtonian drops in stirred dispersions". In: *Chemical Engineering Science* 41.1, pp. 65–72.

Laurent, A., J. C. Charpentier, and C. Prost (1974). "Etude de la cinetique heterogene globale de l'oxydation catalytique d'une solution aqueuse de sulfite de sodium par l'oxygene gazeux en presence de sulfate de cobalt". In: *Journal de Chimie Physique* 71.4, pp. 613–614.

Lee, J. W. and Y. T. Kang (May 2013). "CO2 absorption enhancement by Al2O3 nanoparticles in NaCl aqueous solution". In: *Energy* 53, pp. 206–211.

Lee, J. W., J.-Y. Jung, S.-G. Lee, and Y. T. Kang (Dec. 2011). "CO2 bubble absorption enhancement in methanol-based nanofluids". In: *International Journal of Refrigeration* 34.8, pp. 1727–1733.

Lee, J. K., J. Koo, H. Hong, and Y. T. Kang (Mar. 2010). "The effects of nanoparticles on absorption heat and mass transfer performance in NH3H2O binary nanofluids". In: *International Journal of Refrigeration* 33.2, pp. 269–275.

Lewis, A. C. and D. J. Roberts (Jan. 2005). “New Techniques for Following the Oxidation of Sodium Sulfite in Mass-Transfer Studies”. In: *Industrial & Engineering Chemistry Research* 44.1, pp. 183–185.

Lewis, W. K. and W. G. Whitman (1924). “Principles of Gas Absorption.” In: *Industrial and Engineering Chemistry* 16.12, pp. 1215–1220.

Li, J., D. Liang, K. Guo, R. Wang, and S. Fan (2006). “Formation and dissociation of HFC134a gas hydrate in nano-copper suspension”. In: *Energy Conversion and Management* 47.2, pp. 201–210.

Linek, V. and P. Benes (1976). “A study of the mechanism of gas absorption into oil-water emulsions”. In: *Chemical Engineering Science* 31.11, pp. 1037–1046.

Linek, V. and V. Vacek (1981). “Chemical engineering use of catalyzed sulfite oxidation kinetics for the determination of mass transfer characteristics of gas-liquid contactors”. In: *Chemical Engineering Science* 36.11, pp. 1747–1768.

Linek, V., V. Vacek, and P. Benes (1987). “A critical review and experimental verification of the correct use of the dynamic method for the determination of oxygen transfer in aerated agitated vessels to water, electrolyte solutions and viscous liquids”. In: *Chemical Engineering Journal* 34, pp. 11–34.

Linek, V., T. Moucha, and J. Sinkule (1996). “Gas-liquid mass transfer in vessels stirred with multiple impellers - I. Gas-liquid mass transfer characteristics in individual stages”. In: *Chemical Engineering Science* 51, pp. 3203–3212.

Linek, V., T. Moucha, and M. Kordač (2005a). “Mechanism of mass transfer from bubbles in dispersions - Part I. Danckwerts’ plot method with sulphite solutions in the presence of viscosity and surface tension changing agents”. In: *Chemical Engineering and Processing* 44, pp. 353–361.

Linek, V., M. Kordač, and T. Moucha (2005b). “Mechanism of mass transfer from bubbles in dispersions - Part II: Mass transfer coefficients in stirred gas–liquid reactor and bubble column”. In: *Chemical Engineering and Processing* 44, pp. 121–130.

— (Jan. 2006). “Evaluation of the optical sulfite oxidation method for the determination of the interfacial mass transfer area in small-scale bioreactors”. In: *Biochemical Engineering Journal* 27.3, pp. 264–268.

Linek, V., M. Kordač, and M. Soni (2008). “Mechanism of gas absorption enhancement in presence of fine solid particles in mechanically agitated gas–liquid dispersion. Effect of molecular diffusivity”. In: *Chemical Engineering Science* 63, pp. 5120–5128.

Littlejohns, J. V. and A. J. Daugulis (May 2007). “Oxygen transfer in a gas–liquid system containing solids of varying oxygen affinity”. In: *Chemical Engineering Journal* 129.1-3, pp. 67–74.

Lowe, K. C. (2002). “Perfluorochemical respiratory gas carriers: benefits to cell culture systems”. In: *Journal of Fluorine Chemistry* 118.1–2, pp. 19–26.

Lu, S., M. Xing, Y. Sun, and X. Dong (Sept. 2013). “Experimental and Theoretical Studies of CO2 Absorption Enhancement by Nano-Al2O3 and Carbon Nanotube Particles”. In: *Chinese Journal of Chemical Engineering* 21.9, pp. 983–990.

Lundstedt, T., E. Seifert, L. Abramo, B. Thelin, A. Nyström, J. Pettersen, and R. Bergman (Aug. 1998). “Experimental design and optimization”. In: *Chemometrics and Intelligent Laboratory Systems* 42.1-2, pp. 3–40.

Ma, X., F. Su, J. Chen, and Y. Zhang (2007). “Heat and mass transfer enhancement of the bubble absorption for a binary nanofluid”. In: *Journal of Mechanical Science and Technology* 21, pp. 1813–1818.

Ma, X., F. Su, J. Chen, T. Bai, and Z. Han (Aug. 2009). “Enhancement of bubble absorption process using a CNTs-ammonia binary nanofluid”. In: *International Communications in Heat and Mass Transfer* 36.7, pp. 657–660.

Manikandan, S., N. Karthikeyan, K. S. Suganthi, and K. S. Rajan (2012). “Enhancement of volumetric mass transfert coefficient for oxygen transfer using Fe2O3-water nanofluids”. In: *Asian Journal of Scientific Research* 5.4, pp. 271–277.

Mattiasson, B. and P. Adlercreutz (1983). “Use of perfluorochemicals for oxygen-supply to immobilized cells”. In: *Annals of the New York Academy of Sciences* 413, pp. 545–547.

— (1987). “Perfluorochemicals in biotechnology”. In: *Trends in Biotechnology* 5.9, pp. 250–254.

McMillan, J. D. and D. I. C. Wang (1987). “Enhanced oxygen transfer using oil-in-water dispersions.” In: *Annals of the New York Academy of Sciences* 506.Biochemical Engineering V, pp. 569–582.

— (1990). “Mechanisms of oxygen transfer enhancement during submerged cultivation in perfluorochemical-in-water dispersions”. In: *Annals of the New York Academy of Sciences* 589.Biochemical Engineering VI, pp. 283–300.

Michel, B. J. and S. A. Miller (1962). “Power requirements of gas-liquid agitated systems”. In: *American Institute of Chemical Engineering Journal* 8.2, pp. 262–266.

Mlynek, Y. and W. Resnick (1972). “Drop sizes in an agitated liquid-liquid system”. In: *AIChE Journal* 18.1, pp. 122–127.

Moeser, G. D., K. A. Roach, W. H. Green, P. E. Laibinis, and T. A. Hatton (Sept. 2002). “Water-Based Magnetic Fluids as Extractants for Synthetic Organic Compounds”. In: *Industrial & Engineering Chemistry Research* 41.19, pp. 4739–4749.

Montes, F. J., J. Catan, and M. A. Galan (Sept. 1999). “Prediction of kLa in yeast broths”. In: *Process Biochemistry* 34.6–7, pp. 549–555.

Moo-Young, M. and H. W. Blanch (1981). “Design of biochemical reactors. Mass transfer criteria for simple and complex systems”. In: *Reactors and Reactions*. Vol. 19. Springer Berlin Heidelberg. Chap. Advances I, pp. 1–69.

Moraveji, M. K., M. Golkaram, and R. Davarnejad (Apr. 2013). “Effect of CuO nanoparticle on dissolution of methane in water”. In: *Journal of Molecular Liquids* 180, pp. 45–50.

Nagy, E. (1995). “Three-phase mass transfer: one-dimensional heterogenous model”. In: *Chemical Engineering Science* 50.5, pp. 827–836.

— (June 2003). “On the three-phase mass transfer with solid particles adhered to the gas-liquid interface”. In: *Central European Journal of Chemistry* 1.2, pp. 160–177.

Nagy, E. and P. Hadik (2003). “Three-phase mass transfer: effect of the size distribution”. In: *Industrial & Engineering Chemistry Research* 42, pp. 5363–5372.

Nagy, E. and A. Moser (1995). “Three-phase mass transfer: improved pseudo-homogeneous model”. In: *American Institute of Chemical Engineering Journal* 41.1, pp. 23–34.

Nagy, E., T. Feczko, and B. Koroknai (2007). “Enhancement of oxygen mass transfer rate in the presence of nanosized particles”. In: *Chemical Engineering Science* 62, pp. 7391–7398.

Narita, A., K. Naka, and Y. Chujo (Mar. 2009). “Facile control of silica shell layer thickness on hydrophilic iron oxide nanoparticles via reverse micelle method”. In: *Colloids and Surfaces A: Physicochemical and Engineering Aspects* 336.1-3, pp. 46–56.

Nielsen, D. R., A. J. Daugulis, and P. J. McLellan (Sept. 2003). “A novel method of simulating oxygen mass transfer in two-phase partitioning bioreactors.” In: *Biotechnology and Bioengineering* 83.6, pp. 735–42.

Nielsen, J., J. Villadsen, and G. Lidén (1994). *Bioreaction Engineering Principles*. 2nd editio. Springer.

Nishikawa, M., F. Mori, and S. Fujieda (1987a). “Average drop size in a liquid-liquid phase mixing vessel”. In: *Journal of Chemical Engineering of Japan* 20.1, pp. 82–88.

Nishikawa, M., F. Mori, S. Fujieda, and T. Kayama (1987b). “Scale-up of liquid-liquid phase mixing vessel”. In: *Journal of Chemical Engineering of Japan* 20.5, pp. 454–459.

Nocentini, M., F. Magelli, G. Pasquali, and D. Fajner (Jan. 1988). “A fluid-dynamic study of a gas—liquid, non-standard vessel stirred by multiple impellers”. In: *The Chemical Engineering Journal* 37.1, pp. 53–59.

Olle, B. (2006). “Mechanistic modeling of increased oxygen transport using functionalized magnetic fluids in bioreactors”. Ph.D. Massachusetts Institute of Technology.

Olle, B., S. Bucak, T. C. Holmes, L. E. Bromberg, T. A. Hatton, and D. I. C. Wang (May 2006). "Enhancement of oxygen mass transfer using functionalized magnetic nanoparticles". In: *Industrial & Engineering Chemistry Research* 45.12, pp. 4355–4363.

Ozturk, S., Y. A. Hassan, and V. M. Ugaz (Feb. 2010). "Interfacial complexation explains anomalous diffusion in nanofluids." In: *Nano Letters* 10.2, pp. 665–71.

Painmanakul, P., J. Wachirasak, M. Jamnongwong, and G. Hebrard (Nov. 2009). "Theoretical Prediction of Volumetric Mass Transfer Coefficient (kLa) for Designing an Aeration Tank". In: *Engineering Journal* 13.3, pp. 13–28.

Pang, C., W. Wu, W. Sheng, H. Zhang, and Y. T. Kang (Dec. 2012). "Mass transfer enhancement by binary nanofluids (NH3/H2O + Ag nanoparticles) for bubble absorption process". In: *International Journal of Refrigeration* 35.8, pp. 2240–2247.

Park, S.-W., B.-S. Choi, and J.-W. Lee (Oct. 2006a). "Chemical Absorption of Carbon Dioxide into Aqueous Colloidal Silica Solution with Diethanolamine". In: *Separation Science and Technology* 41.14, pp. 3265–3278.

Park, S.-w., B.-s. Choi, and J.-w. Lee (2006b). "Effect of elasticity of aqueous colloidal silica solution on chemical absorption of carbon dioxide with 2-amino-2-methyl-1-propanol". In: *Korea-Australia Rheology Journal* 18.3, pp. 133–141.

Park, S.-w., B.-s. Choi, S.-s. Kim, and J.-w. Lee (2007). "Chemical Absorption of Carbon Dioxide into Aqueous Colloidal Silica Solution Containing Monoethanolamine". In: *Journal of Industrial Engineering Chemistry* 13.1, pp. 133–142.

Park, S.-W., B.-S. Choi, S.-S. Kim, B.-D. Lee, and J.-W. Lee (Mar. 2008). "Absorption of carbon dioxide into aqueous colloidal silica solution with diisopropanolamine". In: *Journal of Industrial and Engineering Chemistry* 14.2, pp. 166–174.

Perez, J. and O. C. Sandall (1974). "Gas absorption by non-Newtonian fluids in agitated vessels." In: *American Institute of Chemical Engineering Journal* 20, pp. 770–775.

Prasher, R., P. Bhattacharya, and P. E. Phelan (June 2006a). "Brownian-motion-based convective-conductive model for the effective thermal conductivity of nanofluids". In: *Journal of Heat Transfer* 128.6, pp. 588–595.

Prasher, R., P. E. Phelan, and P. Bhattacharya (2006b). "Effect of aggregation kinetics on the thermal conductivity of nanoscale colloidal solutions (nanofluid)". In: *Nano Letters* 6.7, pp. 1529–1534.

Richards, J. W. (1961). "Studies in aeration and agitation". In: *Progress in Industrial Microbiology* 3, pp. 143–172.

Ruthiya, K. C., B. F. M. Kuster, and J. C. Schouten (2003a). "Gas-liquid Mass Transfer Enhancement in a Surface Aeration Stirred Slurry Reactors". In: *The Canadian Journal of Chemical Engineering* 81.August, pp. 632–639.

Ruthiya, K. C., J. van Der Schaaf, B. F. M. Kuster, and J. C. Schouten (Dec. 2003b). "Mechanisms of physical and reaction enhancement of mass transfer in a gas inducing stirred slurry reactor". In: *Chemical Engineering Journal* 96.1-3, pp. 55–69.

Saien, J. and H. Bamdadi (Apr. 2012). "Mass Transfer from Nanofluid Single Drops in Liquid–Liquid Extraction Process". In: *Industrial & Engineering Chemistry Research* 51.14, pp. 5157–5166.

Sara, O., F. İçer, S. Yapici, and B. Sahin (Apr. 2011). “Effect of suspended CuO nanoparticles on mass transfer to a rotating disc electrode”. In: *Experimental Thermal and Fluid Science* 35.3, pp. 558–564.

Sardeing, R., P. Painmanakul, and G. Hébrard (Oct. 2006). “Effect of surfactants on liquid-side mass transfer coefficients in gas–liquid systems: A first step to modeling”. In: *Chemical Engineering Science* 61.19, pp. 6249–6260.

Shen, L., P. E. Laibinis, and T. A. Hatton (1999). “Bilayer Surfactant Stabilized Magnetic Fluids: Synthesis and Interactions at Interfaces”. In: *Langmuir* 15.2, pp. 447–453.

Shen, Y., J. Tang, Z. Nie, Y. Wang, Y. Ren, and L. Zuo (Aug. 2009). “Preparation and application of magnetic Fe3O4 nanoparticles for wastewater purification”. In: *Separation and Purification Technology* 68.3, pp. 312–319.

Smith, J., K. Van’t Riet, and J. Middleton (1977). “Scale up of agitated gas-liquid reactors for mass transfer”. In: *Second European Conference on Mixing*, F4 –51 t0 66.

Sprow, F. B. (1967). “Distribution of drop sizes produced in turbulent liquid—liquid dispersion”. In: *Chemical Engineering Science* 22.3, pp. 435–442.

Subba-Rao, V., P. M. Hoffmann, and A. Mukhopadhyay (Oct. 2011). “Tracer diffusion in nanofluids measured by fluorescence correlation spectroscopy”. In: *Journal of Nanoparticle Research* 13.12, pp. 6313–6319.

Suresh, A. K., T. Sridhar, and O. E. Potter (Jan. 1988). “Mass transfer and solubility in autocatalytic oxidation of cyclohexane”. In: *AIChE Journal* 34.1, pp. 55–68.

Suresh, S., V. C. Srivastava, and I. M. Mishra (2009). "Techniques for oxygen transfer measurement in bioreactors: a review". In: *Journal of Chemical Technology and Biotechnology* 84.8, pp. 1091–1103.

Swiniarski, R. P. (1992). "Rates and efficiencies of oxygen transfer by gas pumping agitators in gas-liquid mixing systems". M.Sc. University of British Columbia.

Turanov, A. N. and Y. V. Tolmachev (Sept. 2009). "Heat- and mass-transport in aqueous silica nanofluids". In: *Heat and Mass Transfer* 45.12, pp. 1583–1588.

Van't Riet, K. (July 1979). "Review of Measuring Methods and Results in Nonviscous Gas-Liquid Mass Transfer in Stirred Vessels". In: *Industrial & Engineering Chemistry Process Design and Development* 18.3, pp. 357–364.

Veilleux, J. and S. Coulombe (2010). "A total internal reflection fluorescence microscopy study of mass diffusion enhancement in water-based alumina nanofluids". In: *Journal of Applied Physics* 108.10, p. 104316.

Wang, C. Y. and R. V. Calabrese (1986). "Drop breakup in turbulent stirred-tank contactors. Part II: relative influence of viscosity and interfacial tension". In: *AIChE Journal* 32.4, pp. 667–676.

Wang, H.-B., Y.-H. Zhang, Y.-B. Zhang, F.-W. Zhang, J.-R. Niu, H.-L. Yang, R. Li, and J.-T. Ma (Sept. 2012). "Pd immobilized on thiol-modified magnetic nanoparticles: A complete magnetically recoverable and highly active catalyst for hydrogenation reactions". In: *Solid State Sciences* 14.9, pp. 1256–1262.

Wang, H., R. Wang, L. Wang, and X. Tian (July 2011). "Preparation of multicore/single-shell OA-Fe3O4/PANI bifunctional nanoparticles via miniemulsion polymerization". In: *Colloids and Surfaces A: Physicochemical and Engineering Aspects* 384.1-3, pp. 624–629.

Wechsler, B., D. Lindsley, and C. Prewitt (1984). "Crystal structure and cation distribution in titanomanganites (Fe3–xTixO4)". In: *American Mineralogist* 69, p. 754.

Wen, J. P., X. Q. Jia, and W. Feng (Jan. 2005). "Hydrodynamic and Mass Transfer of Gas-Liquid-Solid Three-Phase Internal Loop Airlift Reactors with Nanometer Solid Particles". In: *Chemical Engineering & Technology* 28.1, pp. 53–60.

Wu, W.-D., G. Liu, S.-X. Chen, and H. Zhang (Feb. 2013). "Nanoferrofluid addition enhances ammonia/water bubble absorption in an external magnetic field". In: *Energy and Buildings* 57, pp. 268–277.

Yagi, H and F Yoshida (1975). "Gas absorption by Newtonian and non-Newtonian fluids in sparged agitated vessels." In: *Industrial & Engineering Chemistry Process Design and Development* 14, pp. 488–493.

Yang, K., H. Peng, Y. Wen, and N. Li (Mar. 2010). "Re-examination of characteristic FTIR spectrum of secondary layer in bilayer oleic acid-coated Fe3O4 nanoparticles". In: *Applied Surface Science* 256.10, pp. 3093–3097.

Yang, L., K. Du, X. F. Niu, B. Cheng, and Y. F. Jiang (May 2011). "Experimental study on enhancement of ammonia–water falling film absorption by adding nano-particles". In: *International Journal of Refrigeration* 34.3, pp. 640–647.

Yoshida, F., T. Yamane, and Y. Miyamoto (Oct. 1970). "Oxygen Absorption into Oil-in-Water Emulsions. A Study on Hydrocarbon Fermentors". In: *Industrial & Engineering Chemistry Process Design and Development* 9.4, pp. 570–577.

Yu, H. and Z. Tan (2012). "New Correlations of Volumetric Liquid-Phase Mass Transfer Coefficients in Gas-Inducing Agitated Tank Reactors". In: *International Journal of Chemical Reactor Engineering* 10.1.

Zadghaffari, R., J. Moghaddas, and J. Revstedt (Aug. 2010). “Large-eddy simulation of turbulent flow in a stirred tank driven by a Rushton turbine”. In: *Computers & Fluids* 39.7, pp. 1183–1190.

Zhao, S., S. G. Kuttuva, and L. K. Ju (1999). “Oxygen transfer characteristics of multiple-phase dispersions simulating water-in-oil xanthan fermentations”. In: *Bioprocess Engineering* 20, pp. 313–323.

Zhu, H., B. H. Shanks, and T. J. Heindel (Oct. 2008). “Enhancing CO-Water Mass Transfer by Functionalized MCM41 Nanoparticles”. In: *Industrial & Engineering Chemistry Research* 47.20, pp. 7881–7887.

— (2009). “Effect of Electrolytes on CO- Water Mass Transfer”. In: *Industrial & Engineering Chemistry Research* 48.6, pp. 3206–3210.

Zhu, H., B. H. Shanks, D. W. Choi, and T. J. Heindel (Nov. 2010). “Effect of functionalized MCM41 nanoparticles on syngas fermentation”. In: *Biomass and Bioenergy* 34.11, pp. 1624–1627.

Zon, M van der, P. J. Hamersma, E. K. Poels, and A. Bliek (Jan. 1999). “Gas–solid adhesion and solid–solid agglomeration of carbon supported catalysts in three phase slurry reactors”. In: *Catalysis Today* 48.1-4, pp. 131–138.